2008

Experimental study of a foam flow in horizontal pipes: two flow regimes and its implications

Miodrag Bogdanovic
Louisiana State University and Agricultural and Mechanical College, mbogda1@lsu.edu

EXPERIMENTAL STUDY OF FOAM FLOW IN HORIZONTAL PIPES: TWO FLOW REGIMES AND ITS IMPLICATIONS

A Thesis

Submitted to the Graduate Faculty of the
Louisiana State University and
Agricultural and Mechanical College
in partial fulfillment of the
Requirements for the degree of
Master of Science in Petroleum Engineering

in

The Department of Petroleum Engineering

by

Miodrag Bogdanovic
B.S. M.E, University of Belgrade, Serbia, 2000
August, 2008

ACKNOWLEDGEMENTS

I would like to thank to the Louisiana State University and Craft and Hawkins Department of Petroleum Engineering. Especially, I express my appreciation to my major professor, Dr. Seung Ihl Kam, for his direction, guidance, advice and encouragement. Special thanks to my examining committee members Dr. John Rogers Smith, and Dr. Richard G. Hughes.

I am thankful to The Craft and Hawkins Department of Petroleum Engineering at Louisiana State University for their financial support. Without their support, this work would not have been possible. Additional gratitude is also extended to all professors.

Special thanks are extended to the staff at LSU's Petroleum Engineering Research and Technology Transfer Laboratory (PERTTL), especially Gerry Masterman and Darryl A. Bourgoyne for their help to set the lab equipment and hours spent on this project. Also, I would like to thank to Mr. Fenelon Nunes for his support and presence at the department.

Special thanks to Stepan Co., Northfield, IL, and Baker-Petrolite, Sugar Land, TX, for providing products and information to develop this research.

I wish to thank to my country, Serbia, because through the University of Belgrade and companies Energoproject and PM Lucas I received the academic knowledge and professional experience to be successful in my life.

This work is dedicated to my parents, Vladimir and Javorka, my sister Gordana and her son Andrej.

TABLE OF CONTENTS

ACKNOWLEDGEMENTS……ii

LIST OF TABLES……v

LIST OF FIGURES ……vi

ABSTRACT……xi

1. INTRODUCTION……1
   1.1 Objectives of This Study ……2
   1.2 Chapter Description ……3

2. LITERATURE REVIEW……5
   2.1 Stability of Foam as a Dispersed Phase ……5
   2.2 Yield Stress of Bulk Foam Flow……6
   2.3 Fundamentals of Bulk Foam Rheology in Pipes ……8
   2.4 Two Flow Regimes of Foam in Porous Media……13

3. PROCEDURE AND METHODOLOGY……17
   3.1 Experimental Materials and Setup……17
   3.2 Experimental Procedure and Data Processing……21

4. RESULTS AND DISCUSSIONS ……27
   4.1 Introduction ……27
   4.2 Base Case (Case 1)……28
   4.3 Effect of Surfactant Concentration (Cases 1,2, and 3)……35
   4.4 Effect of Filter Opening Size (Cases 4,5, and 6)……39
   4.5 Effect of Surfactant Formulation (Cases 7,8,9 and 10)……44
   4.6 Effect of Pipe Diameter (Cases 11 and 12)……53
   4.7 Flow Experiments at Fixed Foam Quality (Cases 13 and 14)……57
   4.8 Discussions ……63
   4.9 Implication of Two Flow Regimes in Field Applications……68

5. CONCLUSIONS AND RECOMMENDATIONS……70
   5.1 Conclusions ……70
   5.2 Recommendations ……72

REFERENCES ……74

APPENDIX
   A. EXPERIMENTAL DATA FOR CASES 1 THROUGH 12……80

B. DERIVATION OF REYNOLDS NUMBER AND POWER-LAW EXPONENT.....93

VITA ……..…..97

LIST OF TABLES

3.1 A brief summary of all 14 experimental cases conducted in this study……..…….……22

3.2 Different combinations of gas and liquid injection rates in 1 inch ID stainless steel pipe (cf. Cases 11 and 12 as shown in Table 3.1)……...…..…….……..22

3.3 Different combinations of gas and liquid injection rates in 0.5 inch ID pipes (cf. Cases 1 through 10 as shown in Table 3.1)……..…….…….....23

4.1 Flow rates used for Case 13 (cf. Fig. 4.28) at fixed foam quality of 98.4%.....58

4.2 Flow rates used for Case 14a (cf. Fig. 4.29) at fixed foam quality of 98.4%.....59

4.3 Flow rates used for Case 14b (cf. Fig. 4.30) at fixed foam quality of 98.4%.....59

LIST OF FIGURES

2.1 Two dimensional representation of the origin of yield stress in the presence of foams: the interaction between different layers of foams causes a resistance to flow [upper schematic figure from Princen, 1983; lower diagram from Prud'homme, 1981]..……. 7

2.2 Experimental data of yield stress of foam as a function of foam quality [from Blauer et al., 1974]: the yield stress increases sharply above a threshold value in which bubble to bubble interaction becomes significant…….....……..... 7

2.3 The origin of yield stress of foam-solid mixtures: the concept of a representative unit cell in Princen-Prud'hommes model (Fig. 2.1) is still applicable in three-phase foam-solid mixtures [from Kam et al., 2002]
(a) Dimensionless force resisting flow at different values of gas fraction (F_g) (solid fraction (F_s) is fixed at 49.8 %)…….……..... 9
(b) Dimensionless resisting force as a function of three-phase fractions (gas liquid, and solids)…….……. 9

2.4 Bingham plastic viscosity of foam as a function of foam quality [from Blauer et al., 1974]: the increase in foam texture causes an increase in plastic viscosity…....…….. 11

2.5 The change in foam viscosity (x axis) as a function of shear stress (y axis) at different tube diameters: foams behave as shear-thinning [from David and Marsden, 1969].
(a) Foam quality between 81 % and 89 %..... 13
(b) Foam quality between 90 % and 96 %..... 13

2.6 Steady-state pressure contours during foam flow in a 2-ft long sandpack [from Osterloh and Jante, 1992]: There exist two different flow regimes in which foam behaves quite distinctly……..... 15

2.7 Steady-state pressure-gradient contours during foam flow in 530-md Berea sandstone [from Alvarez et al., 2001]: the presence of two flow regimes are identified in a wide range of experimental conditions……...……..... 16

3.1 A schematic of experimental setup for foam flow in pipe used in this study…..…… 17

3.2 Experimental setup……... 18

3.3 Visual cell……. 18

3.4 Pipe inlet with upstream foam generator and gas flow meter……..... 18

3.5 Pressure transducers……....……. 18

3.6 Brooks microprocessor flow control unit……. 20

3.7 Positive displacement Optos Pumps……. 20

3.8 Dead weight tester…… 21

3.9 0.5 and 1 inch stainless steel pipes……... 21

3.10 0.5 and 1 inch pipe outlets…… 21

3.11 Foam disposal……... 21

3.12 A schematic of Newtonian fluid (α=1), shear-thinning (α<1), and shear-thickening fluid (α>1)…….....……... 26

3.13 Determination of power-law exponent (α)……..... 26

4.1 Pressure response as a function of time with a stepwise change in gas and liquid injection rates (Case 1; also base case): (0.5 inch ID stainless steel pipe, 1 wt% surfactant concentration using Cedepal FA-406, 50 μm filter……..... 30

4.2 Pressure response as a function of time with a stepwise change in gas and liquid injection rates, continued (Case 1; also base case): (0.5 inch ID stainless steel pipe, 1 wt% surfactant concentration using Cedepal FA-406, 50 μm filter opening size)..... 31

4.3 Pressure response as a function of time with a stepwise change in gas and liquid injection rates, continued (Case 1; also base case): (0.5 inch ID stainless steel pipe, 1 wt% surfactant concentration using Cedepal FA-406, 50 μm filter opening size)…...… 32

4.4 Steady-state pressure drops, in psi, as a function of superficial gas and liquid injection velocities (Case 1; also base case): (0.5 inch ID stainless steel pipe, 1 wt% surfactant concentration using Cedepal FA-406, 50 μm filter opening size)……..……..... 34

4.5 Fig. 4.5. Pressure response as a function of time with a stepwise change in gas and liquid injection rates (Case 2): (0.5 inch ID stainless steel pipe, 5 wt% surfactant concentration using Cedepal FA -406, 50 μm filter opening size)opening size)……. 36

4.6 Steady-state pressure drops, in psi, as a function of superficial gas and liquid injection velocities (Case 3): (0.5 inch ID stainless steel pipe, 5 wt% surfactant concentration using Cedepal FA-406, 50 μm filter opening size)……..…… 37

4.7 Pressure response as a function of time with a stepwise change in gas and liquid injection rates (Case 3): (0.5 inch ID stainless steel pipe, 0.1 wt% surfactant concentration using Cedepal FA -406, 50 μm filter opening size)…….. 38

4.8 Steady-state pressure drops, in psi, as a function of superficial gas and liquid injection velocities (Case 3): (0.5 inch ID stainless steel pipe, 0.1 wt% surfactant concentration using Cedepal FA-406, 50 μm filter opening size)……...……... 39

4.9 Pressure response as a function of time with a stepwise change in gas and liquid injection rates (Case 4): (0.5 inch ID stainless steel pipe, 1 wt% surfactant concentration using Cedepal FA -406, 90 μm filter opening size)……. 41

4.10 Steady-state pressure drops, in psi, as a function of superficial gas and liquid injection velocities (Case 4): (0.5 inch ID stainless steel pipe, 1 wt% surfactant concentration using Cedepal FA-406, 90 μm filter opening size)……... 42

4.11 Pressure response as a function of time with a stepwise change in gas and liquid injection rates (Case 5): (0.5 inch ID stainless steel pipe, 5 wt% surfactant concentration using Cedepal FA -406, 90 μm filter opening size)……... 43

4.12 Steady-state pressure drops, in psi, as a function of superficial gas and liquid injection velocities (Case 5): (0.5 inch ID stainless steel pipe, 5 wt% surfactant concentration using Cedepal FA-406, 90 μm filter opening size)……... 44

4.13 Steady-state pressure drops, in psi, as a function of superficial gas and liquid injection velocities (Case 6): (0.5 inch ID stainless steel pipe, 0.1 wt% surfactant concentration using Cedepal FA-406, 90 μm filter opening size)……... 45

4.14 Pressure response as a function of time with a stepwise change in gas and liquid injection rates (Case 7): (0.5 inch ID stainless steel pipe, 1 wt% surfactant concentration using Petrostep CG-50, 50 μm filter opening size)……. 46

4.15 Steady-state pressure drops, in psi, as a function of superficial gas and liquid injection velocities (Case 7): (0.5 inch ID stainless steel pipe, 1 wt% surfactant concentration using Petrostep CG-50, 50 μm filter opening size)……... 47

4.16 Pressure response as a function of time with a stepwise change in gas and liquid injection rates (Case 8): (0.5 inch ID stainless steel pipe, 1 wt% surfactant concentration using Stepanform 1050, 50 μm filter opening size)……... 48

4.17 Steady-state pressure drops, in psi, as a function of superficial gas and liquid injection velocities (Case 8): (0.5 inch ID stainless steel pipe, 1 wt% surfactant concentration using Stepanform 1050, 50 μm filter opening size)……... 49

4.18 Pressure response as a function of time with a stepwise change in gas and liquid injection rates (Case 9): (0.5 inch ID stainless steel pipe, 1 wt% surfactant concentration using Aquet TD-600, 50 μm filter opening size)……... 50

4.19 Steady-state pressure drops, in psi, as a function of superficial gas and liquid injection velocities (Case 9): (0.5 inch ID stainless steel pipe, 1 wt% surfactant concentration using Aquet TD-600, 50 μm filter opening size)……... 51

4.20 Pressure response as a function of time with a stepwise change in gas and liquid injection rates (Case 10): (0.5 inch ID stainless steel pipe, 1 wt% surfactant concentration using Ultra Palmolive, 50 μm filter opening size)……... 52

4.21 Steady-state pressure drops, in psi, as a function of superficial gas and liquid injection velocities (Case 10): (0.5 inch ID stainless steel pipe, 1 wt% surfactant concentration using Ultra Palmolive, 50 μm filter opening size)…… 53

4.22 Pressure response as a function of time (Case 11): (1 inch ID stainless steel pipe, 1 wt% surfactant concentration using Cedepal FA-406, 50 μm filter opening size)……..……..…….. 54

4.23 Pressure response as a function of time (Case 11), continued……..…....…….... 54

4.24 Steady-state pressure drops, in psi, as a function of superficial gas and liquid injection velocities (Case 11): (1 inch ID stainless steel pipe, 1 wt% surfactant concentration using Cedepal FA-406, 50 μm filter opening size)……...…….... 55

4.25 Pressure response as a function of time (Case 12): (1 inch ID stainless steel pipe, 5 wt% surfactant concentration using Cedepal FA -406, 50 μm filter opening size)…….....…….... 56

4.26 Pressure response as a function of time (Case 12), continued …..... 56

4.27 Steady-state pressure drops, in psi, as a function of superficial gas and liquid injection velocities (Case 12): (1 inch ID stainless steel pipe, 5 wt% surfactant concentration using Cedepal FA-406, 50 μm filter opening size)……...…….…….. 57

4.28 Pressure response as a function of time with a stepwise change in gas and liquid injection rates (Case 13): (0.5 inch ID stainless steel pipe, 1 wt% surfactant concentration using Cedepal FA-406, 50 μm filter opening size)……..……..…….... 60

4.29 Pressure response as a function of time with a stepwise change in gas and liquid injection rates (Case 14a): (0.5 inch ID stainless steel pipe, 1 wt% surfactant concentration using Cedepal FA-406, 50 μm filter opening size)……...…….... 61

4.30 Pressure response as a function of time with a stepwise change in gas and liquid injection rates (Case 14b): (0.5 inch ID stainless steel pipe, 0.5 wt% surfactant concentration using Cedepal FA-406, 50 μm filter opening size)……..…..…….... 62

4.31 Schematic representation of two flow regimes and pressure contours……...…… 63

4.32 Sequence of photos taken from the 0.5 inch pipe outlet showing repetition of free gas and foam slug within high-quality regime at foam quality above 99%..... 64

4.33 Sequence of homogeneous foam flow within low-quality regime at 0.5 inch pipe outlet at foam quality below 99%..... 65

4.34 Photos taken in the upstream visual cell: left with stable foam in the low-quality and right with unstable foam in the higher foam qualities .....…….. 65

4.35 Schematic representation of constant-total-injection-velocity experiment at varying foam quality (f_g)……..……... 67

4.36 Implication of the change in gas fraction (vertical dotted line), in liquid fraction (horizontal dotted line) or in f_g* ……...…….……..... 69

ABSTRACT

Although foam has been widely used in many scientific and engineering applications, the current understanding of foam rheology in pipes is still very limited because of its complex nature. This experimental study, for the first time, investigates the flow rheology of foams in pipes by placing a special emphasis on two distinct foam flow regimes.

A wide range of experimental conditions are examined in this study, which include five different surfactant formulations (Cedepal FA-406, Petrostep CG-50, Stepanform 1050, Aquet TD-600, and Ultra-Palmolive), three different surfactant concentrations (0.1, 1, and 5 wt %), two different pipe diameters (0.5 and 1 inch nominal size stainless steel pipes), and two different filter opening sizes (50 μm and 90 μm) for upstream foam generation.

The experiments revealed the following characteristics: (1) foam flow in pipes exhibited two different flow regimes called “high-quality” regime and “low-quality” regime, (2) the high-quality regime was characterized by unstable and oscillating pressure response which resulted from repeating free gas and foam slug, whereas the low-quality regime was characterized by stabilized pressure response which resulted from the flow of uniform and homogeneous foams, (3) different patterns of pressure contours were observed - the pressure contours were relatively steep in the high-quality regime but relatively gentle, or even almost horizontal, in the low-quality regime, (4) foam rheology in the high-quality regime was shear thickening to liquid injection velocity in all cases, and foam rheology in the low-quality regime was not consistent, and (5) the value of foam quality (f_g*) that splits the two flow regimes was shown to be affected by experimental conditions such as surfactant formulations and concentrations.

These observations imply that the rheology in the high-quality regime is primarily governed by dynamic mechanisms of lamella creation and coalescence during the flow, and the

rheology in the low-quality regime is primarily governed by interactions between individual bubbles and/or interactions between bubbles and pipe wall. Therefore, the high-quality regime is likely to expand (or, the low-quality regime is likely to contract, equivalently) with a reduction in surfactant foamability.

Implications of distinct foam behaviors in two flow regimes in practical applications are also discussed.

1. INTRODUCTION

Foam is an agglomeration of bubbles separated by thin liquid films [Bikerman, 1973] often referred to as “lamella” (in singular) or “lamellae” (in plural). The presence of surface active agents, called surfactants, reduces the interfacial tension between immiscible phases and endows the liquid films between dispersed bubbles with great stability [Bikerman, 1973; Schramm, 1994].

Understanding foam flow in pipes is a challenging and complicated issue. Some of the major problems can be summarized as follows [Bikerman, 1973; Wilson, 1989; Schramm, 1994; Prud'homme and Khan, 1996; Briceño and Joseph, 2003]: First, any realistic modeling and simulation of foam flow should be based on the description of average bubble size and bubble size distribution which, cannot be measured or estimated reliably in many cases. Second, complications occur because of dynamic behavior of bubble generation and coalescence when the foam is in motion. Bubbles are continuously generated near the pipe wall under high shear stress and merged to form larger bubbles near the center of the flow conduit at which the shear stress is minimal. These bubbles are rearranged constantly responding to the change in flow conditions. Third, foam quality (f_g), which is defined as the fraction of gas flow to the total flow, can change significantly during the flow because of gas compressibility, which is indirectly related to dynamics of bubble generation and coalescence. Phase exchange between internal gas phase and external liquid phase may add another difficulty in estimating foam quality precisely. Last, perhaps the biggest challenge in decades of foam research, experimental data accumulated at particular test conditions cannot scale up or down easily, because the issues of bubble size, bubble size distribution, bubble creation and coalescence, bubble rearrangements, and the change in foam texture are nonlinearly commingled one another. There is no doubt that other

components relevant to surfactant chemistry such as salt concentration, pH, temperature, additives, and so on should also be factored in.

A simple approach to model foam is to assume that foam is a homogeneous mixture following either Newtonian or non-Newtonian fluid (Bingham plastic) behavior in which the external liquid and internal gas phase travel almost at the same velocity [Wilson, 1989]. Although this simple approach may work reasonably well in some applications, it obviously does not fully reflect the complexity of foam rheology in a comprehensive manner.

Recent experimental studies on foam rheology in porous media show interesting behaviors during steady-state foam flow in consolidated porous rocks and unconsolidated sand- or bead-packs [Osterloh and Jante, 1992, Alvarez et al., 2002, Kam et al., 2007a]. When the steady-state pressure gradients are plotted as a function of gas and liquid injection velocities in x and y axes, there exist two distinct flow regimes: a regime with relatively high gas fraction having pressure-gradient contours almost independent of gas injection velocity; and the other regime with relatively low gas fraction having pressure-gradient contours almost independent of liquid injection velocities. The concept of two flow regimes is very helpful in designing foam applications in improved or enhanced oil recovery processes. No efforts have been made so far regarding how this two flow regime concept present in porous media can be extended to foam flow mechanisms in pipes.

1.1. Objectives of This Study

Foam flow in pipe has been regarded as a separate issue from foam flow in porous media because of the difference in flow mechanisms, especially the role of capillary pressure which is minimal in the former but is crucial in the latter. But there are some common interests shared by the two topics: (1) when the gas fraction is relatively high, bubbles become less stable and thus foam rheology is governed by dynamics of bubble creation and coalescence in a water-deficient

environment and (2) when the liquid fraction is relatively high, bubbles become stable and thus the transport of stable bubbles is the key to foam rheology.

The major objective of this study is to conduct laboratory foam flow experiments at different test conditions in order to understand the rheological properties of foams in pipes. This study, for the first time, focuses on the interpretation of foam rheology using the concept of two flow regimes (i.e., high-quality regime and low-quality regime) as shown in recent foam flow experiments in porous media. The experimental results are to be analyzed (1) to distinguish two distinct flow regimes based on the steady-state pressure contours, (2) to identify whether the flow rheology of each regime can be approximated by near-Newtonian, shear thinning, or shear thickening behavior, and (3) to investigate the factors that influence the boundary between the two flow regimes, i.e., the value of foam quality (f_g*) that splits the map into two regimes.

The implications of two flow regimes during foam flow in pipe are also discussed.

1.2. Chapter Description

This study consists of five chapters which can be summarized as follows:

Chapter 1 briefly introduces the complexity of foam flow in general and overviews theoretical background. The scope and objectives of this study are also listed.

Chapter 2 summarizes the fundamentals of foams in terms of foam stability, yield stress, flow modeling, flow rheology in pipes, and flow rheology in porous media. It also reviews the concept of two steady-state strong-foam regimes experimentally observed in recent studies of foam flow in porous media.

Chapter 3 describes the details about experimental instruments, layouts, and procedures employed in this study in order to measure and analyze foam rheology in pipes. The first half depicts the materials and different components of experimental system, and the second half

outlines how the data obtained from the experiments can be processed and translated into the format reported in the result section.

Chapter 4 provides the results of foam flow experiments over a broad range of experimental conditions, i.e., at varying gas and liquid injection velocities under different surfactant concentrations, surfactant formulations, opening sizes of foam generator, and/or diameters of stainless steel pipe. The description of experimental results is followed by discussions of significance and implication of the results in practical field applications.

Chapter 5 covers a summary of this study with conclusions and recommendations for future work.

2. LITERATURE REVIEW

This chapter briefly reviews previous studies on the fundamentals of foams and bubbles, factors affecting foam characteristics, and flow rheology of foams in pipes and porous media.

2.1. Stability of Foam as a Dispersed Phase

A system has a tendency to reduce its energy level as designed by Mother Nature. Any dispersed systems such as foams and emulsions are therefore unstable, and eventually break down and segregate into immiscible phases minimizing its interfacial area and energy level. The presence of surface active agents, called surfactants, can retard the process of segregation significantly, however. Anionic surfactants, often used in petroleum reservoir applications, have negatively charged hydrophilic head groups and hydrophobic tail groups, and the electrostatic repulsive force between the head groups endows foam films with stability [Schramm, 1994].

Once stable liquid films are formed and present with the help of surfactant molecules at the interface, Laplace equation defines the pressure difference across the interface, which can be described as follows:

$$P_c = P_{gas} - P_{liq} = \sigma\left(\frac{1}{R_1} + \frac{1}{R_2}\right) \qquad \text{,……...……...…} \quad (2.1)$$

where, P_{gas} and P_{liq} are gas and liquid pressures, P_c is the pressure drop across the interface between gas and liquid phases (i.e., capillary pressure), σ is interfacial tension, and R_1 and R_2 are two principal radii. Eq. (2.1) indicates that a curved interface between gas and liquid phases in the presence of foam ends up with non-uniform pressure between gas and liquid. This implies that gas mass in smaller bubbles can diffuse into larger bubbles because a foam mixture has a wide range of bubble sizes. This in turn implies that even though the stability of thin liquid films is guaranteed mechanically, dispersed gas phase can still decay and be segregated from liquid phase by diffusion process.

In general, foams are more stable once a larger quantity of surfactant solution is available in the surrounding area. A variable called "foam quality", f_g, defines the fraction of gas in foams. For stationary foams, foam quality (f_g) is expressed by the volume fraction, i.e.,

$$f_g = \frac{V_{gas}}{V_{gas} + V_{liq}} \quad ,\ldots\ldots\ldots\ldots\ldots\ldots\ldots\ldots\ldots\ldots\ldots\ldots\ldots\ldots\ldots\ldots\ldots\ldots\ldots\ldots\ldots. \text{(2.2)}$$

while for foams in motion, foam quality (f_g) is defined as the rate fraction, i.e.,

$$f_g = \frac{q_{gas}}{q_{gas} + q_{liq}} = \frac{u_{gas}}{u_{gas} + u_{liq}} \quad ,\ldots\ldots\ldots\ldots\ldots\ldots\ldots\ldots\ldots\ldots\ldots\ldots\ldots\ldots\ldots\ldots\ldots. \text{(2.3)}$$

where, V_{gas} and V_{liq} are gas and liquid volumes, q_{gas} and q_{liq} are gas and liquid flow rates, u_{gas} and u_{liq} are gas and liquid superficial velocities.

Foam texture is another important term to characterize foam properties. Foams with small bubble size are called "fine-textured", where foams with large bubble size are called "coarse-textured".

2.2. Yield stress of Bulk Foam Flow

Foam in bulk is known for its yield stress, which can be approximated using the Bingham plastic model as follows:

$$\tau = \tau_0 + \mu_p \dot{\gamma} \ ,\ldots\ldots\ldots\ldots\ldots\ldots\ldots\ldots\ldots\ldots\ldots\ldots\ldots\ldots\ldots\ldots\ldots\ldots\ldots\ldots\ldots\ldots\ldots. \text{(2.4)}$$

where τ is shear stress, τ_o is yield stress, μ_p is plastic viscosity, and $\dot{\gamma}$ is shear rate. The yield stress results from the fact that the flow of bulk foam requires deformation of individual bubbles resisting to the flow. Fig. 2.1 shows a two-dimensional schematic of representative unit cells which illustrates how the change in shear stress (τ) and shear strain (γ) can be related to the change in bubble shape [Prud'homme, 1981; Princen, 1983]. The stress-strain diagram at the bottom of Fig. 2.1 shows a periodic response when a foam mixture is under constant shear rate in a flow conduit.

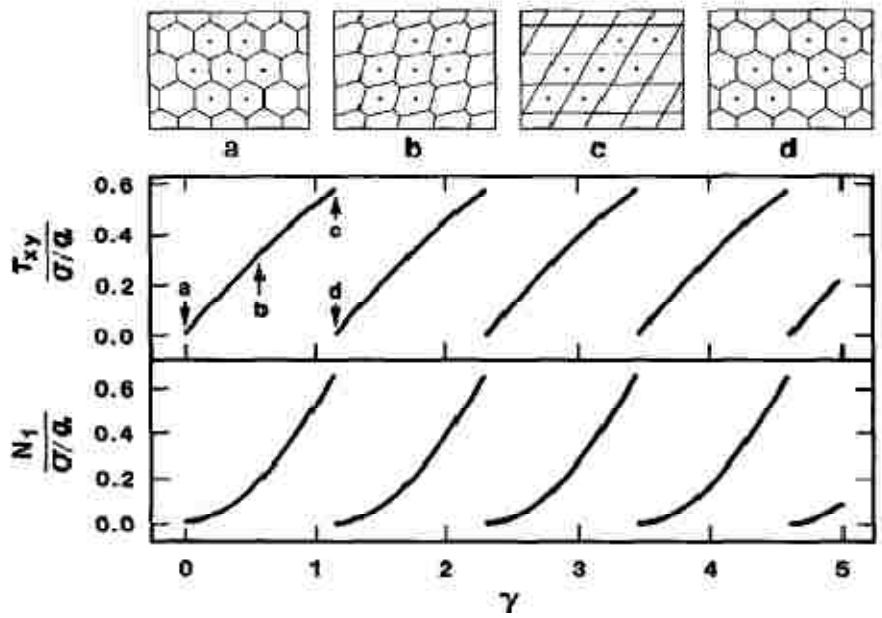

Fig. 2.1. Two dimensional representation of the origin of yield stress in the presence of foams: the interaction between different layers of foams causes a resistance to flow [upper schematic figure from Princen 1983; lower diagram from Prud'homme, 1981].

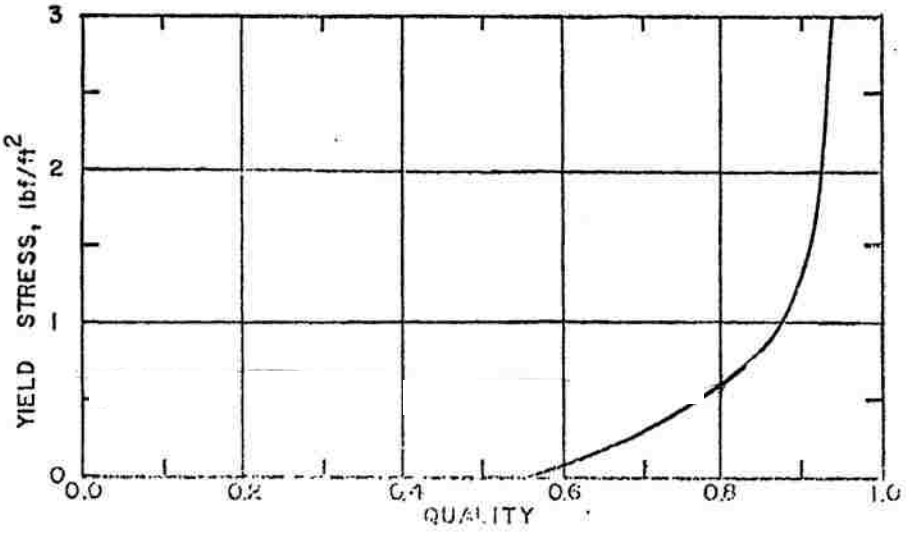

Fig. 2.2. Experimental data of yield stress of foam as a function of foam quality [from Blauer et al., 1974]: the yield stress increases sharply above a threshold value in which bubble to bubble interaction becomes significant.

The maximum resistance to the flow, which defines the yield stress, is known to be sensitive to foam quality as illustrated in Fig. 2.2 [Blauer et al., 1974; Princen, 1983; Kraynik, 1988]: (1) at low foam quality, the yield stress is negligible because dispersed bubbles do not

interact each other; (2) at intermediate foam quality, the yield stress increases with increasing foam quality because bubbles in different shear layers begin to interfere each other and the degree of interference increases with foam quality, and (3) at high foam quality, there is a sudden reduction in the magnitude of yield stress due to the coalescence of bubbles (or, instability of foam mixtures) at dry conditions. The first and second points are well demonstrated experimentally in the study of [Blauer et al., 1974].

The same concept of periodic unit cells can be used to investigate the origin of the yield stress of foam-solid mixtures theoretically [Kam et al., 2002; Kam and Rossen 2002]. These studies also show that although three-phase systems are more complicated, the yield stress of foam-solid mixtures still primarily depends on the interactions between bubbles. For example, Fig. 2.3(a) shows that the magnitude of dimensionless resistance force on the y axis changes with the shear displacement (x axis) and the minimum value of the force, which is proportional to the yield stress, increases with increasing gas fraction when the solid fraction is fixed at 49.8%. Fig. 2.3(b) shows that the resistance force depends on the fractions of three phases, and also demonstrates the importance of bubble deformation and bubble-to-bubble and/or bubble-to-solid interactions to quantify the yield stress. The trend of the yield stress as shown in Fig. 2.3 is consistence with experimental findings [Harris et al., 1991; Bejuijen et al., 1999].

2.3. Fundamentals of Bulk Foam Rheology in Pipes

Understanding the origin of yield stress provides insights into the rheological properties of bulk foams. Earlier studies point out that foam can be treated as a single uniform and homogeneous fluid whose viscosity is significantly greater than either of gas or liquid phases [Einstein, 1906; Hatschek, 1910; Mitchell, 1969, 1971]. These studies show that when the foam quality is less than approximately 52%, gas bubbles are mostly spherical and uniformly dispersed, implying that bubbles do not interfere each other significantly during the flow. For

foam qualities less than 52%, the yield stress of foam is also negligible by the same token and the rheology of foam is similar to that of the external liquid phase. This is why foam is shown to behave similar to Newtonian fluid at low foam quality.

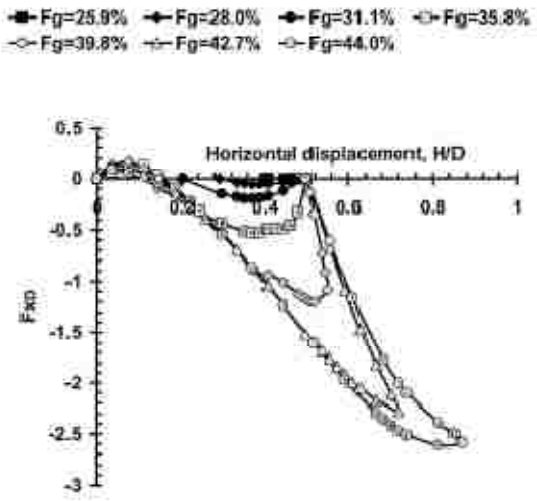

(a) Dimensionless force resisting flow at different values of gas fraction (F_g) (solid fraction (F_s) is fixed at 49.8 %)

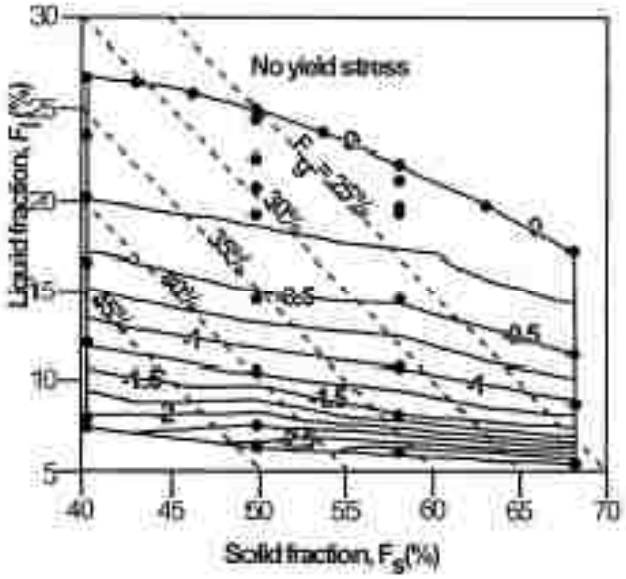

(b) Dimensionless resisting force as a function of three-phase fractions (gas liquid, and solids)

Fig. 2.3. The origin of yield stress of foam-solid mixtures: the concept of a representative unit cell in Princen-Prud'hommes model (Fig. 2.1) is still applicable in three-phase foam-solid mixtures [from Kam et al., 2002].

Other studies, including Hatschek [1910], indicate that for foam qualities ranging from approximately 52% to 74%, gas bubbles begin to deform and interfere with each other. The apparent viscosity therefore increases with foam quality. Hatschek also experimentally observed that this increase in foam viscosity with foam quality is more dramatic for foam quality greater than about 74%. He concluded that the rapid increase in foam viscosity is due to the additional resistance caused by the change in bubble shape (i.e., from spheres to hexagons or dodecahedra), which agrees well with modeling studies on foam yield stress [Princen, 1983; Kraynik, 1988].

Fig. 2.4 shows an example experimental result of the Bingham plastic viscosity of foam as a function of foam quality [Blauer et al., 1974]. At foam quality very close to zero, which is very close to a single phase, the Bingham plastic viscosity is close to 1 centipoise (cp). As foam quality increases to around 52%, the viscosity increases linearly with foam quality. The slope is relatively gentle because of moderate interactions between spherical bubbles. The interaction becomes more active as foam quality increases greater than 52%, which is accompanied by a significant rise in the Bingham plastic viscosity.

Fig. 2.4 implies that foam can also be described by a power-law or Hershel-Bulkley model, as described by previous studies [Valco et al., 1992; Gardiner et al., 1999; Briceño and Joseph, 2003; Bonilla et al., 2000], i.e.,

$\tau = K\dot{\gamma}^n$, for power-law fluid and …….. (2.5)

$\tau = \tau_0 + K\dot{\gamma}^n$, for Hershel-Bulkley fluid ……... (2.6)

where τ is shear stress, K is consistency index, n is power-law exponent, τ_o is yield stress, and $\dot{\gamma}$ is shear rate.

Whether the fluid is shear-thinning, shear-thickening, or near-Newtonian is primarily dependent upon dynamic mechanisms of bubble creation and coalescence, the size and shape of the bubbles, and the level of bubble interactions in a confined flow conduit.

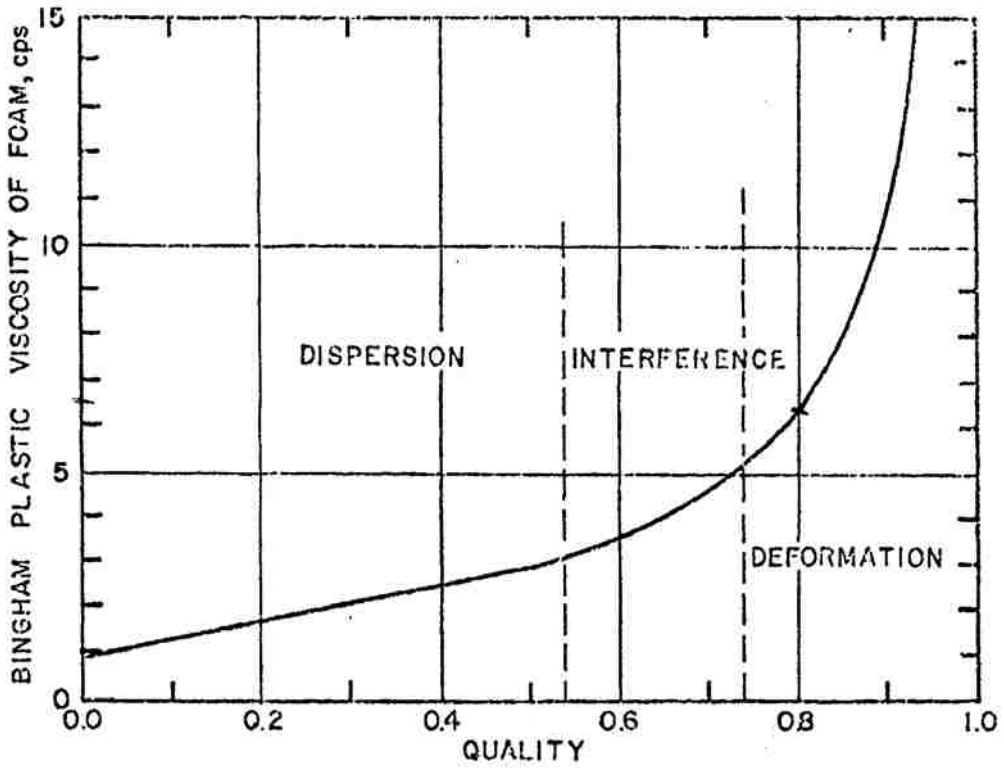

Fig. 2.4. Bingham plastic viscosity of foam as a function of foam quality [from Blauer et al., 1974]: the increase in foam texture causes an increase in plastic viscosity.

Briceño and Joseph's study [2003] visualizes how foam texture changes depending upon injection rates and injection velocities: fine-textured foams present at low foam quality (about f_g < 73 %), repetition of foam and gas slug at high foam quality (about f_g > 97 %), and coarse-textured foams present in between. Fig. 2.5 shows such an example resulting from laboratory experiments in a small tube. In both foam qualities tested (foam qualities from 81 to 89 % and from 90 to 96 %), apparent foam viscosity decreases with the shear stress because of fine textured foams created at higher shear rate, meaning that foam is a shear-thinning fluid. It can also be observed that at the same shear stress, the apparent viscosity of foams increases as tube diameter increases. This implies that although higher shear stress in a smaller diameter is a favorable condition to create fine-textured foams, higher capillary pressure has a dominant effect to keep foam texture coarser in smaller tubes. Some studies found that the effective viscosity of

foams in pipes may decrease as the shear rate increases, because of the interplay between shear stress, shear rate, foam texture, and dynamics of lamella creation and coalescence during foam flow, which is a typical behavior of pseudo-plastic fluid [Mooney, 1931; Raza and Marsden, 1967; David and Marsden, 1969; Okpobiri and Ikoku, 1986]. This is consistent with previous understanding that bubble size and bubble size distribution are the key to analyze foam rheology.

When it comes to a comparison between foam flow in relatively large pipe diameters and foam flow in small tubes or pores, however, caution is needed because there are different controlling mechanisms. The flow mechanism in small tubes or pores is primarily governed by capillary phenomenon, while the flow mechanism in pipes is dominated by gravity, shear stress/strain, and interaction between bubbles in pipes. The characteristics of foam flow in pores are further explained in the following section.

Just like other fluids, the presence of two different flow patterns such as laminar and turbulent flows also has a similar impact to foam flow in pipes. Blauer et al.'s study [1974] shows that Moody's chart that relates friction factor to Reynolds number at different pipe roughness [Bird et al., 1960] is applicable to foam flow in pipes and correctly describes the transition from laminar to turbulent flow at Reynolds numbers between 2000 and 2500. Constructing a velocity-dependent flow-regime map, which consists of stratified flow, slug flow, plug flow, and annular-mist flow, is also investigated [Guzman et al., 2005] to find that the outcome is qualitatively in agreement with the flow regime map reported by Taiter and Dukler [1976] but the exact location of transition from one regime to another deviates. Laboratory-measured mean bubble size and bubble size distribution should be monitored during data interpretation as shown by Raza and Marsden [1967] and Becher [1965].

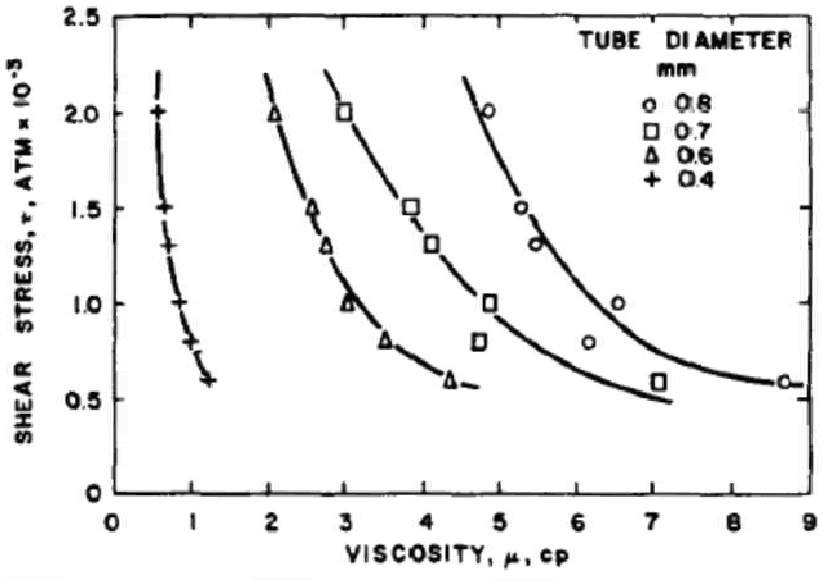

(a) Foam quality between 81 % and 89 %

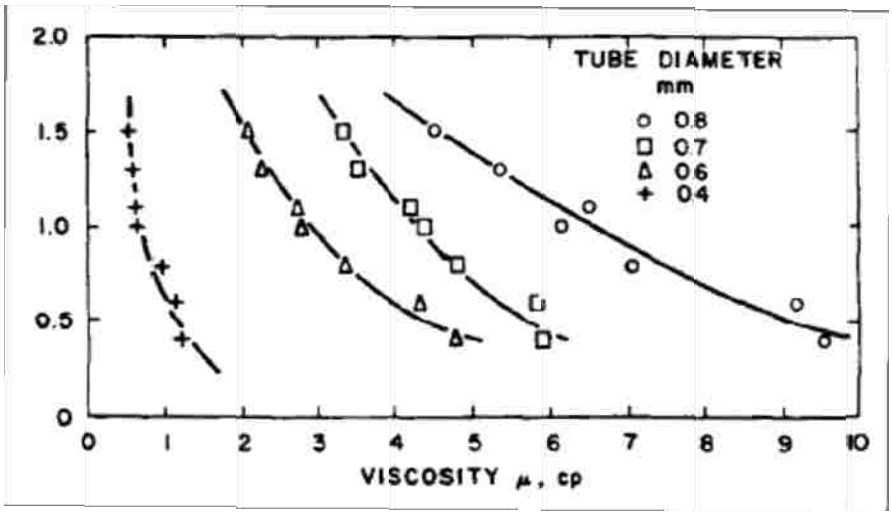

(b) Foam quality between 90 % and 96 %

Fig. 2.5. The change in foam viscosity (x axis) as a function of shear stress (y axis) at different tube diameters: foams behave as shear-thinning [from David and Marsden, 1969], x-axes are apparent viscosity in cp and y-axes are shear stress in ATM ^{x} 10^{-5}.

2.4. Two Flow Regimes of Foam in Porous Media

One use of foams in the petroleum industry is in foam-assisted improved and enhanced oil recovery applications in which bubbles are placed in a tiny pore structure [Schramm, 1994]. The flow mechanisms in porous media are different from flow mechanisms in pipes in that

capillary pressure plays significant and dominant roles in the way fluids are distributed and the way different phases interact with each other [Rossen, 1996]. Capillary pressure also influences flow rheology of foams in porous media by affecting the stability of foam films.

Laboratory flow experiments show that foam has three different states in porous media [Gauglitz et al., 2002]: fine-textured foams with a significant reduction in gas mobility, coarse-textured foams with a slight reduction in gas mobility, and foams with a moderate reduction in gas mobility. They are also referred to as strong foam state, weak foam state, and intermediate state. Similar to foam rheology in pipes, these three states are characterized by foam texture resulting from complicated interactions between gas and liquid phases in a complicated pore network [Kam and Rossen, 2003].

A number of studies put an emphasis on the rheology of strong foams in order to identify how gas viscosity is affected by a wide range of experimental conditions including surfactant formulations, surfactant concentrations, porosity and permeability of the medium, wettability of solids, and so on. Osterloh and Jante's study [1992] was the first to plot the measured steady-state pressure drop during strong foam flow in porous media in a form of pressure contours as a function of gas and liquid injection velocities, as shown in Fig. 2.6.

The experimental data during co-injection of nitrogen gas and surfactant solutions into a 2-ft long sandpack show that the pressure contours are vertical in the upper and left-hand side of the plot while the pressure contours are horizontal in the lower and right-hand side of the plot. The presence of two flow regimes of strong foam in porous media was further studied comprehensively by Alvarez et al. [2001] using a wide range of experimental conditions including different surfactant formulations, surfactant concentrations, rock types (Berea sandstone, glass bead pack and sand pack), permeabilities, and backpressures. As shown in Fig. 2.7, their results are very similar to those in Osterloh and Jante's study [1992]. Many other

studies also support the presence of two steady-state strong-foam regimes [Mamun et al., 2002; Rong, 2002; Kim et al., 2005; Kam et al., 2007a; Kam et al., 2007b].

These two flow regimes are known to be governed by two different mechanisms [Alvarez et al. 2001; Kam and Rossen, 2003; Dholkawala et al., 2007]. The regime in which the pressure contours are vertical, which is called "high-quality regime" (i.e., high quality meaning relatively higher gas fraction), is dominated by the bubble coalescence mechanism [Khatib et al., 1988, Aronson et al., 1994, Kidodeaux, 1997]. The other regime in which the pressure contours are horizontal is dominated by bubble trapping and mobilization in porous media [Rossen and Wang, 1999; Kam et al., 2007b]. The high-quality regime is characterized by an unstable foam flow near a limiting capillary pressure and the low-quality regime is characterized by a stable flow of bubbles at low capillary pressure.

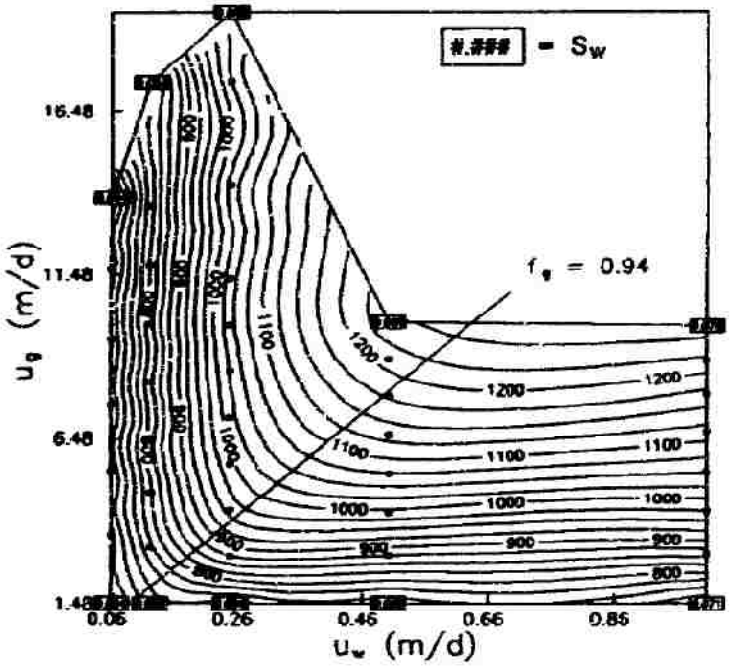

Fig. 2.6. Steady-state pressure contours during foam flow in a 2-ft long sandpack [from Osterloh and Jante, 1992]: There exist two different flow regimes in which foam behaves quite distinctly.

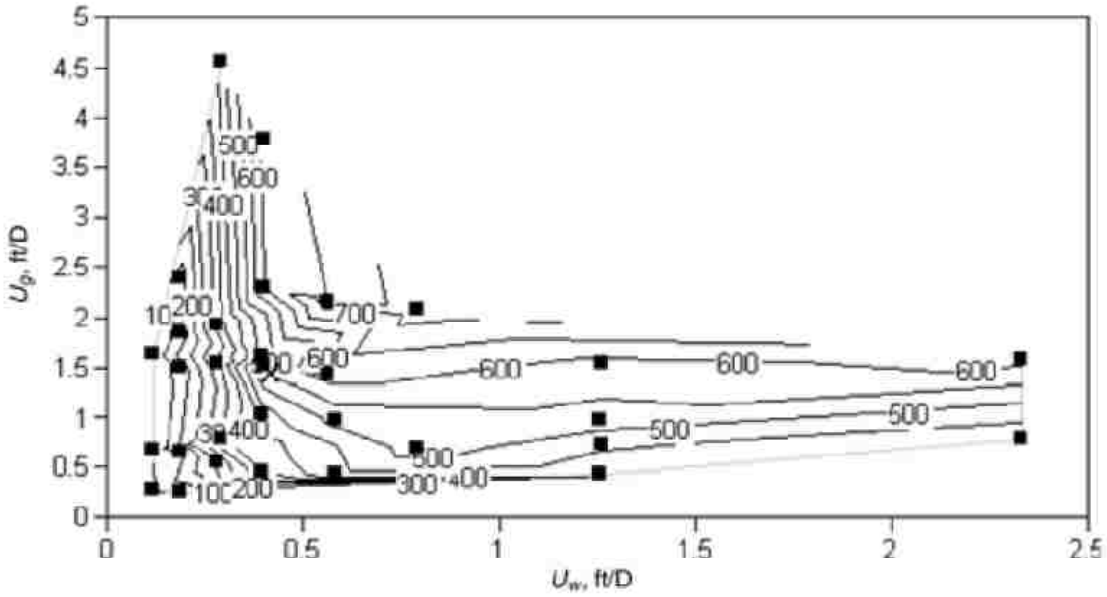

Fig. 2.7. Steady-state pressure-gradient contours during foam flow in 530-md Berea sandstone [from Alvarez et al., 2001]: the presence of two flow regimes are identified in a wide range of experimental conditions.

3. PROCEDURE AND METHODOLOGY

This chapter outlines how foam flow experiments were conducted to measure and analyze foam rheology in pipes: the first section details the experimental design and materials used, and the second section presents data interpretation and processing techniques.

3.1. Experimental Materials and Setup

A schematic of the laboratory setup used in this study is shown in Fig. 3.1.

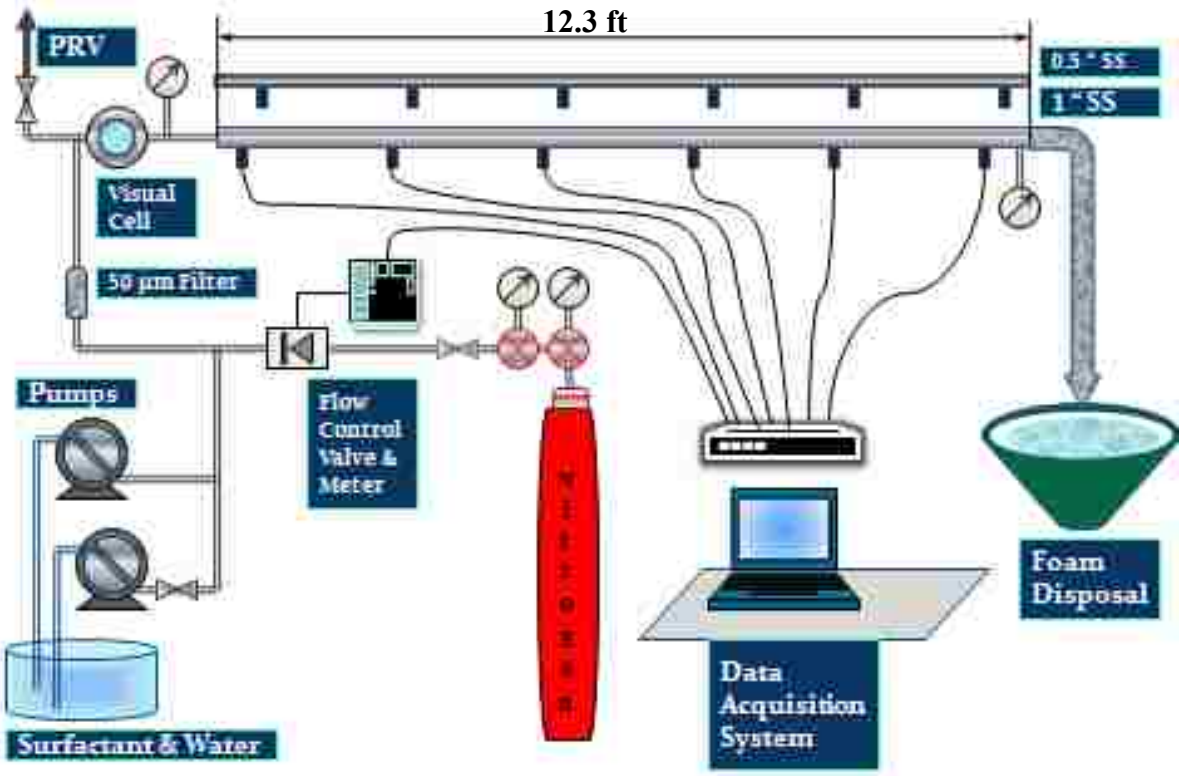

Fig. 3.1. A schematic of experimental setup for foam flow in pipe used in this study

The experiments were conducted by injecting gas and surfactant solutions simultaneously into a filter with either 50 µm or 90 µm opening size to generate fine-textured foams at the upstream end of the pipe section. The fine-textured foams flowed through a visual cell, and then into the pipe which was positioned in a horizontal direction. The pipe had multiple pressure ports

which allowed the sectional pressure drops to be measured along the pipe. The visual cell installed at the inlet permitted a direct observation of bubble size or foam texture. The pressure ports were connected to pressure transducers, and the pressure signals transmitted into the pressure transducers were collected and recorded in a computer on a real-time basis. Figs. 3.2 through 3.5 show photos of actual laboratory equipment used in this study.

Fig. 3.2. Experimental setup

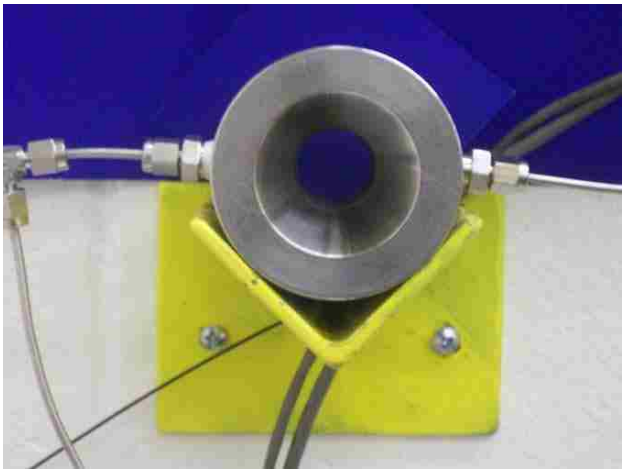

Fig. 3.3. Visual cell

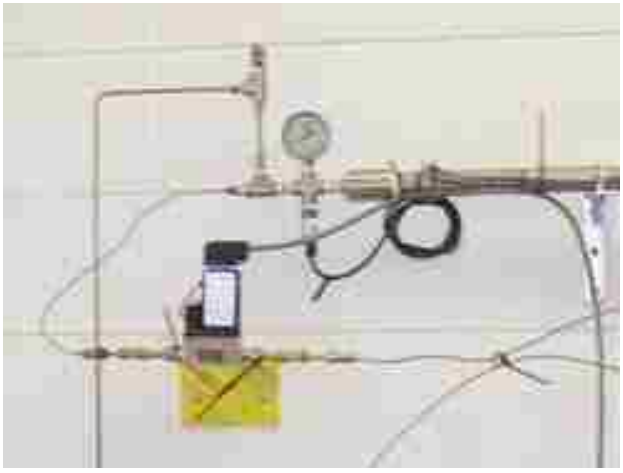

Fig. 3.4. Pipe inlet with upstream foam generator and gas flow meter

Fig. 3.5. Pressure transducers

Five different surfactants, four of which are commonly used in the petroleum industy and one of which is popular in our daily activities of washing and cleaning, were used as a foamer in

the experiments: CEDEPAL F-406, Petrostep CG-50, and Stepanform 1050 (all from STEPAN Co., Northfield, IL), Aquet TD-600 (Baker-Petrolite, Sugar Land, TX), and Ultra-Palmolive (Colgate-Palmolive Company, NY). All of these are anionic surfactants. CEDEPAL FA-406, Petrostep CG-50, Stepanform 1050, and Aquet TD-600 are surfactants actively used in drilling and completion processes in the petroleum industry. CEDEPAL FA-406 was selected as the base-case surfactant because foam stability experiments with test tubes showed that CEDEPAL FA-406 created fine-textured foams more easily and the foam formed by CEDEPAL FA-406 exhibited better stability compared to other surfactants at the same concentration. Many experiments were performed at different surfactant concentrations by adding surfactant delivered from the manufacturers into distilled and de-ionized water. The surfactant concentration was reported in weight percent, wt %.

A fixed rate of the gas phase was injected by a Brooks Mass Flow Controller 5850E (Brooks Instruments, PA), and the flow rate was regulated by a Brooks Microprocessor Control & Readout Unit 0152 (Brooks Instrument, PA). Nitrogen was used as the gas phase in all experiments and the range of flow rates was varied from 0 to 5000 Sccm (standard cubic centimeters per minute). The surfactant solution was injected by a high-accuracy positive-displacement Optos 3HM Pump (Eldex, CA) which has the rate range of 0.04 to 80 cc/min.

Two different sizes of pipes were used: 0.5 inch and 1 inch NPS (Nominal Pipe Size) stainless steel pipes, with 0.36 inch and 0.957 inch ID, respectively. Pressure ports with an opening size of 0.125 inch ID were drilled and positioned along the stainless steel pipes, instead of tee-joints, in order to minimize possible disturbance during the flow. The 1 inch pipe was about 12 ft long, while the 0.5 inch pipe was about 12.3 ft long. The pipes consisted of seven segments with eight pressure ports, named from pressure port A through H. They are equally spaced (approximately 1.7 ft apart for the 0.5 inch NPS pipe and 1.72 ft apart for the 1 inch NPS

pipe), port A being installed just before the inlet and port H being installed just after the outlet. Because the inlet and outlet tubing was 0.5 inch NPS, the pressure measurements in the first and last ports (ports A and H) in the 1 inch pipe experiments were not included in the analysis because of the inlet and outlet effect.

Pressure was measured by Omega Voltage Pressure Transducers (Omega Engineering Inc., CT), with the pressure range of 30, 100, and 500 psia. They provided good precision, with possible error within 0.02% of the maximum pressure range. These pressure transducers were calibrated with a Dead Weight Tester (Refinery Supply Company, Inc., Tulsa, OK) from time to time throughout the experiments to ensure the accuracy of pressure measurements. A DIN-113 5V Input/RS-485 Output pressure demodulator (Omega Engineering Inc., CT) was used for signal processing. The data were collected and processed by an in-house data acquisition system built in Excel. Each pressure signal from the pressure transducer was collected at a time interval of about 5 seconds. Figs. 3.6 through 3.11 show additional items of equipment described in this section.

Fig. 3.6. Brooks microprocessor flow control unit

Fig. 3.7. Positive displacement Optos pumps

Fig. 3.8. Dead weight tester

Fig. 3.9. 0.5 and 1 inch stainless steel pipes

Fig. 3.10. 0.5 and 1 inch pipe outlets

Fig. 3.11. Foam disposal

3.2. Experimental Procedure and Data Processing

This study carried out nearly 500 sets of experiments grouped into 14 experimental cases in order to obtain the steady-state pressure responses at different experimental conditions. Table 3.1 shows a summary of 14 different cases of experiments.

At given experimental conditions (Case 1 through Case 14), a series of experiments was conducted at varying gas and liquid injection velocities in order to measure the steady-state pressure drops between the pressure ports. Once the system reached a steady state by showing stable pressure responses, a new combination of gas and liquid injection rates was imposed.

Occasionally the same sets of gas and liquid injection rates were repeated so as to check reproducibility of pressure measurements. In all cases tested, the experimental results were repeatable. Table 3.2 and 3.3 show different combinations of gas and liquid injection rates used in 1 inch NPS and 0.5 inch NPS stainless steel pipes, respectively.

Table 3.1. A brief summary of all 14 experimental cases conducted in this study

Exp. Case	Pipe Size [inch]	Filter Size [μm]	Surfactant Concentration [wt%]	Surfactant Type
1	0.5	50	1%	Cedepal FA-406
2	0.5	50	5%	Cedepal FA-406
3	0.5	50	0.1%	Cedepal FA-406
4	0.5	90	1%	Cedepal FA-406
5	0.5	90	5%	Cedepal FA-406
6	0.5	90	0.1%	Cedepal FA-406
7	0.5	50	1%	Petrostep CG-50
8	0.5	50	1%	Stepanform 1050
9	0.5	50	1%	Aquet TD-600
10	0.5	50	1%	Ultra-Palmolive
11	1	50	1%	Cedepal FA-406
12	1	50	5%	Cedepal FA-406
13	0.5	50	1%	Cedepal FA-406
14	0.5	n/a	1%	Cedepal FA-406
Case 1 - Base Case			Cases 13 & 14 at fixed foam quality of 98.425 %	

Table 3.2. Different combinations of gas and liquid injection rates in 1 inch NPS, (0.957 inch ID stainless steel pipe) (cf. Cases 11 and 12 as shown in Table 3.1)

Pressure Drop or Pressure Gradient		Gas Flow Rate [Scc/min]				
		1000	2000	3000	4000	5000
Liquid Flow Rate ml/min	20	x	x	x	x	x
	40	x	x	x	x	x
	60	x	x	x	x	x
	80	x	x	x	x	x

(1000 cc/min is equivalent to 0.036 m/s or 0.178 ft/sec)

Table 3.3. Different combinations of gas and liquid injection rates in 0.5 inch NPS, (0.36 inch ID pipe) (cf. Cases 1 through 10 as shown in Table 3.1)

Pressure Drop or Pressure Gradient		Gas Flow Rate [Scc/min]					
		500	1000	2000	3000	4000	5000
Liquid Flow Rate ml/min	20	x	x	x	x	x	x
	40	x	x	x	x	x	x
	60	x	x	x	x	x	x
	80	x	x	x	x	x	x

(1000 cc/min is equivalent to 0.254 m/s or 0.83 ft/s)

Variables reported in this study are defined as follows: foam quality (f_g) is a function of the volumetric flow rates of the gas and liquid phases

$$f_g = \frac{q_{gas}}{q_{gas} + q_{liq}}, \qquad \text{..... (3.1)}$$

where q_{gas} and q_{liq} represent volumetric flow rates of gas and liquid, respectively. The values for f_g in this study ranged from 86 % to 99.6 %.

The reported pressure values are time averaged once the system is believed to be in the steady state. Therefore, the pressure at location i (P_i) can be calculated by

$$P_i = \frac{\sum_{n=1}^{N} P_n}{N} \qquad \text{..... (3.2)}$$

where, N is the number of the data points used for this calculation. The pressure drop between any two of pressure ports i and j can then be expressed by

$$\Delta P_{ij} = P_i - P_j \qquad \text{..... (3.3)}$$

where, ΔP_{ij} is the pressure drop between the two pressure ports i and j, and P_i and P_j represent the time-averaged value of pressure at pressure ports i and j, respectively. Note that ΔP_{ij} is always greater than zero if the port i is positioned further upstream compared to the port j. It is sometimes convenient to report the results in terms of the pressure gradient (dP/dL) rather than

the absolute pressure value, which is

$$\frac{dP}{dL} = \frac{\Delta P_{ij}}{\Delta L_{ij}} = \frac{P_i - P_j}{\Delta L_{ij}} \qquad \text{,……..……} \quad (3.4)$$

where, ΔL_{ij} is the distance between the two pressure ports i and j.

For 1 inch NPS diameter pipe, the average system pressure (P_{avg}) is defined by the average pressure values between the second (port B) and second last (port G) pressure ports, P_B and P_G respectively, to avoid interference from the inlet and outlet of the pipe, because the inlet and outlet tubing was 0.5 inch. Therefore,

$$P_{avg} = \frac{P_B + P_G}{2} \qquad \text{,……..……} \quad (3.5a)$$

while for 0.5 inch NPS pipe, the average system pressure (P_{avg}) is defined by the average pressure values between the inlet (port A) and outlet (port H) ports. Therefore

$$P_{avg} = \frac{P_A + P_H}{2} \qquad \text{,……..……} \quad (3.5b)$$

Using the ideal gas law, the average gas flow rate (q_{gas}) can be determined by correcting the gas flow rate measured at standard condition ($q_{gas,sc}$)

$$q_{gas} = \frac{P_{sc} q_{gas,sc}}{P_{avg}} \qquad \text{,……..……} \quad (3.6)$$

Note that the standard pressure (P_{sc}) was 14.7 psia and room temperature (T) was about 70 ºF throughout the experiments. The compressibility factor (or, Z factor) does not change significantly within the range of pressure variations observed in this study. One can use gas and liquid velocities rather than flow rates as shown below:

$$u_{gas} = \frac{q_{gas}}{A} \quad \text{and} \qquad \text{,……..……} \quad (3.7)$$

$$u_{liq} = \frac{q_{liq}}{A} \qquad ,\ldots\ldots (3.7)$$

where u_{gas} and u_{liq} are superficial velocities of gas and liquid phases, respectively, and A represents the cross-sectional area of the pipe given by

$$A = \frac{\pi\ d^2}{4} \qquad ,\ldots\ldots (3.8)$$

where d is the inner diameter of the pipe.

Previous studies show that foam can be approximated by shear-thickening, shear-thinning, or Newtonian fluid. Fig. 3.12 shows the behavior of near-Newtonian fluid (α = 1), shear-thickening fluid (α > 1), and shear-thinning fluid (α < 1) using the pressure drops and corresponding flow rates.

The power-law exponent, α, has been estimated by analyzing pressure drops and corresponding superficial gas and liquid velocities by using

$$\frac{\Delta P_2}{\Delta P_1} = \left(\frac{q_2}{q_1}\right)^{\alpha} \qquad ,\ldots\ldots (3.9)$$

which can be written as follows:

$$\alpha = \frac{\ln\left(\frac{\Delta P_2}{\Delta P_1}\right)}{\ln\left(\frac{q_2}{q_1}\right)} \qquad ,\ldots\ldots (3.10)$$

Figure 3.13 graphically shows how to determine α from the steady-state pressure drops as a function of superficial gas and liquid velocities. Derivation of Eqs. (3.9) and (3.10) is shown in Appendix B. It should be noted that, as proved in Appendix B, all experimental conditions in this study correspond to laminar flow reaching Reynolds number well below 400 to 500 due to the increase in foam viscosity.

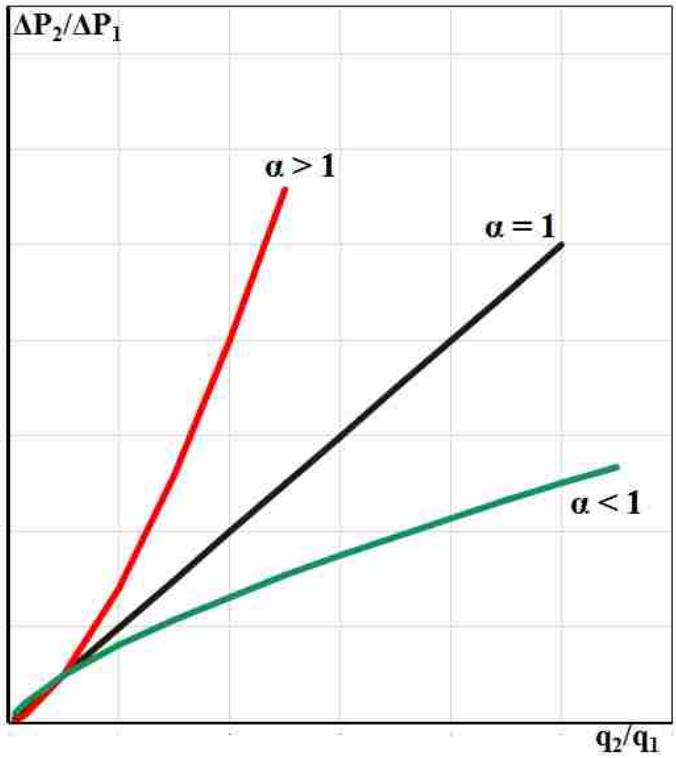

Fig. 3.12. A schematic of Newtonian fluid (α=1), shear-thinning (α<1), and shear-thickening fluid (α>1).

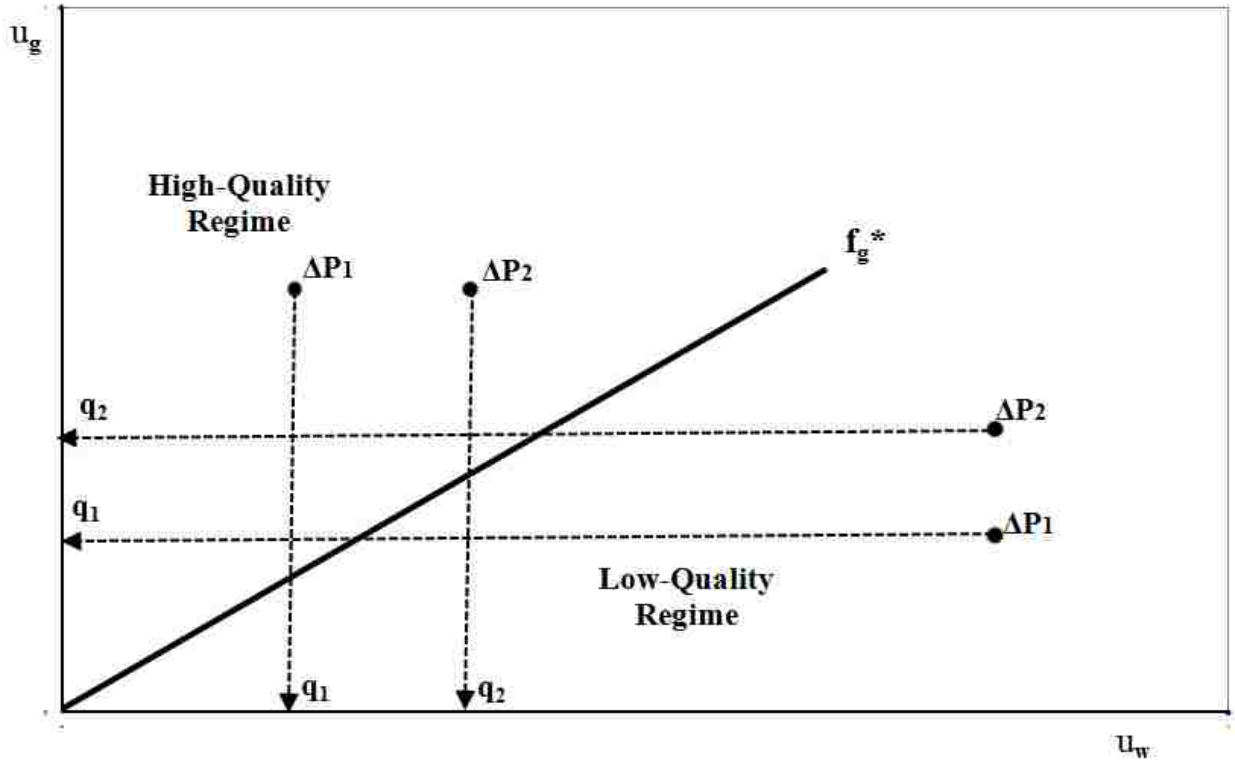

Fig. 3.13. Determination of power-law exponent (α)

4. RESULTS AND DISCUSSIONS

4.1. Introduction

This chapter describes the results of foam experiments over a wide range of gas and liquid injection rates at different test conditions. These include different pipe diameters, surfactant formulations, surfactant concentrations, and opening sizes of filters (used as foam generators). The foam quality, f_g, in most of the experiments is relatively high, ranging from 86.0 % to 99.6%.

A total of 14 different cases of flow experiments are of interest in this study. They are referred to as Case 1 through Case 14 (cf. Table 3.1). Further details of these 14 cases are outlined as follows:

Case 1: co-injection of nitrogen and 1 wt% of Cedepal FA-406 surfactant solution; use of 50μm opening size filter as a foam generator; 0.5 inch NPS stainless steel pipe (Base Case)

Case 2: 5 wt% of Cedepal FA-406 surfactant solution rather than 1 wt% of Cedepal FA-406 surfactant solution; other conditions are the same as those in the base case

Case 3: 0.1 wt% of Cedepal FA-406 surfactant solution rather than 1 wt% of Cedepal FA-406 surfactant solution; other conditions are the same as those in the base case

Case 4: 90μm opening size filter rather than 50μm opening size filter; other conditions are the same as those in the base case

Case 5: 5 wt% of Cedepal FA-406 surfactant solution rather than 1 wt% of Cedepal FA-406 surfactant solution; other conditions are the same as those in Case 4

Case 6: 0.1 wt% of Cedepal FA-406 surfactant solution rather than 1 wt% of Cedepal FA-406 surfactant solution; other conditions are the same as those in Case 4

Case 7: 1 wt% of Petrostep CG-50 surfactant solution rather than 1 wt% of Cedepal FA-406 surfactant solution; other conditions are the same as those in the base case

Case 8: 1 wt% of Stepanform 1050 surfactant solution rather than 1 wt% of Cedepal FA-406 surfactant solution; other conditions are the same as those in the base case

Case 9: 1 wt% of Aquet TD-600 surfactant solution rather than 1 wt% of Cedepal FA-406 surfactant solution; other conditions are the same as those in the base case

Case 10: 1 wt% of Ultra Palmolive surfactant solution rather than 1 wt% of Cedepal FA-406 surfactant solution; other conditions are the same as those in the base case

Case 11: 1 inch NPS stainless steel pipe rather than 0.5 inch stainless steel pipe; other conditions are the same as those in the base case

Case 12: 5 wt% of Cedepal FA-406 surfactant solution rather than 1 wt% of Cedepal FA-406 surfactant solution; other conditions are the same as those in Case 11

Case 13: co-injection of gas and surfactant solution at varying total injection velocities keeping foam quality constant (foam first created by the upstream 50μm opening size filter then bypassing the filter); experimental conditions are the same as those in the base case

Case 14: repetition of Case 13 in the absence of the upstream filter at two different concentrations (1 wt% (Case 14a) and 0.5 wt% (Case 14b)) of Cedepal FA-406.

Experimental results from these tests are provided in the sections below, followed by discussions and implications. In addition, the experimental data and pressure drop values for the first twelve cases are included in Appendix A.

4.2. Base Case (Case 1)

The base case consists of 24 different combinations of gas and liquid injection velocities (cf. Table 3.2), with foam quality varying from 86.2 % to 99.6 % step by step. Some of the experimental results are shown in Figs. 4.1, 4.2, and 4.3 in which both gas and liquid flow rates, in cc/min, are specified in a box on the top of the corresponding pressure data. In most of the experiments, it took less than a few minutes for the system to reach a steady state. The flow

injection was continued for another five to ten minutes in order to guarantee the steady-state pressure values and to minimize measurement errors. The pressure values were collected once every 5 seconds normally.

Fig. 4.1 shows one example experimental output with pressures at eight different locations (pressure ports A through H) as a function of time. The pressure response from port C is neglected because its behavior does not match well with the responses from other ports even after multiple calibration attempts. Fig. 4.1 shows an interesting pattern which depends on foam quality: (1) when foam quality is relatively high (i.e., relatively dry foam) at the time between 2200 and 3600 seconds (x axis), the measured pressure values fluctuate in all pressure ports; and (2) when foam quality is relatively low (i.e., relatively wet foam) at the time other than between 2200 and 3600 seconds, the measured pressure values are rather stable. As further described in the following sections, this study refers to the former as the typical response of the "high-quality regime" in which the system is governed by unstable fluctuation in its intrinsic nature, while the later as the typical response of the "low-quality regime" in which the system is governed by a stable system behavior.

Figs. 4.2 and 4.3 show additional results at the same experimental conditions: one with increasing liquid injection rate at fixed gas injection rate and the other with increasing gas injection rate at fixed liquid injection rate, respectively. It is observed that the pressure data respond differently to the stepwise change in injection rates – the steady-state pressure drop decreases with increasing liquid injection rate (cf. Fig. 4.2) but the steady-state pressure drop increases with increasing gas injection rate (cf. Fig. 4.3). Fig. 4.2 provides another important insight into the transition between the high-quality regime and the low-quality regime. There is a threshold value of foam quality above which the pressure response starts to fluctuate, moving into the high-quality regime.

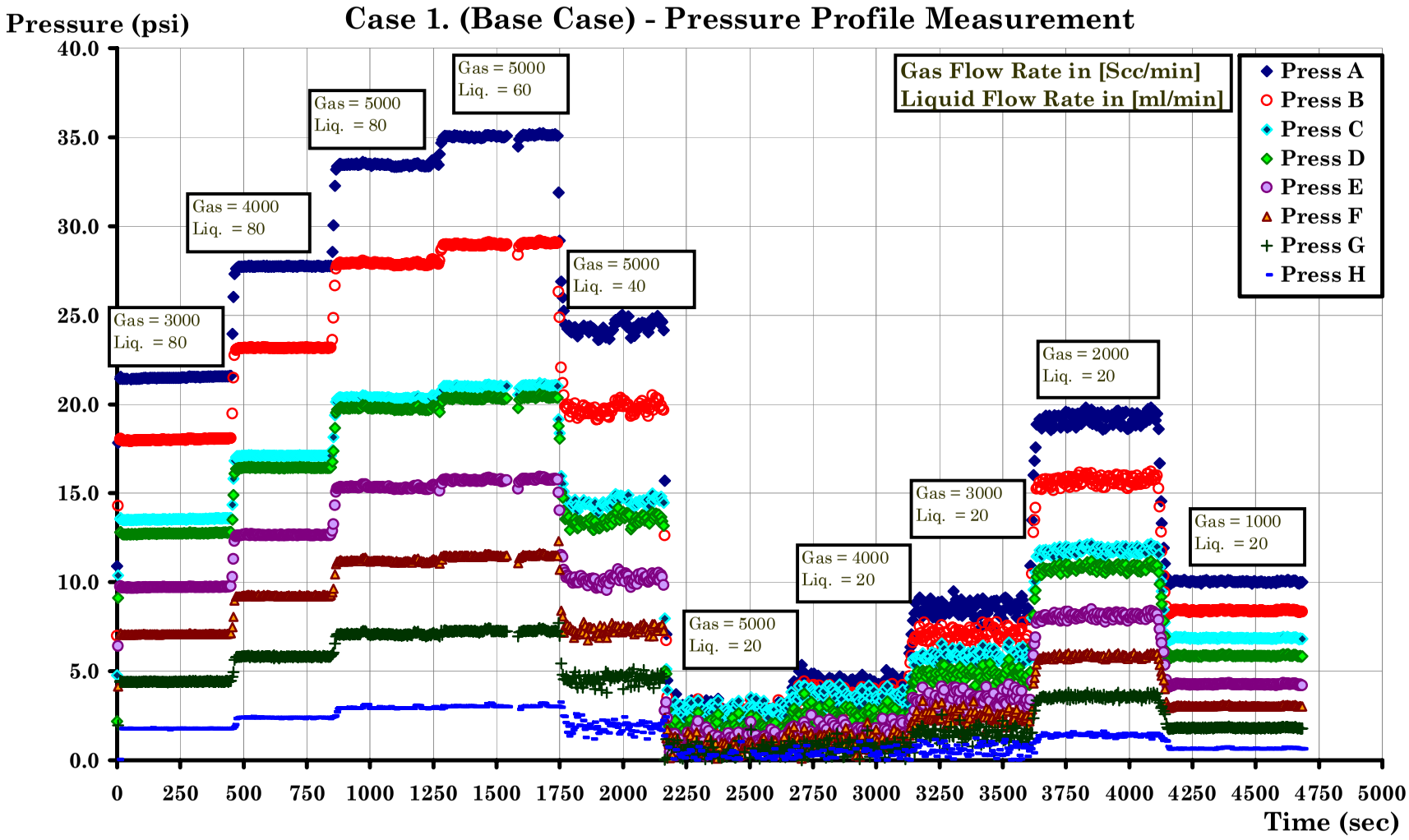

Fig. 4.1. Pressure response as a function of time with a stepwise change in gas and liquid injection rates (Case 1; base case): (0.5 inch NPS stainless steel pipe, 1 wt% surfactant concentration using Cedepal FA -406, 50 µm filter opening size)

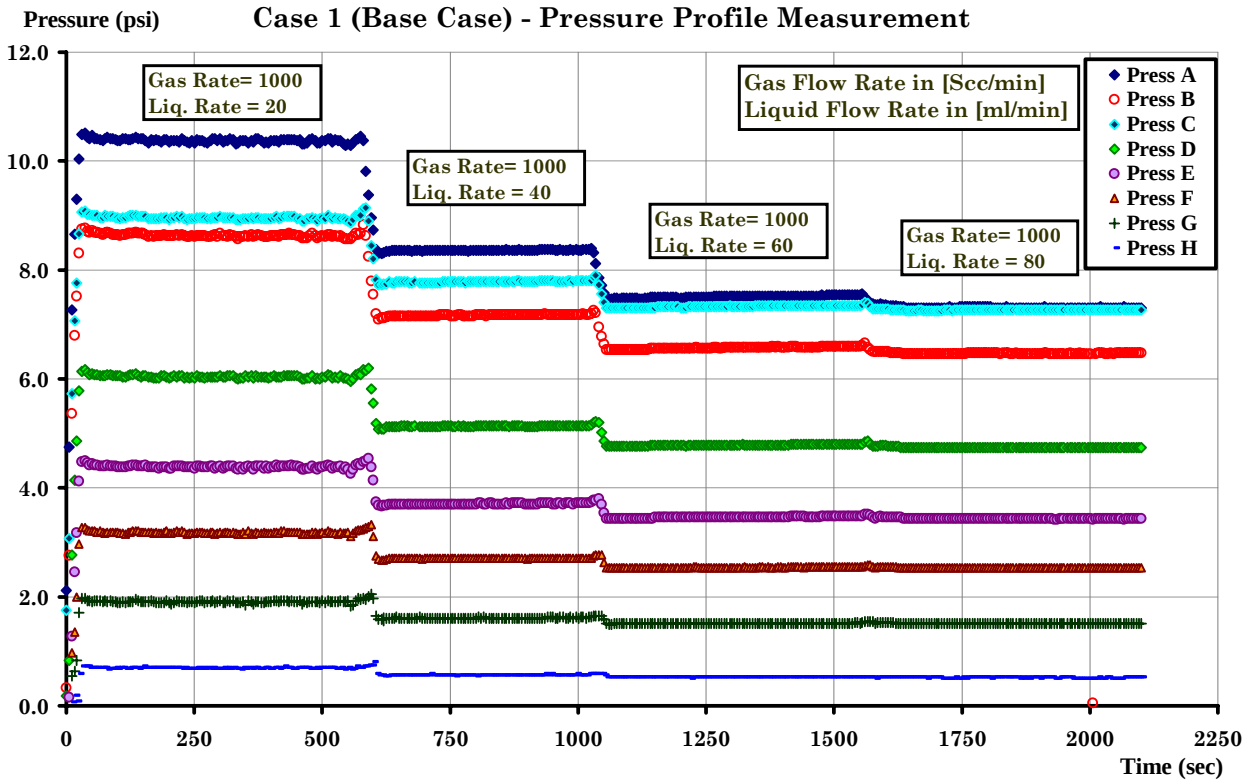

Fig. 4.2. Pressure response as a function of time with a stepwise change in gas and liquid injection rates, continued (Case 1; also base case): (0.5 inch NPS stainless steel pipe, 1 wt% surfactant concentration using Cedepal FA -406, 50 μm filter opening size)

For example, the pressure data are relatively smooth and stable at liquid injection rates of 40, 60, and 80 cc/min while the pressure data look oscillating at liquid injection rate of 20 cc/min. Although not shown here, similar experiments that repeat those in Fig. 4.2 exhibit the same behavior consistently, indicating the presence of the threshold foam quality that separates the two regimes. Subsequent experiments varying gas injection rate at fixed liquid injection rate also show the presence of a threshold foam quality. The importance and implication of this behavior is further discussed in the following sections.

The pressure data obtained from Figs. 4.1 through 4.3 can be plotted in a two-dimensional space with superficial liquid velocity on the x-axis and superficial gas velocity on the y-axis, as shown in Fig. 4.4. Note that the gas injection velocities in the plot are adjusted at

the average pressure in the system after considering gas compressibility. Each point in the plot has corresponding gas and liquid injection velocities, and the measured pressure drop between the pressure ports A and H (P_A-P_H) is specified in psi. Two pressure contours with the pressure drops of 7 psi and 22 psi are delineated based on the steady-state pressure-drop measurements.

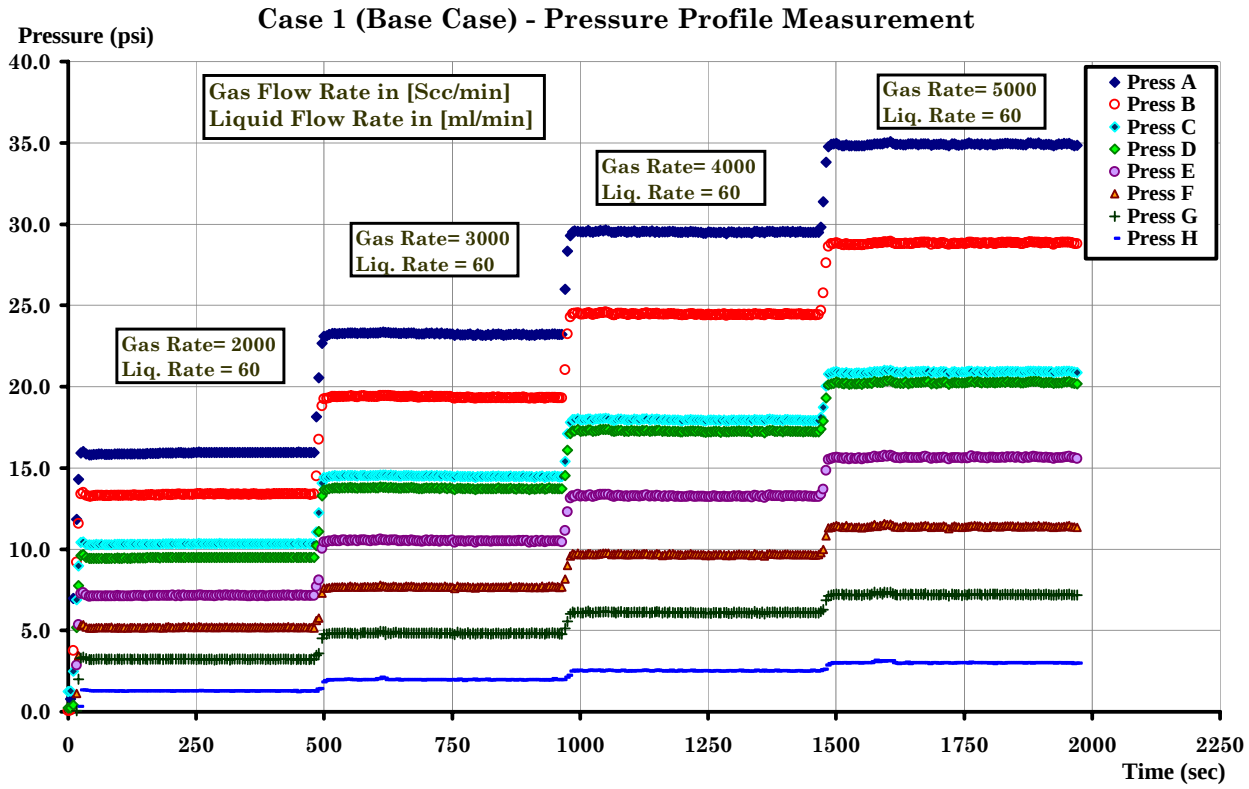

Fig. 4.3. Pressure response as a function of time with a stepwise change in gas and liquid injection rates, continued (Case 1; also base case): (0.5 inch NPS stainless steel pipe, 1 wt% surfactant concentration using Cedepal FA -406, 50 µm filter opening size)

Fig. 4.4 demonstrates a few important features of foam flow in pipe. First, the whole two-dimensional domain can be separated into two parts by a straight line that represents the threshold foam quality (f_g*). The upper and left-hand side is called high-quality regime and the lower and right-hand side is called low-quality regime. The value of f_g* in the base case is shown to be relatively high, about 99%, but this value can vary depending on many experimental

conditions as shown in later sections. Second, the slope of the pressure contour in the high-quality regime is much higher than that in the low-quality regime. The almost horizontal pressure contours (or, the pressure contours with gentle slope) in the low-quality regime imply that the steady-state pressure drop is primarily determined by gas injection velocity, being relatively insensitive to liquid injection velocity. The pressure contours in the high-quality regime imply that the steady-state pressure drop is strongly affected by both gas and liquid injection velocities. Third, if an experiment were carried out by increasing gas injection velocity at fixed liquid injection velocity (i.e., following an imaginary vertical line in Fig. 4.4), the pressure drop would increase with gas injection velocity until it reaches a maximum, and then the pressure drop would decrease with gas injection velocity. If an experiment were carried out such that the liquid injection velocity was increased at fixed gas injection velocity (i.e., following an imaginary horizontal line in Fig. 4.4), the pressure drop would increase with liquid injection velocity until it reaches a maximum, and then the pressure drop would stay almost at the same level or decrease very gradually with further increase in gas injection velocity. Last, the contours indicate that both "foam rheology to the liquid injection velocity" in the high-quality regime and "foam rheology to the gas injection velocity" in the low-quality regime are slightly shear thickening with the power-law exponent of around 1.5 to 1.6. This means that doubling the injection rate roughly results in 2.83 to 3.03 times increase in pressure drop. (This study does not interpret "foam rheology to the gas injection velocity" in the high-quality regime because of very small pressure drops and "foam rheology to the liquid injection velocity" in the low-quality regime because of negligible pressure changes.)

In addition to different pressure contours, there are some other aspects that distinguish the two regimes. As pointed out in Fig. 4.1, the high-quality regime is characterized by an oscillating and unstable pressure response, while the low-quality regime is characterized by a stable

pressure response. These characteristics are consistent with the observations made at the outlet: a very fine-textured homogeneous mixture was observed for the low-quality regime foams, but a sequence of free gas and fine-textured foam slug was observed in the high-quality regime foams. This implies that there are two different mechanisms governing foam rheology in the high-quality and low-quality regimes. This is further discussed in later sections.

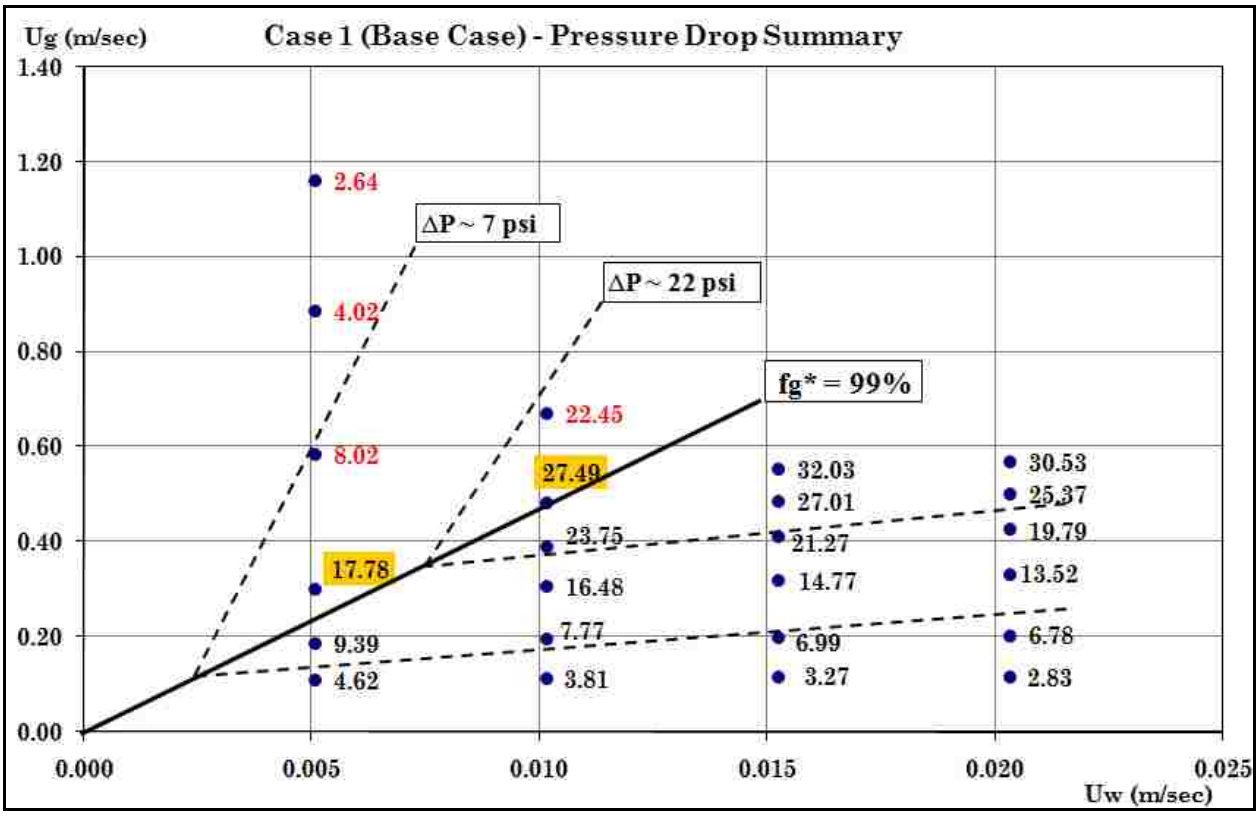

Fig. 4.4. Steady-state pressure drops, in psi, as a function of superficial gas and liquid injection velocities (Case 1; also base case): (0.5 inch NPS stainless steel pipe, 1 wt% surfactant concentration using Cedepal FA-406, 50 μm filter opening size)

It is also worthwhile to point out that the two values of pressure drops, “17.78” psi and “27.49” psi highlighted in Fig. 4.4, were the onset of unstable flow behavior during the experiments where the gas injection velocity was being increased at fixed liquid injection velocity. This implies that the transition from stable to unstable flow characteristics coincides

roughly with the f_g* that separates the two flow regimes based on the pressure contours. In addition, the two values of pressure drops are shown to be the maximum pressure drops along the vertical line (i.e., varying gas injection velocity at fixed liquid injection velocity), which implies that the maximum pressure drops are likely to happen near the transition from one regime to the other, or near f_g* equivalently. These concepts are shown to be consistent and true in all experiments as shown in the following sections.

The similar pressure response shown by the pressure contours (i.e., 7 psi and 22 psi) in Fig. 4.4 are observed consistently in all experiments. Therefore, it is believed that they represent the rheology of the steady-state foam flow in pipes within the experimental conditions covered in this study. The pressure contours, however, are not drawn in the figures below in order to avoid a biased interpretation.

4.3. Effect of Surfactant Concentration (Cases 1, 2, and 3)

Two other series of experiments are conducted in order to investigate the effect of surfactant concentrations. Experimental conditions are identical to those in Case 1 (i.e., the base case) except that the surfactant concentrations are 5 wt% and 0.1 wt% in Case 2 and Case 3, respectively.

Fig. 4.5 shows the pressure response of Case 2 with 5 wt% Cedepal FA-406 surfactant solution, which can be compared with Figs. 4.1 through 4.3. Unlike the base case, the pressure responses are relatively stable within the entire range of gas and liquid injection velocities tested. The steady-state pressure drops between ports A and H, as shown in Fig. 4.6, illustrate that the entire set of data points lie in the low-quality regime. This implies that the value of f_g* in this case is greater than 99.6%, the highest foam quality tested in the experiments.

Fig. 4.7 shows the pressure response of Case 3 with 0.1 wt% Cedepal FA-406 surfactant solution, which can be compared with Figs. 4.1 through 4.3 or Fig. 4.5.

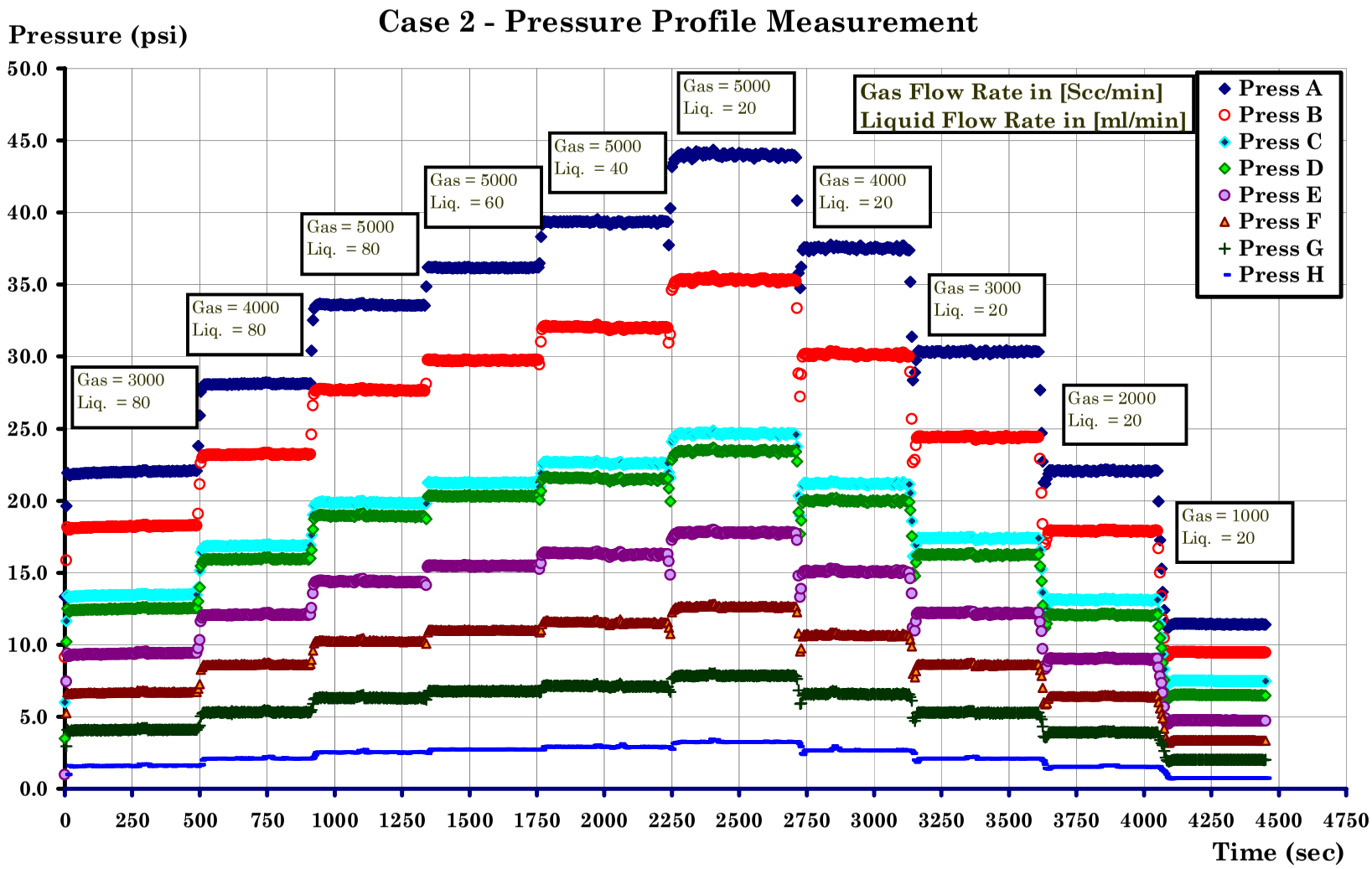

Fig. 4.5. Pressure response as a function of time with a stepwise change in gas and liquid injection rates (Case 2): (0.5 inch NPS stainless steel pipe, 5 wt% surfactant concentration using Cedepal FA -406, 50 µm filter opening size

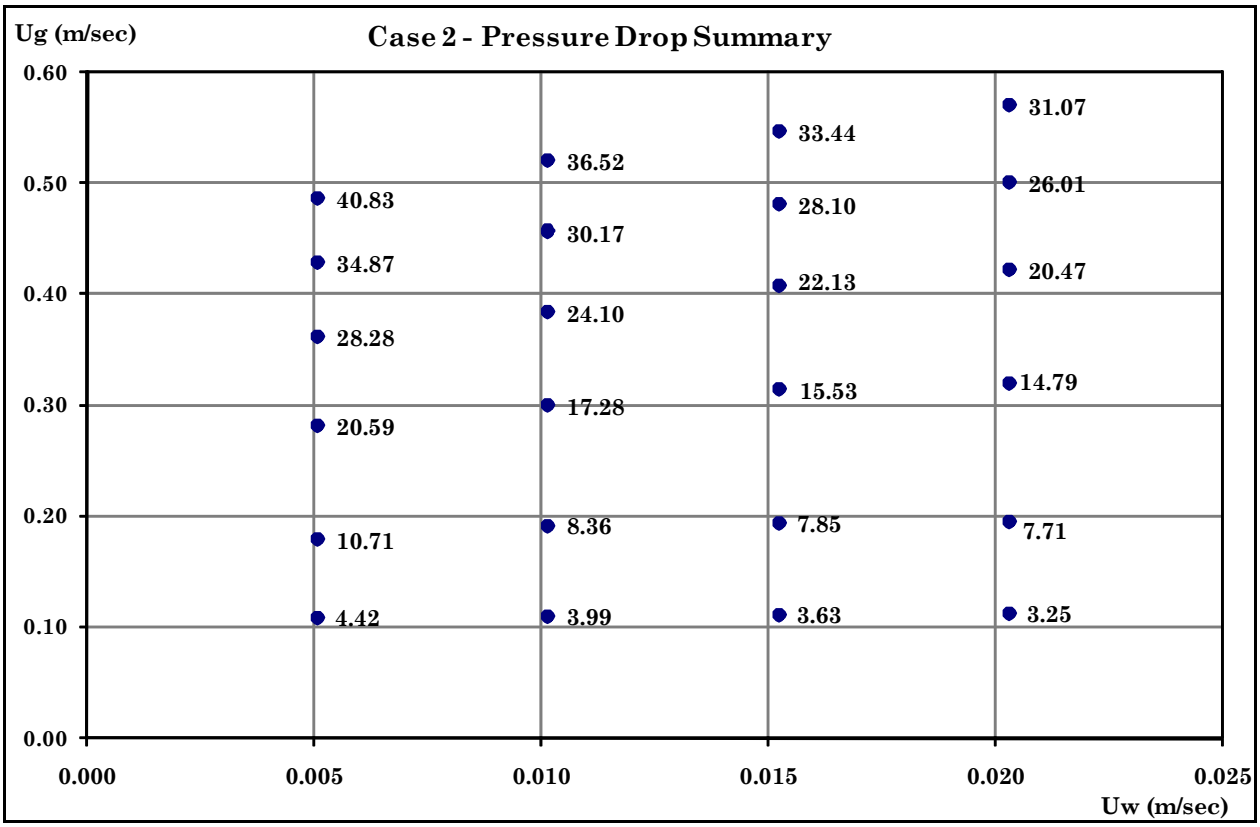

Fig. 4.6. Steady-state pressure drops, in psi, as a function of superficial gas and liquid injection velocities (Case 2): (0.5 inch NPS stainless steel pipe, 5 wt% surfactant concentration using Cedepal FA-406, 50 μm filter opening size)

In contrast to Case 2 (cf. Fig. 4.5), the pressure responses are relatively scattered in many combinations of gas and liquid injection velocities. The steady-state pressure drops in Fig. 4.8 show that the two-dimensional domain is separated by a much lower value of f_g*, around 92 to 93%, or possibly even lower than that.

Comparing Figs. 4.4, 4.6, and 4.8, it can be concluded that a decrease in surfactant concentration generally decreases the value of f_g*, spanning the region occupied by the high-quality regime. This is consistent with our intuition in that the reduction in surfactant concentration is likely to cause foams to be less stable, resulting in the stretch of unstable high-quality regime. This implies that a surfactant with poor foamability may tend to decrease the value of f_g* by the same token which is discussed in the later section.

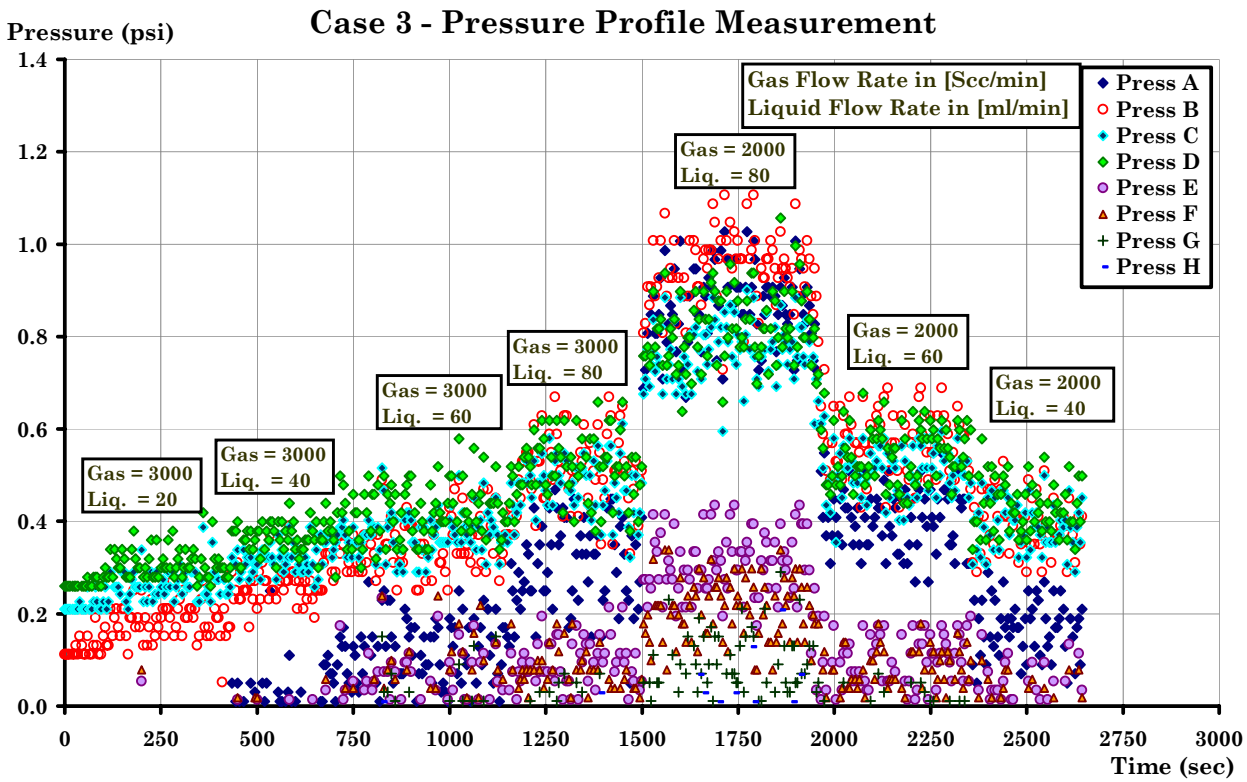

Fig. 4.7. Pressure response as a function of time with a stepwise change in gas and liquid injection rates (Case 3): (0.5 inch NPS stainless steel pipe, 0.1 wt% surfactant concentration using Cedepal FA -406, 50 µm filter opening size)

The foam flow rheology to the gas injection velocity in the low-quality regime in Case 2 (cf. Fig. 4.6) shows shear-thickening behavior with a power-law exponent of around 1.5 to 1.6, which is identical to that in the base case. The foam flow rheology to the liquid injection velocity in the high-quality regime in Case 3 (cf. Fig. 4.8) also shows shear thickening behavior but with much higher power-law exponent, ranging from 2.3 to 3.3. It should be noted again that this study does not interpret “foam rheology to the gas injection velocity” in the high-quality regime because of very small pressure drops and “foam rheology to the liquid injection velocity” in the low-quality regime because of negligible pressure changes.

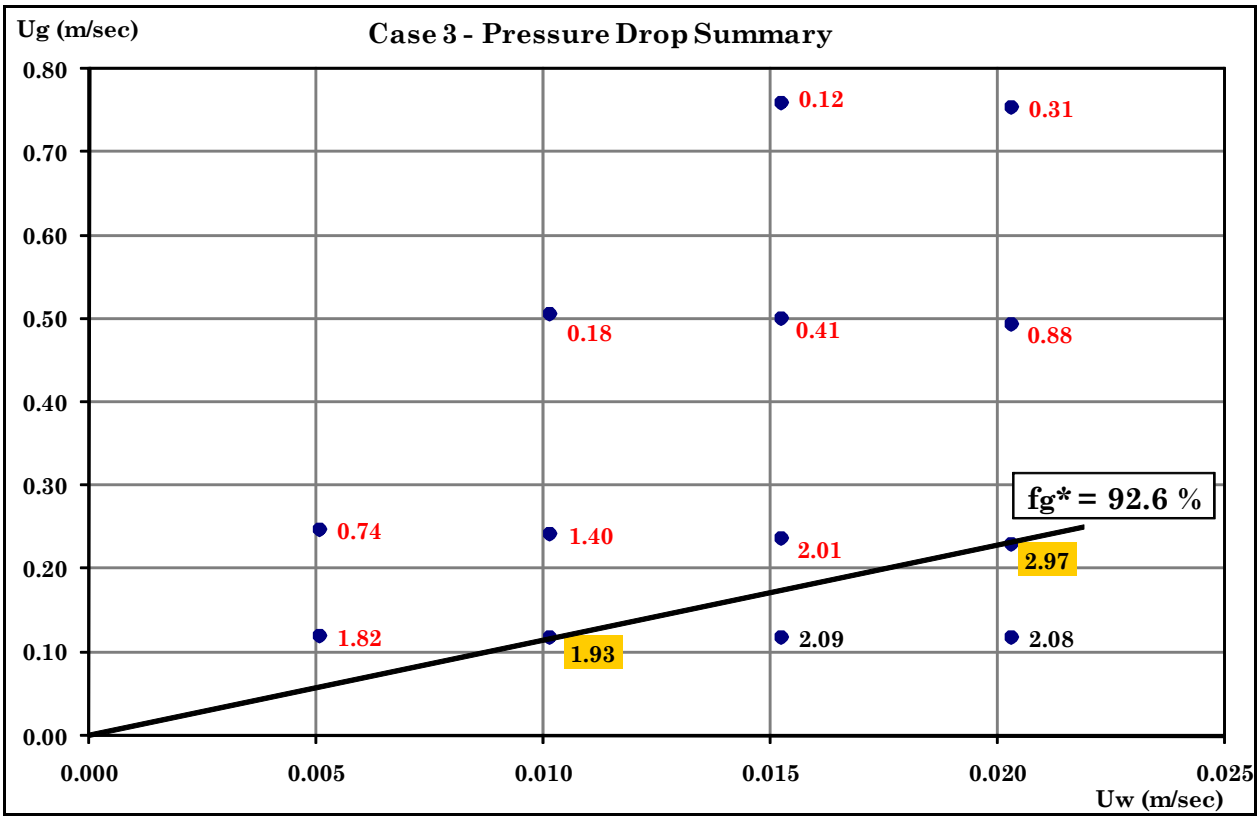

Fig. 4.8. Steady-state pressure drops, in psi, as a function of superficial gas and liquid injection velocities (Case 3): (0.5 inch NPS stainless steel pipe, 0.1 wt% surfactant concentration using Cedepal FA-406, 50 μm filter opening size)

4.4. Effect of Filter Opening Size (Cases 4, 5, and 6)

Further experiments were conducted in order to study the effect of filter opening size. Because a filter installed upstream of the pipe inlet serves as a foam generator, foam rheology in the pipe might be affected by the opening size. If the measured pressure responses are insensitive to the filter opening size, it implies that the fine-textured foam artificially created upstream coarsens and rearranges rapidly such that foam could reach its steady-state texture within the pipe quickly.

Three series of experiments (Cases 4, 5, and 6) repeat Cases 1, 2, and 3 respectively, but using 90μm filter opening size instead of 50μm opening size. All other experimental conditions were kept unchanged. Although foam generation in this experiment occurs at very high injection

rates, a 1.8 times increase in opening size would roughly correspond to 5.83 times increase in bubble volume, if the flow rate were relatively low and the bubbles were created by snap-off mechanism.

Fig. 4.9 shows the results of Case 4 with 90μm filter opening size at 1 wt% Cedepal FA-406 surfactant solution, and Fig. 4.10 shows the corresponding plot of pressure drops as a function of gas and liquid injection velocities. As compared with Figs. 4.1 and 4.4 in the base case (i.e., 50μm filter opening size at 1 wt% Cedepal FA-406 surfactant), no significant differences are observed – the pressure data show both high-quality and low-quality regimes and the pressure values at the corresponding gas and liquid injection velocities are comparable.

Figs. 4.11 and 4.12 show the results of Case 5 with 90μm filter opening size at 5 wt% Cedepal FA-406 surfactant solution which can be compared and contrasted to Figs. 4.5 and Fig. 4.6 in Case 2 (i.e., 50μm filter opening size at 5 wt% Cedepal FA-406 surfactant). Again, there are no significant differences between these two cases – all of the pressure data fall within the low-quality regime and individual pressure values are comparable.

Figs. 4.13 shows the steady-state pressure drops of Case 6 with 90μm filter opening size at 0.1 wt% Cedepal FA-406 surfactant solution which can be compared with Fig. 4.8 in Case 3 (i.e., 50μm filter opening size at 0.1 wt% Cedepal FA-406 surfactant).

The earlier observation that the high-quality regime stretches with decreasing surfactant concentration with 50μm filter opening size seems still valid with 90μm filter opening size. Further the transition between the two flow regimes looks similar. Although the individual pressure values are slightly higher for the smaller filter size, there is no strong evidence that the overall pressure responses in Case 6 are not consistent with those in Case 3. The magnitude of pressure values and the difference in the pressure data between Case 3 and Case 6 are too small (i.e., less than 3 psi and many of them less than 1 psi) to draw any particular firm conclusions.

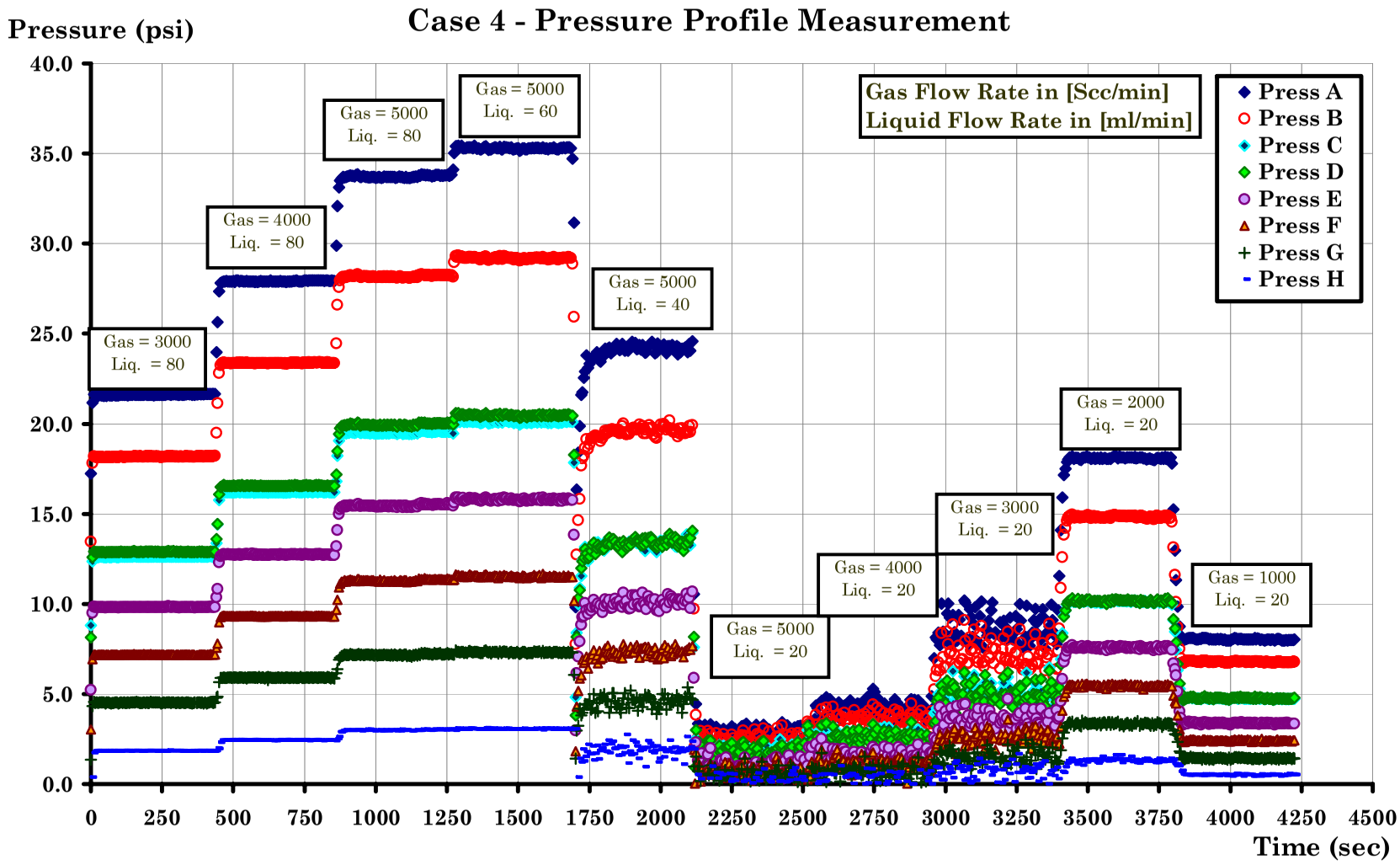

Fig. 4.9. Pressure response as a function of time with a stepwise change in gas and liquid injection rates (Case 4): (0.5 inch NPS stainless steel pipe, 1 wt% surfactant concentration using Cedepal FA -406, 90 µm filter opening size)

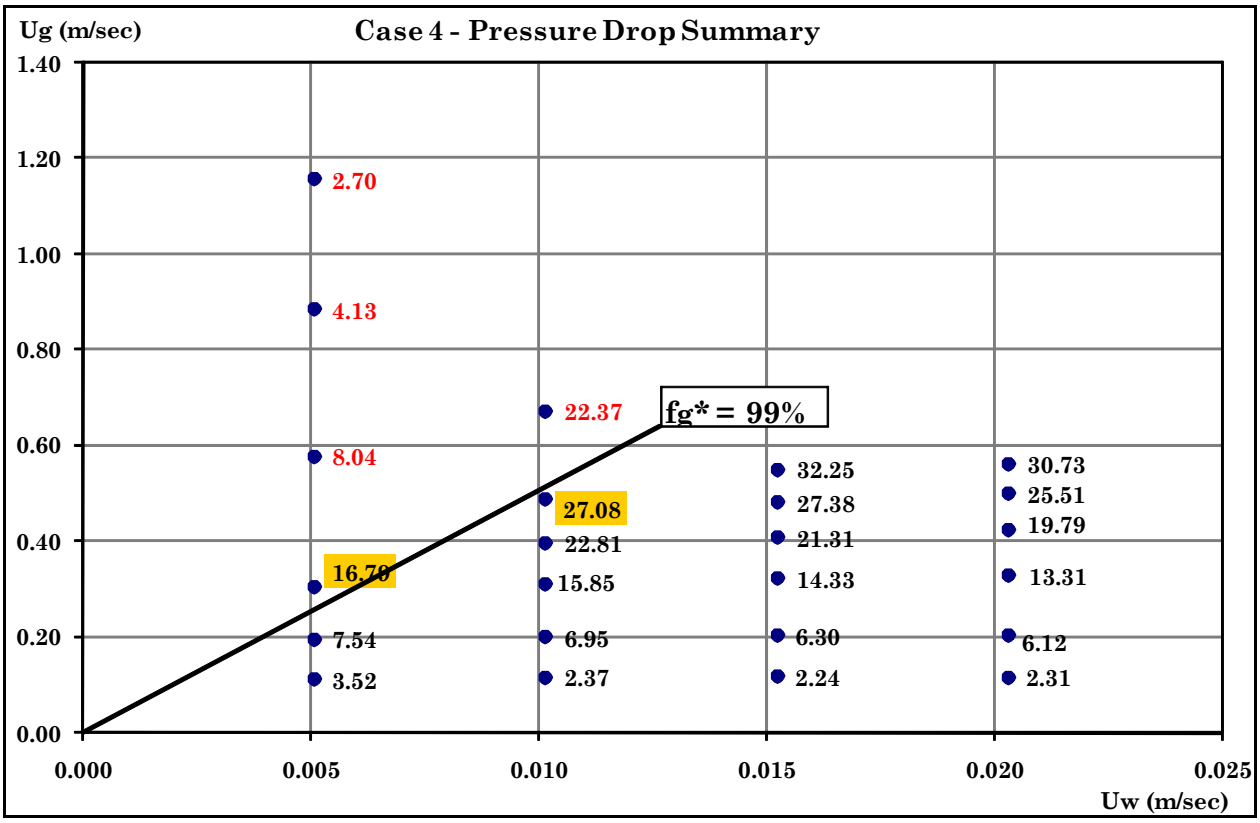

Fig. 4.10. Steady-state pressure drops, in psi, as a function of superficial gas and liquid injection velocities (Case 4): (0.5 inch NPS stainless steel pipe, 1 wt% surfactant concentration using Cedepal FA-406, 90 μm filter opening size)

The fact that the pressure response in the high-quality regime oscillates adds another difficulty.

The results from Figs. 4.9 through 4.13 indicate that the measured pressure responses with 90μm filter opening size do not differ meaningfully from those with 50μm filter opening size at three different surfactant concentrations. This suggests that the steady-state pressure drops measured in pipes are not markedly affected by the filter opening size as long as fine-textured foams are formed prior to reaching the pipe inlet. The influence of foam generator is investigated in more details within Cases 13 and 14. This is important to understand the role of foam generator in the experiments, because fined-textured foams can be pre-generated in the upstream tubing (1/8 inch ID) and connections prior to flowing into the pipe.

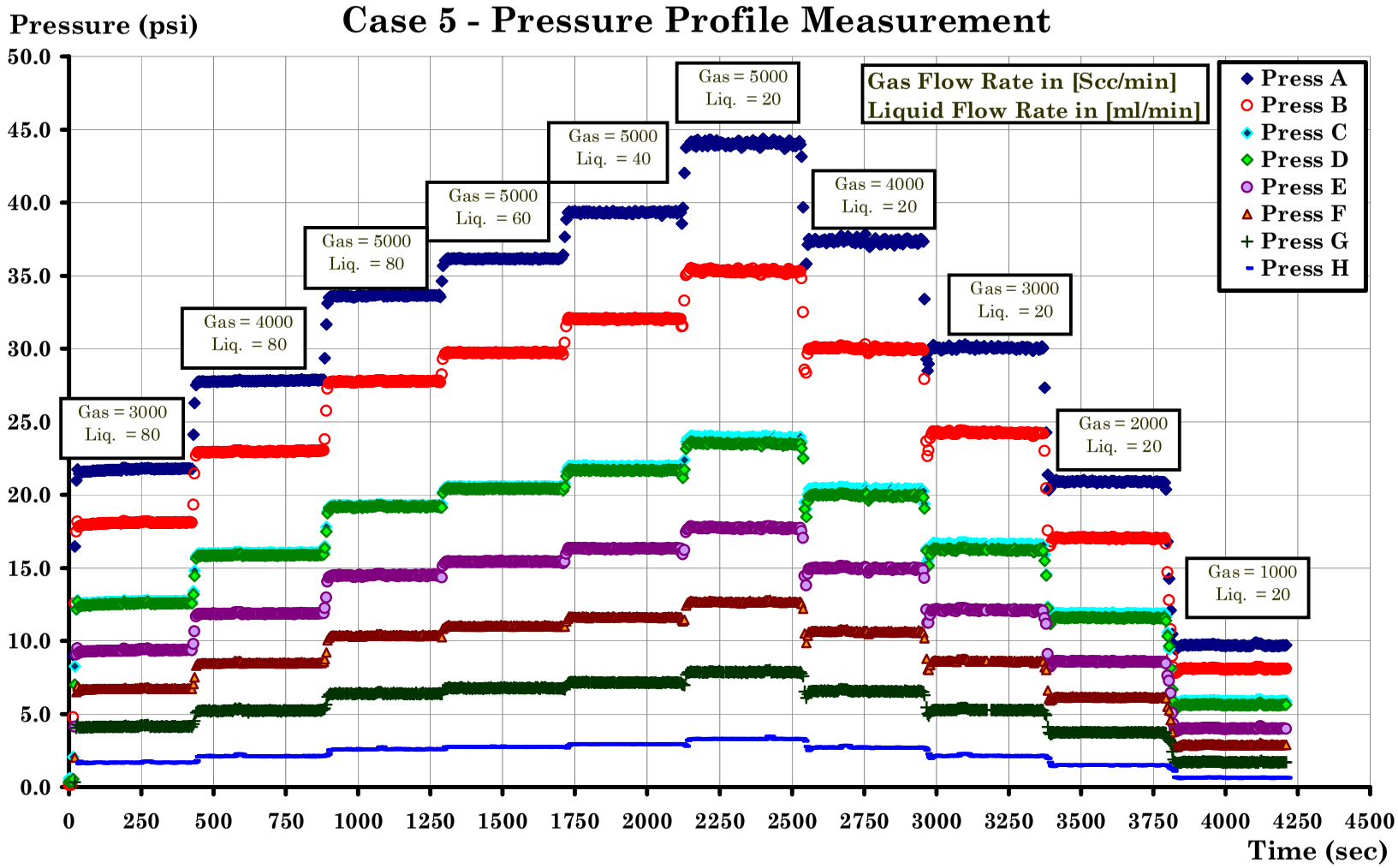

Fig. 4.11. Pressure response as a function of time with a stepwise change in gas and liquid injection rates (Case 5): (0.5 inch NPS stainless steel pipe, 5 wt% surfactant concentration using Cedepal FA -406, 90 µm filter opening size)

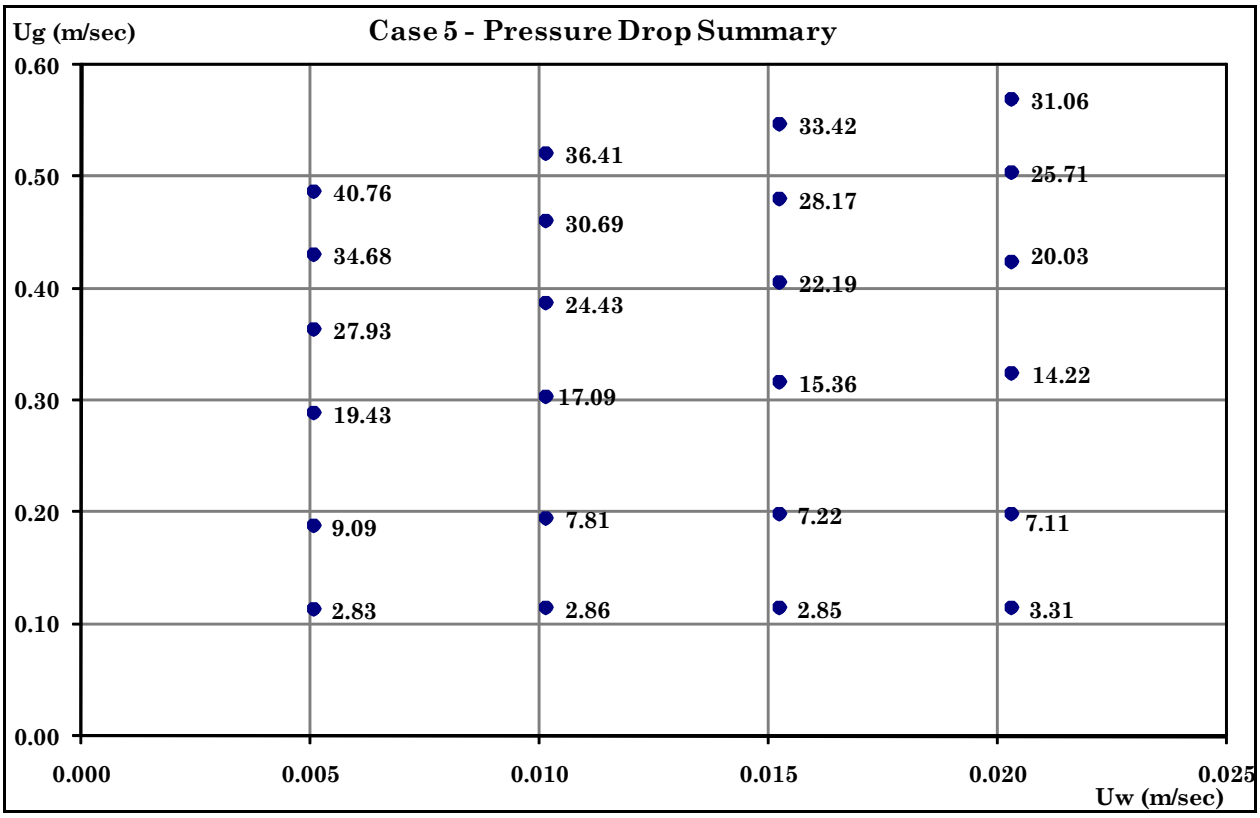

Fig. 4.12. Steady-state pressure drops, in psi, as a function of superficial gas and liquid injection velocities (Case 5): (0.5 inch NPS stainless steel pipe, 5 wt% surfactant concentration using Cedepal FA-406, 90 μm filter opening size)

4.5. Effect of Surfactant Formulation (Cases 7, 8, 9, and 10)

Surfactant formulation has been known to be an important parameter because it affects the stability of thin films and the interactions between gas, liquid, and pipe surface through surface chemistry. This study employs Cedepal FA-406 as the base-case surfactant, because Cedepal FA-406 was shown to be superior to other surfactants tested (Petrostep CG-50, Stepanform 1050, Aquet TD-600, and Ultra Palmolive) in simple test-tube foam stability tests at the same surfactant concentration. All of these experiments, which are called Cases 7, 8, 9, and 10, are conducted at the experimental conditions identical to the base case (i.e., 1 wt% surfactant concentration, 0.5 inch NPS (Nominal Pipe Size) stainless steel pipe, 50 μm filter opening size) except for the surfactant formulations.

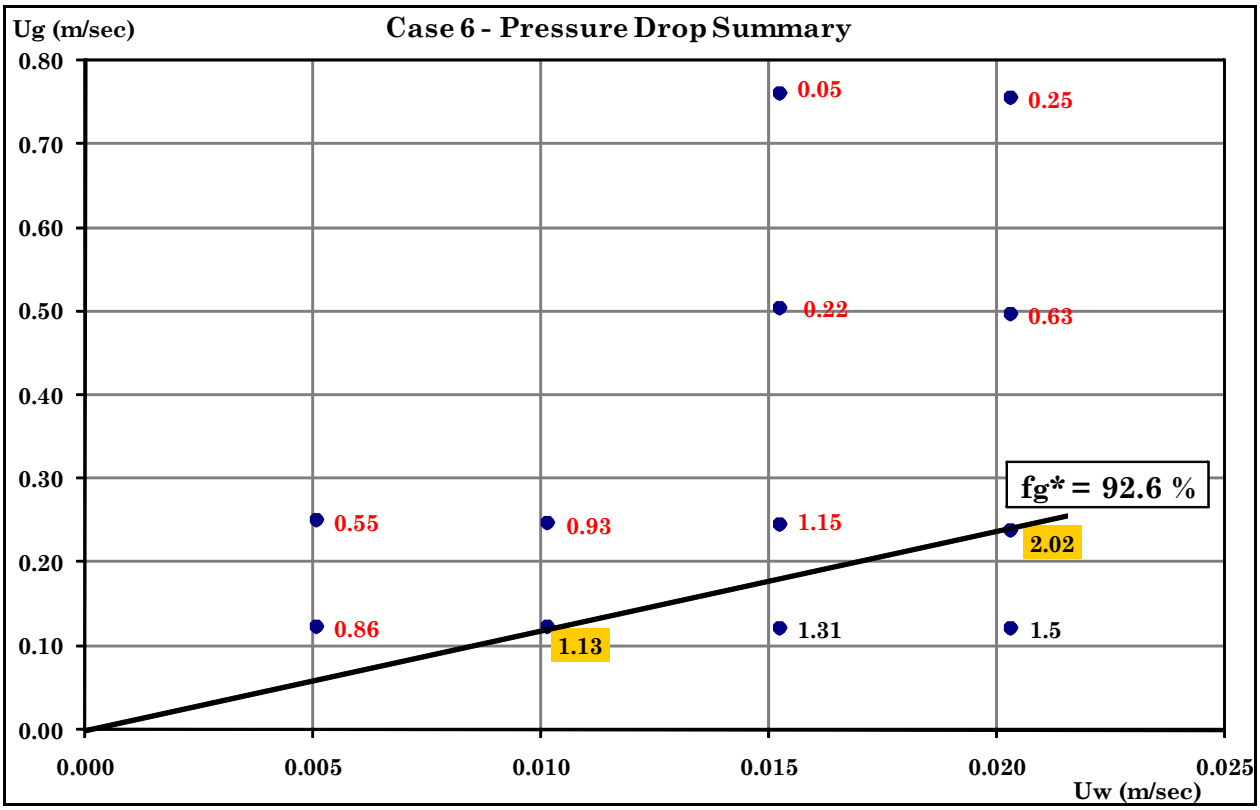

Fig. 4.13. Steady-state pressure drops, in psi, as a function of superficial gas and liquid injection velocities (Case 6): (0.5 inch NPS stainless steel pipe, 0.1 wt% surfactant concentration using Cedepal FA-406, 90 μm filter opening size)

Figs. 4.14 and 4.15 show the results with 1 wt% of Petrostep CG-50 (Case 7). Compared with Fig. 4.1 (base case), Fig. 4.14 shows more fluctuation in the pressure data. This is consistent with the understanding that Petrostep CG-50 is a weaker foamer than Cedepal FA-406 in foam stability tests. Fig. 4.15 shows the steady-state pressure responses. In contrast to Fig. 4.4 (base case), two different aspects can be easily observed in Fig. 4.15: (1) the magnitude of pressure drop is reduced in all gas and liquid injection velocities tested and, especially, the maximum pressure drop in Case 7 is less than a third of that in the base case (i.e., 32.03 psi in Fig. 4.4 vs. 10.07 psi in Fig. 4.15) and (2) the value of f_g* that separates the two regimes is reduced to about 96% in Case 7 rather than 99% in the base case. These two features are also consistent with the fact that Petrostep CG-50 is a weaker foamer than Cedepal FA-406.

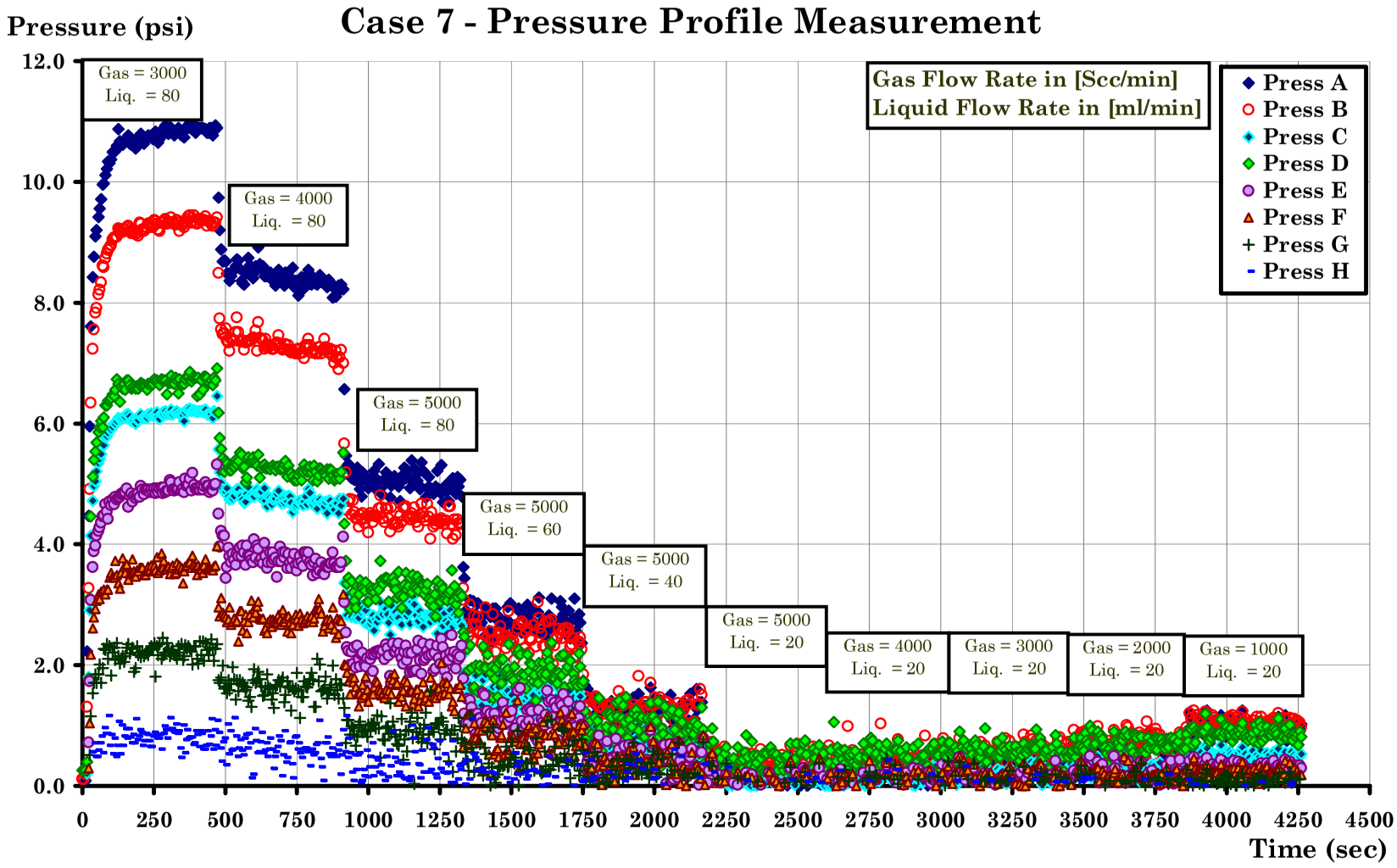

Fig. 4.14. Pressure response as a function of time with a stepwise change in gas and liquid injection rates (Case 7): (0.5 inch NPS stainless steel pipe, 1 wt% surfactant concentration using Petrostep CG-50, 50 µm filter opening size)

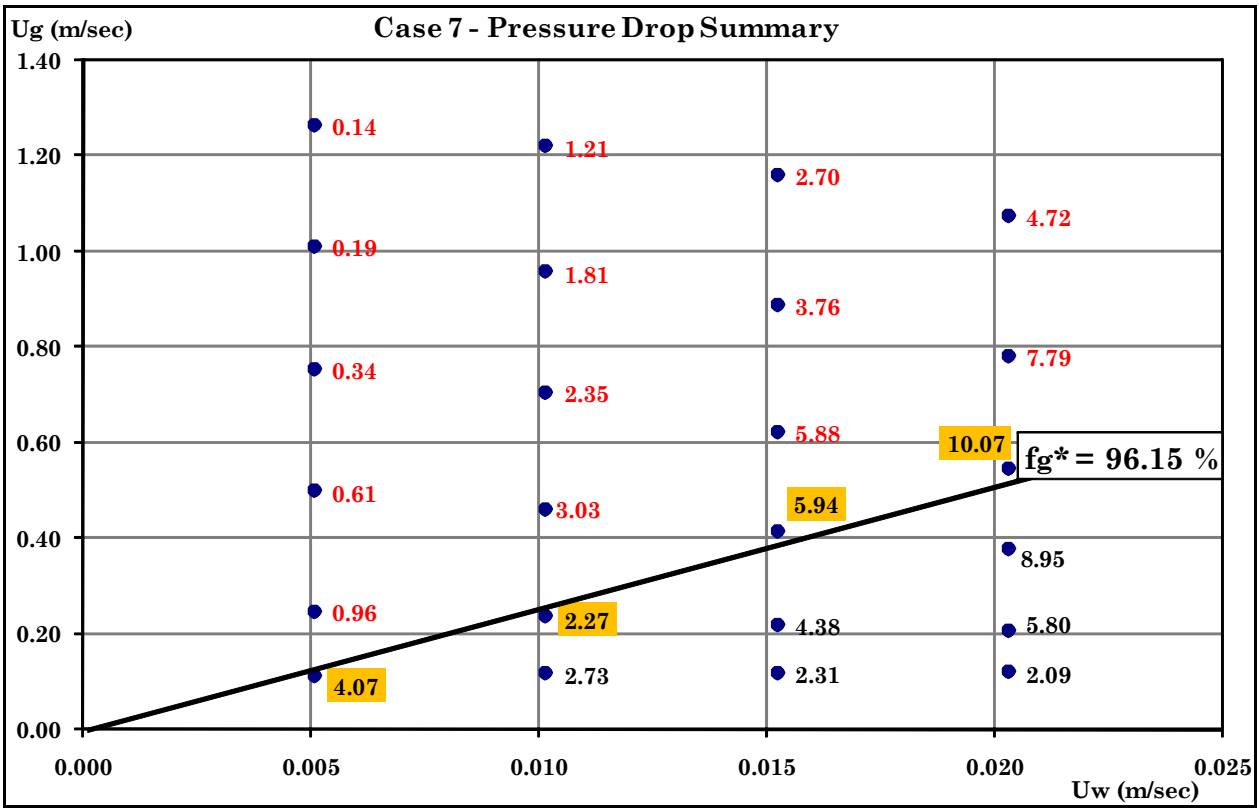

Fig. 4.15. Steady-state pressure drops, in psi, as a function of superficial gas and liquid injection velocities (Case 7): (0.5 inch NPS stainless steel pipe, 1 wt% surfactant concentration using Petrostep CG-50, 50 µm filter opening size)

Both regimes show shear-thickening behavior to the liquid injection velocity in the high-quality regime and to the gas injection velocity in the low-quality regime. The power-law exponent in the high-quality regime ranges from 1.8 to 2.4, which is somewhat greater than the exponent in the base case (i.e., 1.5 to 1.6), while the power-law exponent in the low-quality regime ranges from 1.3 to 1.8, which is comparable to the base case.

Figs. 4.16 and 4.17 show the results with 1 wt% of Stepanform 1050 (Case 8). If a comparison is made with the base case, the individual pressure values tend to be either comparable or reduced slightly, and the f_g* seems to be lowered somewhat. The power-law exponents are around 1.8 to the liquid injection velocity in the high-quality regime, and 1.4 to 1.6 to the gas injection velocity in the low-quality regime.

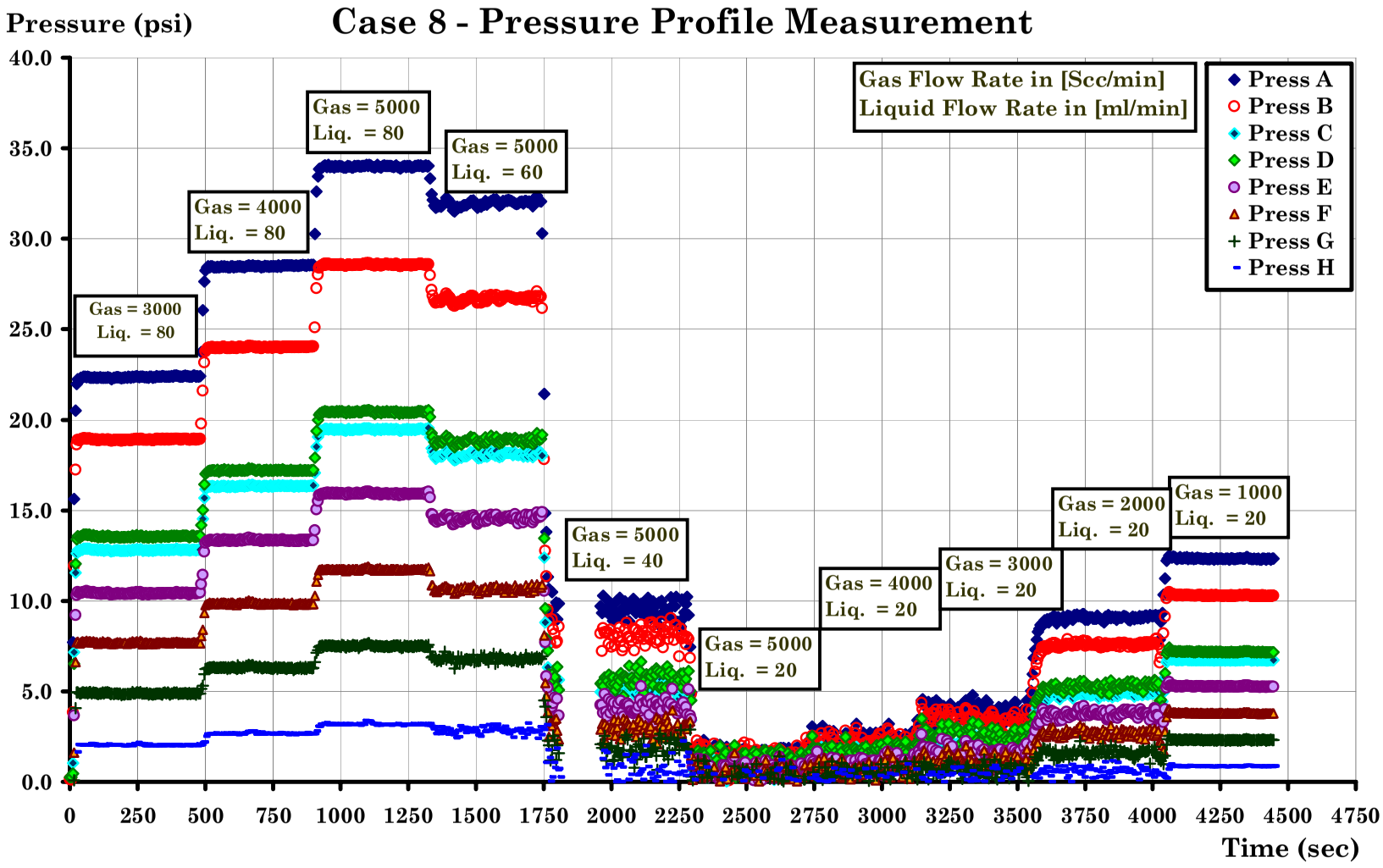

Fig. 4.16. Pressure response as a function of time with a stepwise change in gas and liquid injection rates (Case 8): (0.5 inch NPS stainless steel pipe, 1 wt% surfactant concentration using Stepanform 1050, 50 um filter opening size)

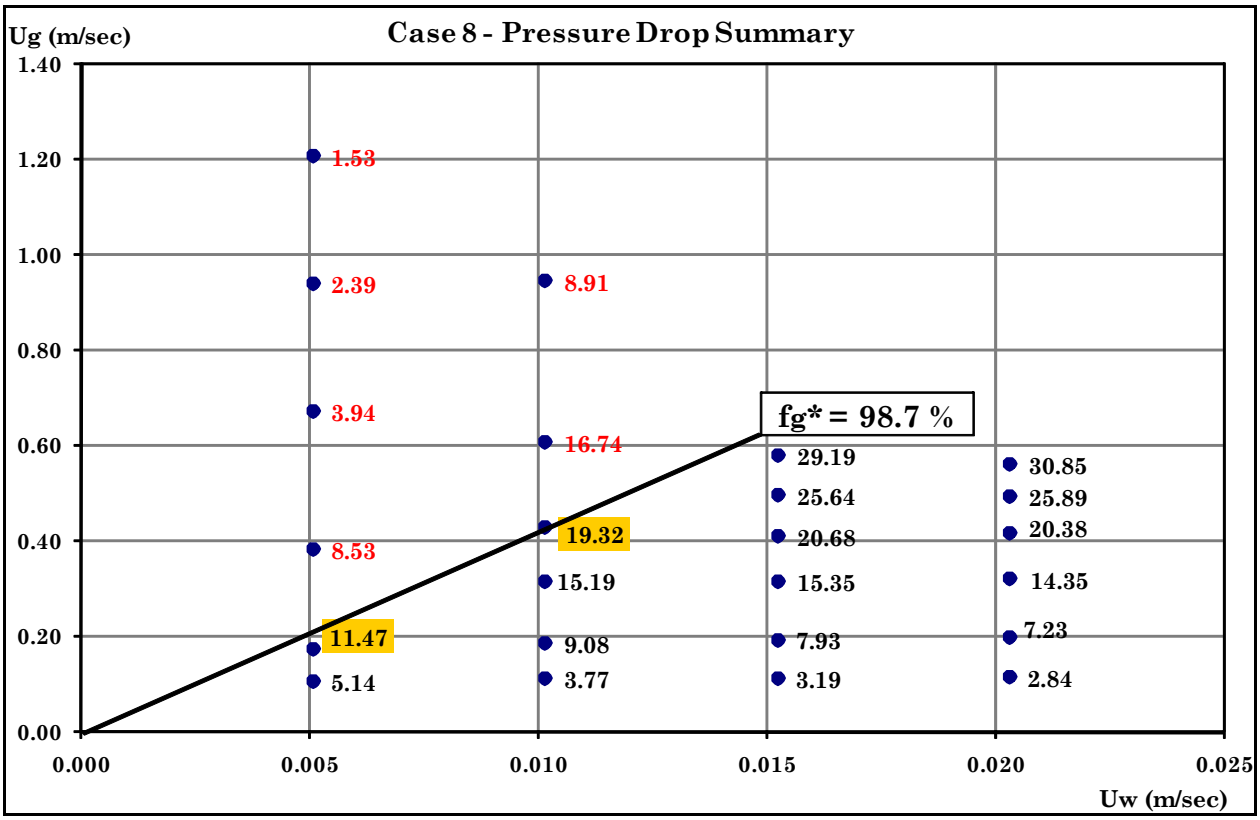

Fig. 4.17. Steady-state pressure drops, in psi, as a function of superficial gas and liquid injection velocities (Case 8): (0.5 inch NPS stainless steel pipe, 1 wt% surfactant concentration using Stepanform 1050, 50 μm filter opening size)

Figs. 4.18 and 4.19 show the results of Case 9 which uses 1 wt% of Aquet TD-600. The pressure responses fluctuate significantly for the entire range of gas and liquid injection velocities and, as a result, the high-quality regime is extended compared with the base case (cf. Fig. 4.4). As a result, the f_g* value is lowered from 99% to around 96%, which is significant change taking into consideration the very narrow range of foam qualities (86% to 99.6%) analyzed in this study.

The high-quality regime shows shear-thickening behavior to the liquid injection velocity with the power-law exponent about 1.3 to 1.5. Although the low-quality regime also seems to exhibit shear-thickening behavior to the gas injection velocity, there is a lack of data for further interpretation.

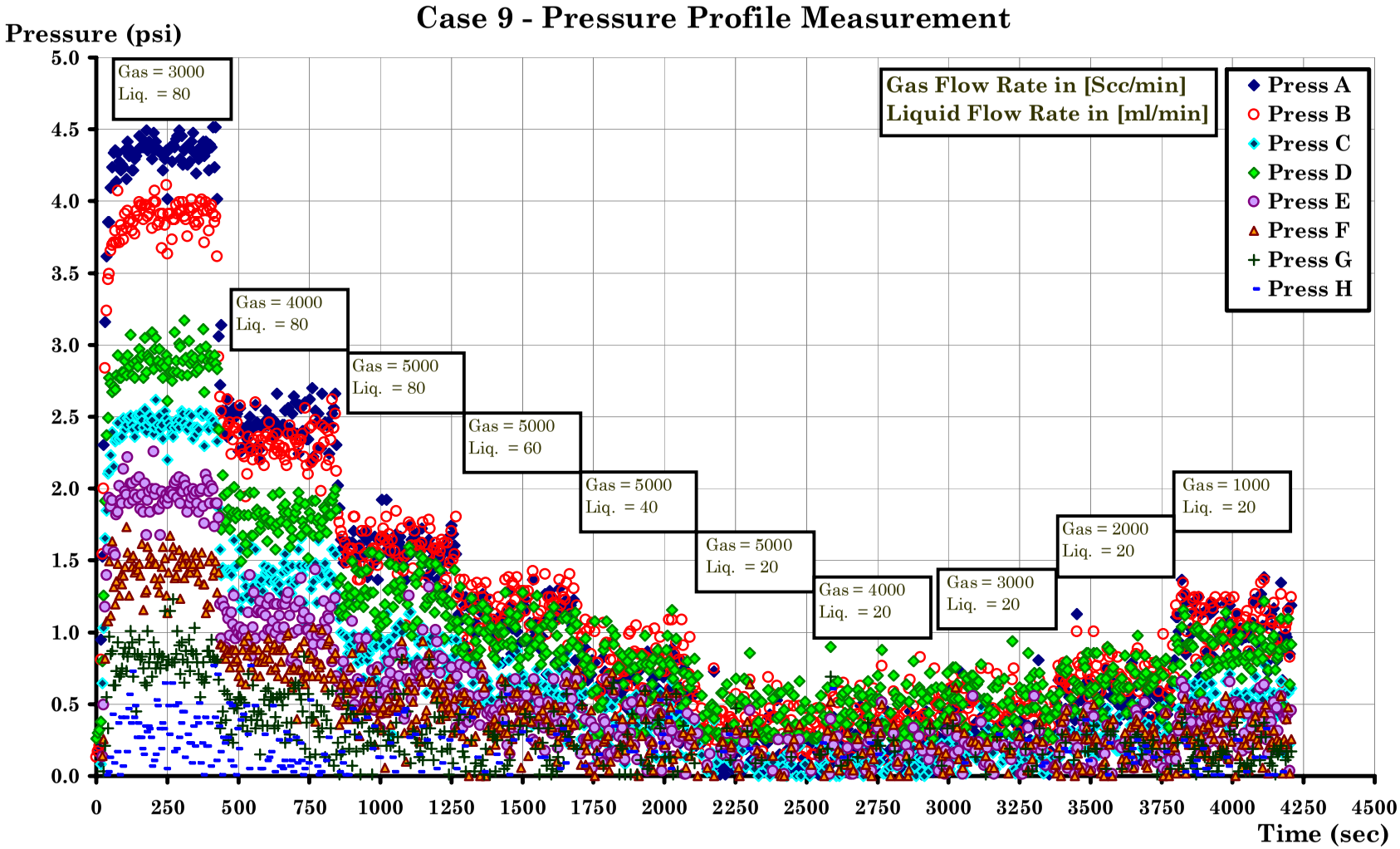

Fig. 4.18. Pressure response as a function of time with a stepwise change in gas and liquid injection rates (Case 9): (0.5 inch NPS stainless steel pipe, 1 wt% surfactant concentration using Aquet TD-600, 50 µm filter opening size)

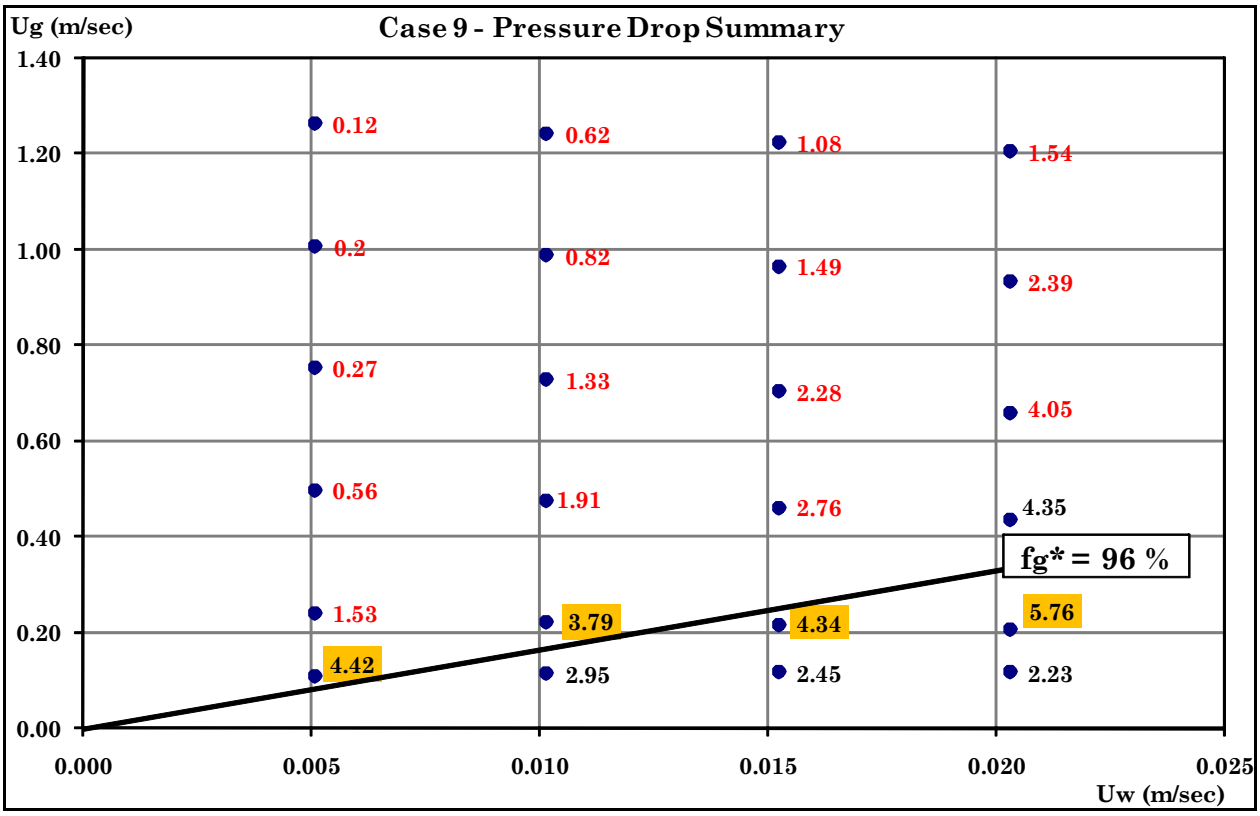

Fig. 4.19. Steady-state pressure drops, in psi, as a function of superficial gas and liquid injection velocities (Case 9): (0.5 inch NPS stainless steel pipe, 1 wt% surfactant concentration using Aquet TD-600, 50 μm filter opening size)

The experimental results with 1 wt% of Ultra Palmolive are shown in Figs. 4.20 and 4.21 (Case 10). Although the use of Ultra Palmolive is for household purposes instead of use in the petroleum industry, the presence of two flow regimes observed in the previous experiments can also be found consistently. The value of f_g* is about 97.5%. Foam rheology to the liquid injection velocity in the high-quality regime is shear-thickening with the power-law exponent of about 1.7, but the foam in the low-quality regime does not display any consistency, showing both shear thinning and shear thickening. The results from Fig. 4.14 through Fig. 4.21 show that the use of stronger foamer makes bubbles more stable during the flow and thus results in the expansion of low-quality regime and increase in f_g*. This agrees well with what was conjectured in the earlier section to investigate the effect of surfactant concentration.

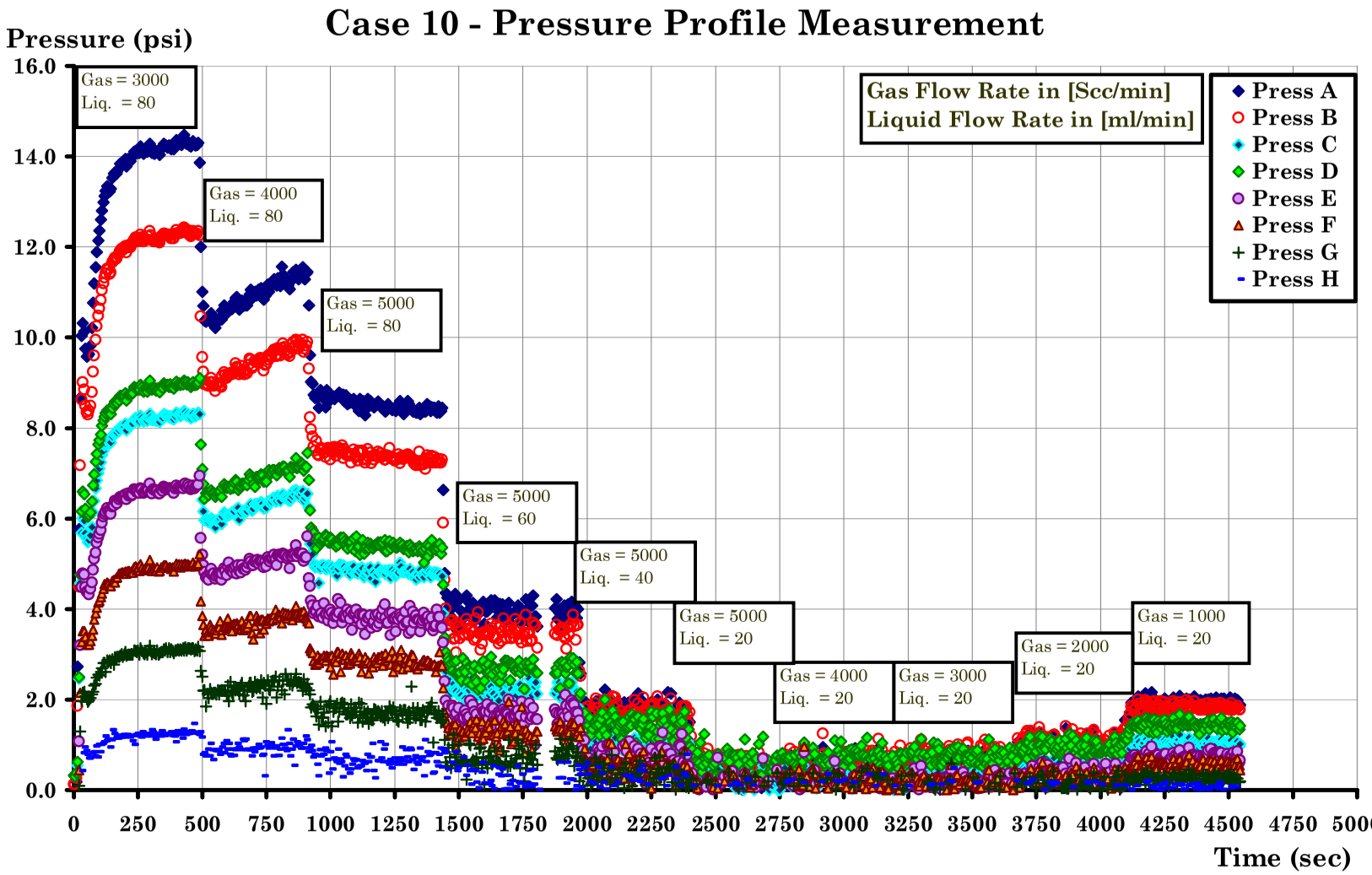

Fig. 4.20. Pressure response as a function of time with a stepwise change in gas and liquid injection rates (Case 10): (0.5 inch NPS stainless steel pipe, 1 wt% surfactant concentration using Ultra Palmolive, 50 µm filter opening size)

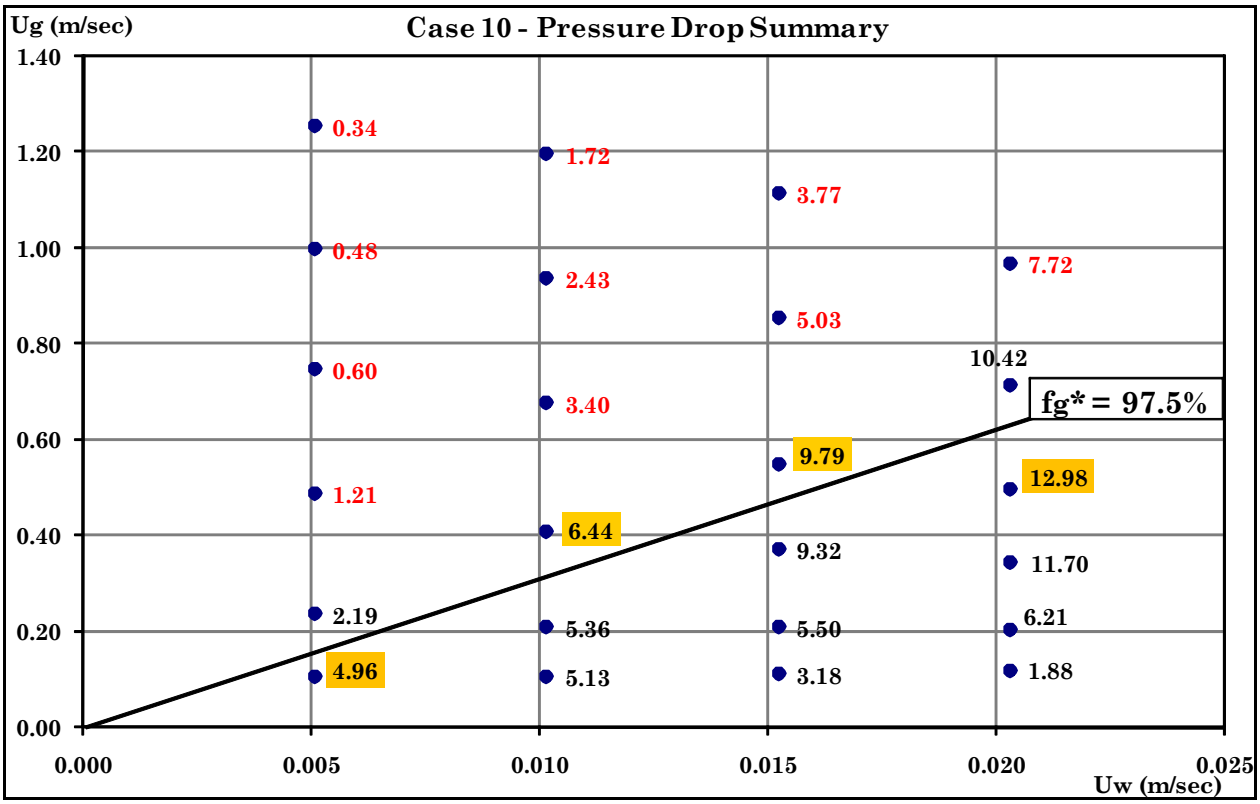

Fig. 4.21. Steady-state pressure drops, in psi, as a function of superficial gas and liquid injection velocities (Case 10): (0.5 inch NPS stainless steel pipe, 1 wt% surfactant concentration using Ultra Palmolive, 50 μm filter opening size)

4.6. Effect of Pipe Diameter (Cases 11 and 12)

Additional experiments were conducted to investigate the effect of flow conduit size by repeating Case 1 (base case) and Case 2 in 1 inch NPS (Nominal Pipe Size) pipe rather than 0.5 inch pipe. The pressure data from ports B through G are used for the interpretation of steady-state foam rheology because of the inlet and outlet effects.

Figs. 4.22 through 4.24 show the result of Case 11 in which nitrogen and 1 wt% Cedepal FA-406 surfactant solution flow into the 1 inch stainless steel pipe.

The presence of two regimes is shown to be obvious, again the high-quality regime characterized by the unstable and fluctuating pressure response and the low-quality regime characterized by the stabilized pressure response and by homogeneous fine-texture foam.

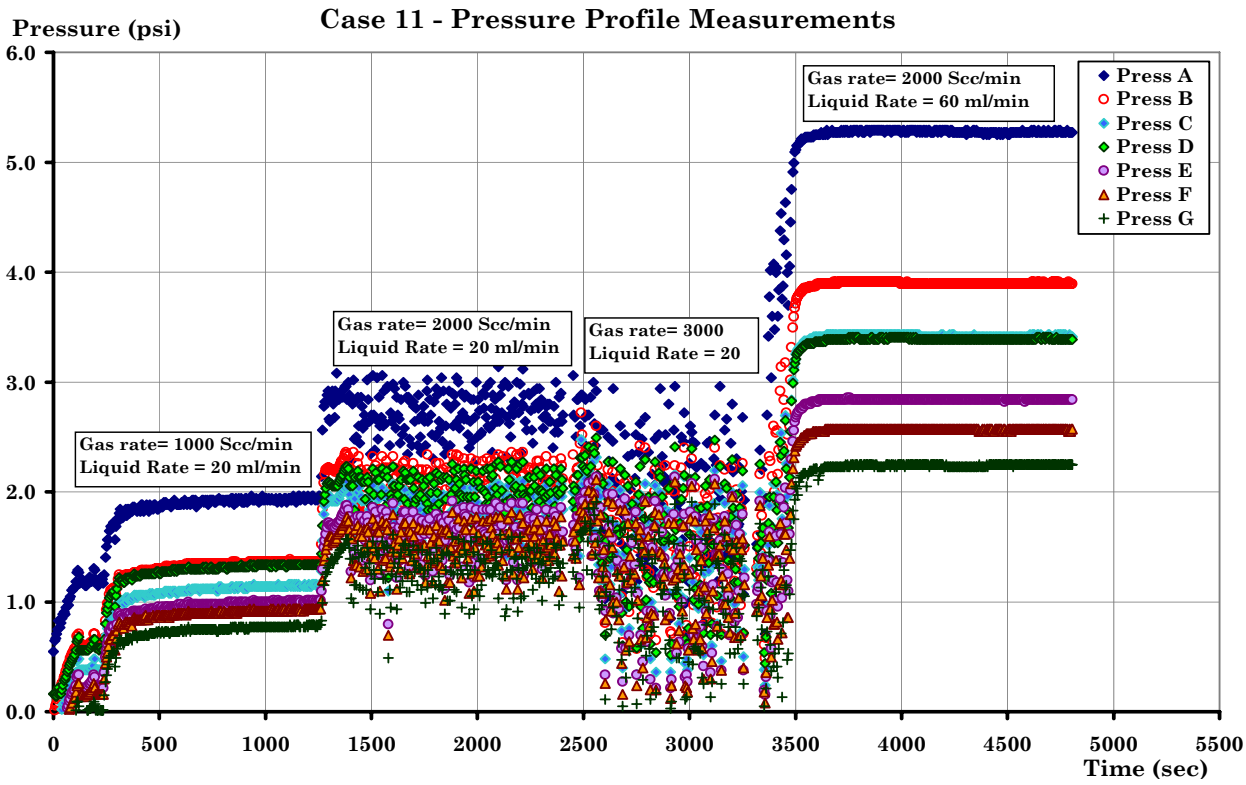

Fig. 4.22. Pressure response as a function of time (Case 11): (1 inch NPS stainless steel pipe, 1 wt% surfactant concentration using Cedepal FA -406, 50 µm filter opening size)

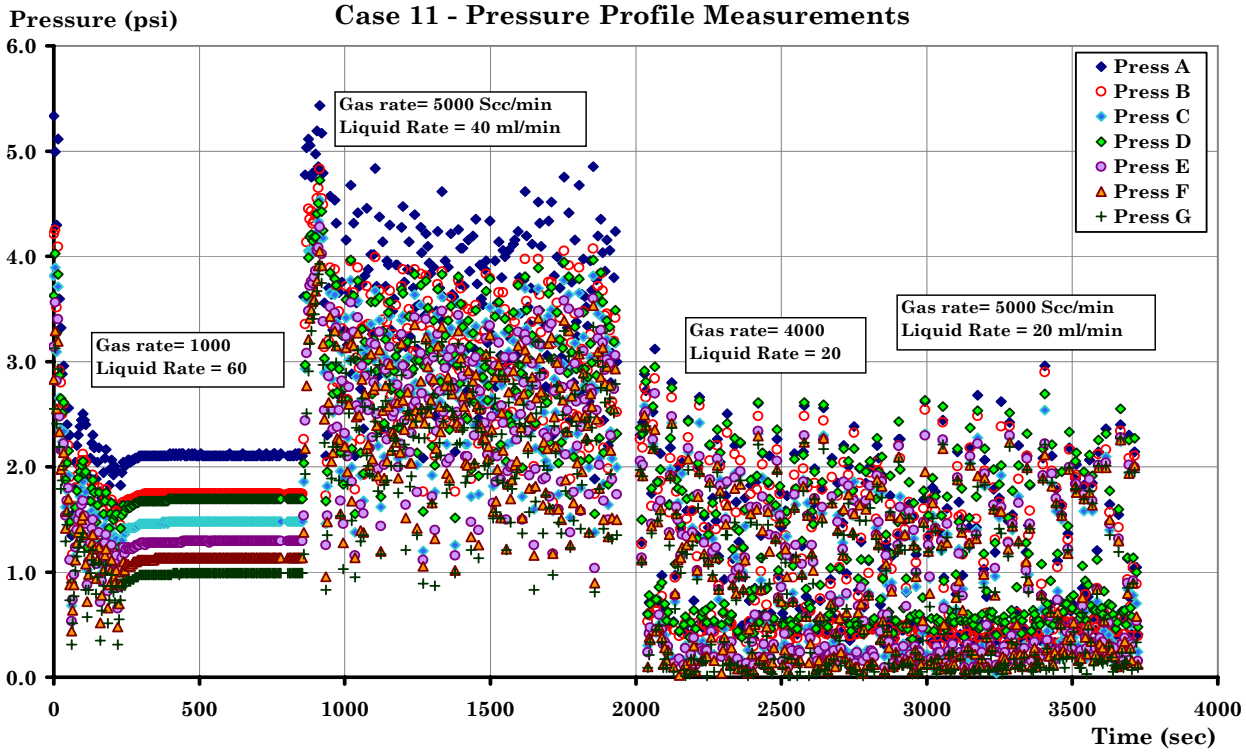

Fig. 4.23. Pressure response as a function of time (Case 11), continued

The magnitude of the pressure drop is reduced significantly due to the increase in the cross-sectional area to the flow. The rheology to the liquid injection velocity in the high-quality regime is shear thickening with the exponent around 1.2-1.4, while the rheology to the gas injection velocity in the low-quality regime is nearly Newtonian with the exponent around 0.9 to 1. The value of f_g* does not seem to be affected significantly, as shown in Fig. 4.24.

Figs. 4.25 through 4.27 show the result of Case 12 in which 5 wt% Cedepal FA-406 surfactant solution is used together with the 1 inch stainless steel pipe. The pressure responses are mostly stable and therefore low-quality regime prevails. In contrast to Case 2 and Case5, the steady-state pressure plot shows the presence of high-quality regime once f_g is about 95.5%. The low-quality regime shows nearly Newtonian flow behavior to the gas injection velocity.

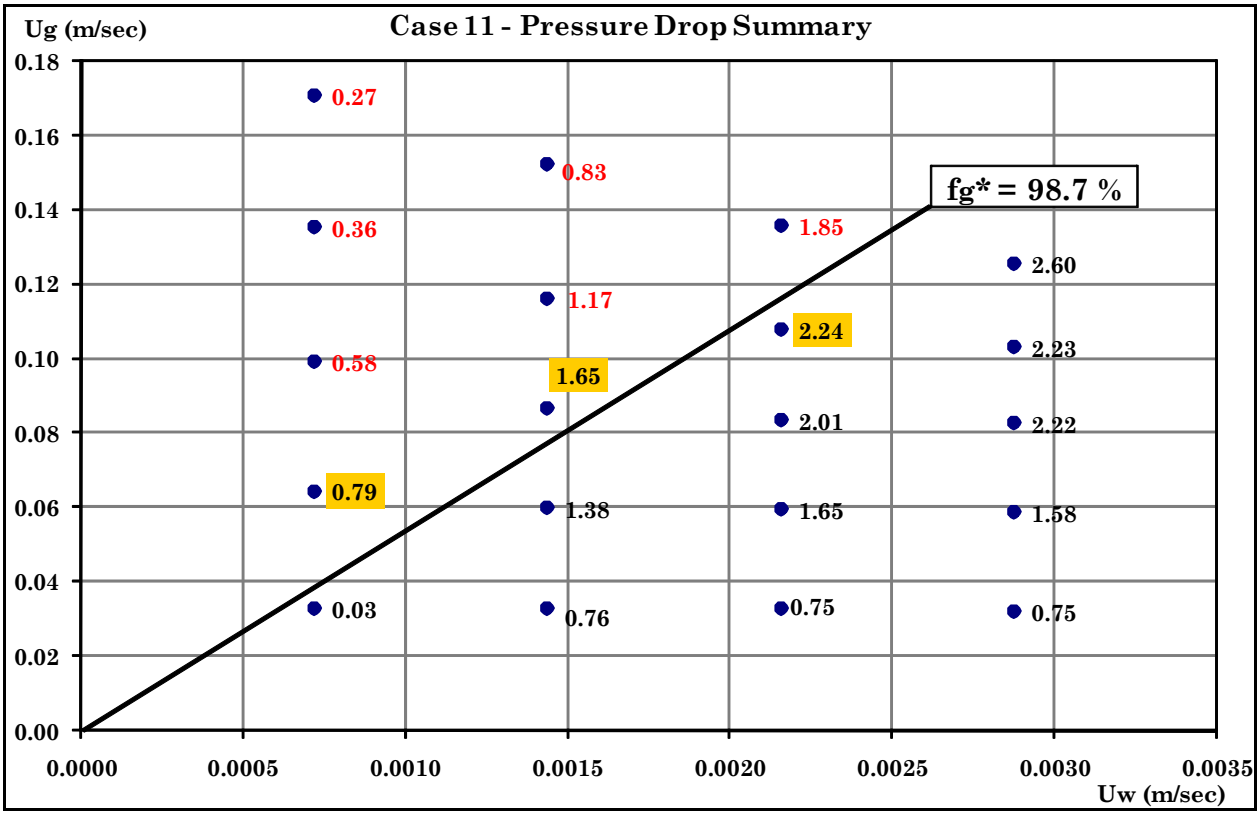

Fig. 4.24. Steady-state pressure drops, in psi, as a function of superficial gas and liquid injection velocities (Case 11): (1 inch NPS stainless steel pipe, 1 wt% surfactant concentration using Cedepal FA-406, 50 μm filter opening size)

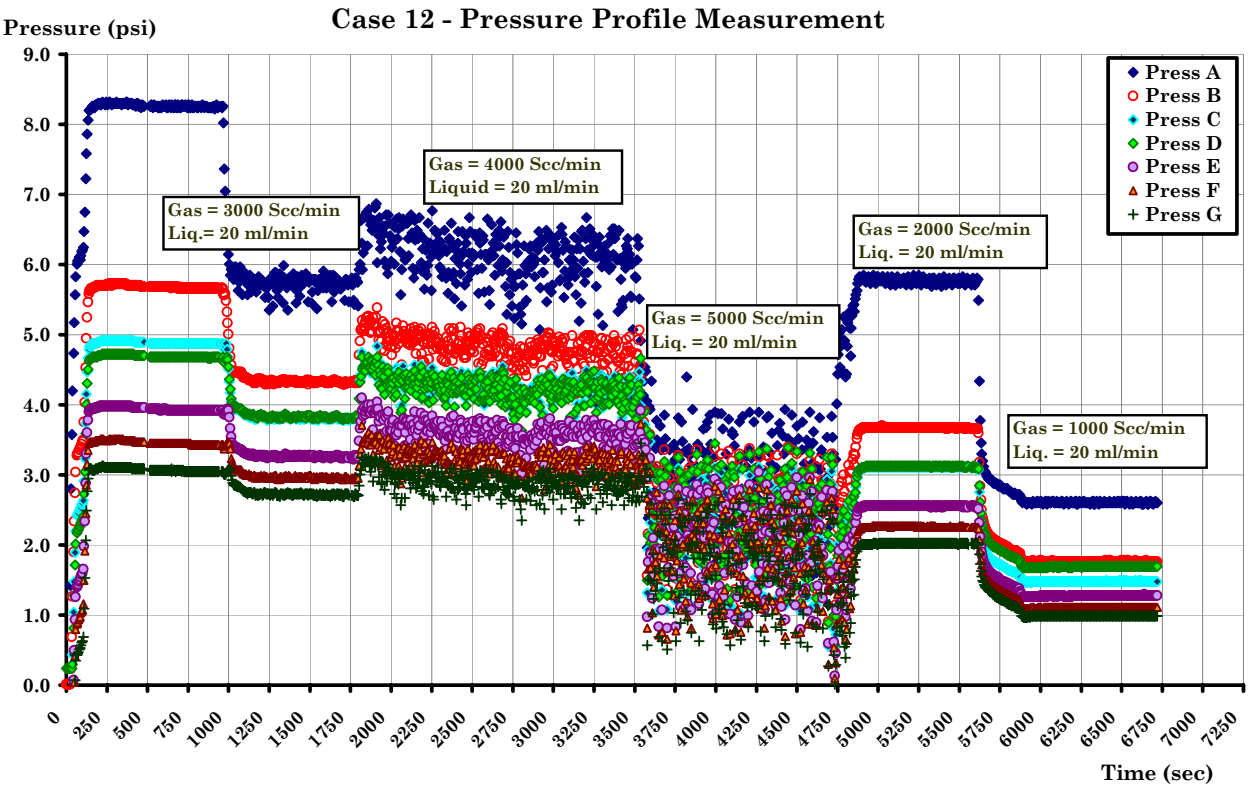

Fig. 4.25. Pressure response as a function of time (Case 12): (1 inch NPS stainless steel pipe, 5 wt% surfactant concentration using Cedepal FA -406, 50 µm filter opening size)

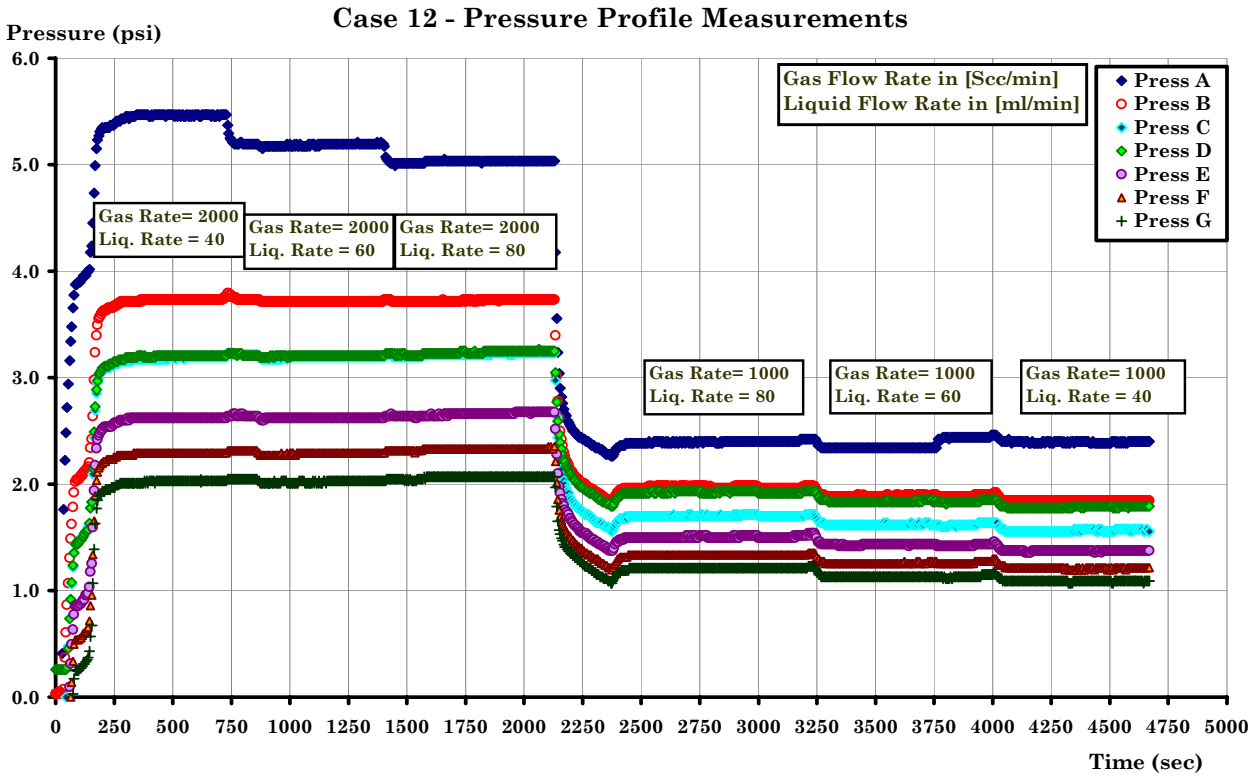

Fig. 4.26. Pressure response as a function of time (Case 12), continued

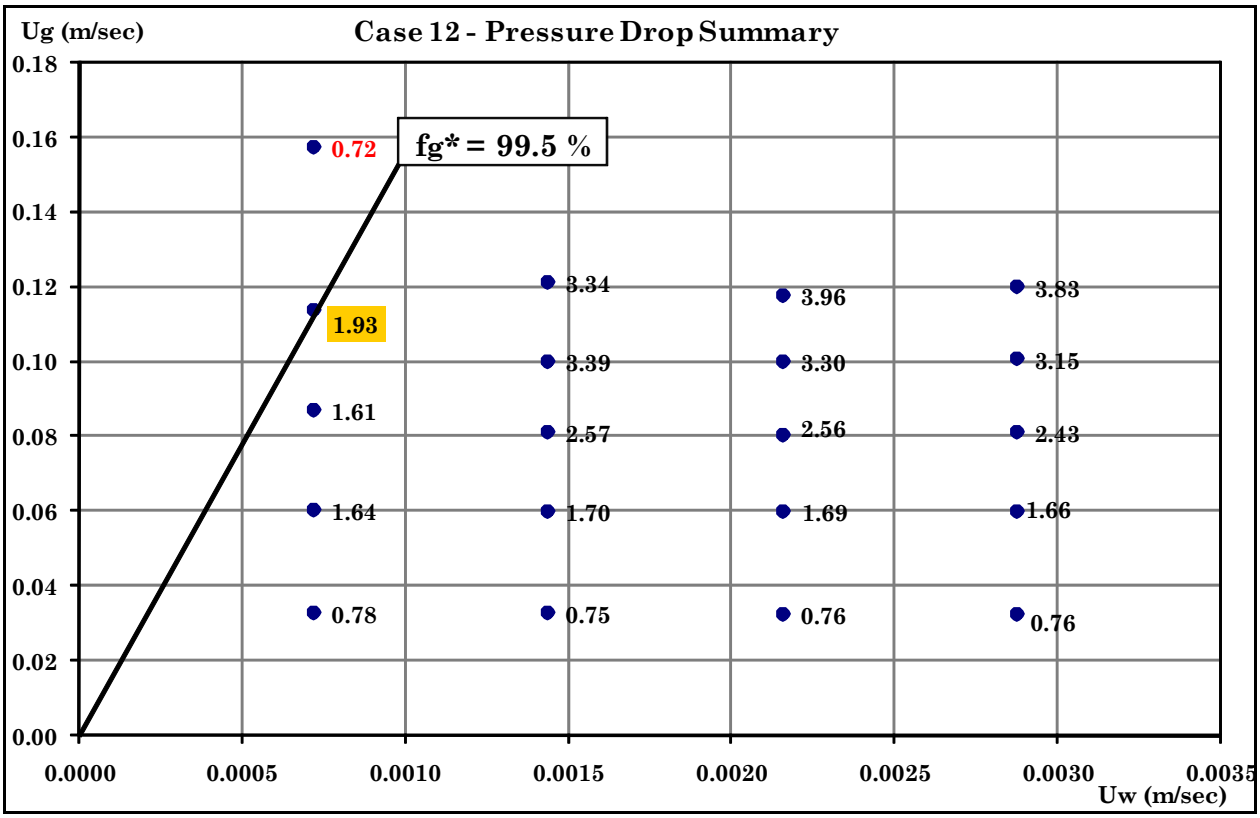

Fig. 4.27. Steady-state pressure drops, in psi, as a function of superficial gas and liquid injection velocities (Case 12): (1 inch NPS stainless steel pipe, 5 wt% surfactant concentration using Cedepal FA-406, 50 µm filter opening size)

4.7. Flow Experiments at Fixed Foam Quality (Cases 13 and 14)

Additional experiments were designed in Case 13 and 14 to investigate (1) the impact of the upstream foam generator and (2) the reproducibility or precision of the system. The former is important to understand the role of foam generator in the experiments, because fined-textured foams can be pre-generated in the upstream tubing (1/8 inch ID) and connections prior to flowing into the pipe. These experiments were conducted at fixed foam quality (98.4%) by changing total injection velocity (u_t). For simplicity, foam qualities and gas injection velocities in Case 13 and 14 are reported at atmospheric pressure, rather than being adjusted by the average system pressure. Table 4.1 lists gas and liquid flow rates used in Case 13, and the corresponding change in pressure response is shown in Fig. 4.28. The experiments start at the flow rates shown

by test number “0” in which fine-textured foams are generated flowing gas and liquid mixture through 50 μm opening size filter. Then, by changing the direction of a three-way valve, the flow is diverted into different directions such that the flow bypasses the filter at the same gas and liquid flow rates as shown by “1” in Table 4.1 and Fig. 28. In subsequent experiments, the total flow rate is reduced step by step, shown by “2” through “9”, and increased back up following the same total flow rates, shown by “8’” through “2’”, still bypassing the filter upstream.

Table 4.1 Flow rates used for Case 13 (cf. Fig. 4.28) at fixed foam quality of 98.4%

Test No.	Gas Rate [Scc/min]	Liquid Rate [ml/min]	Gas Velocity [m/sec]	Liquid Velocity [m/sec]
0	4500	72.01	0.1616	0.0026
1	4500	72.01	0.1616	0.0026
2 & 2'	4000	64.01	0.1437	0.0023
3 & 3'	3500	56.01	0.1257	0.0020
4 & 4'	3000	48.01	0.1077	0.0017
5 & 5'	2500	40.01	0.0898	0.0014
6 & 6'	2000	32.00	0.0718	0.0011
7 & 7'	1500	24.00	0.0539	0.0009
8 & 8'	1000	16.00	0.0359	0.0006
9	500	8.00	0.0180	0.0003

Fig. 4.28 shows the overall pressure response, which indicates that (1) bypassing the upstream filter reduces the steady-state pressure drop somewhat but the magnitude is not very significant (cf. “0” vs. “1”) and (2) the steady-state pressure drops measured in “2” through “8” are consistent with those measured in “2’” through “8’”, demonstrating a good reproducibility and precision. Fig. 4.28 also shows that the pressure responses are stable in all flow rates tested. This was expected because the foam quality of 98.4% tested lies in the low-quality regime (cf. f_g^* = 99% in Fig. 4.4). Table 4.2 and Fig. 4.29 show the flow rates and the corresponding pressure response (Case 14a), which basically repeats Case 13 except that the entire experiments are conducted in the absence of the upstream foam generator. The results are comparable with

Case 13 indicating that the use of a foam generator does not substantially affect the results of subsequent experiments.

Table 4.2 Flow rates used for Case 14a (cf. Fig. 4.29) at fixed foam quality of 98.4%

Test No.	Gas Rate Scc/min	Liquid Rate ml/min	Gas Velocity [m/sec]	Liquid Velocity [m/sec]
1	4000	64.01	0.1437	0.0023
2 & 2'	3500	56.01	0.1257	0.0020
3 & 3'	3000	48.01	0.1077	0.0017
4 & 4'	2500	40.01	0.0898	0.0014
5 & 5'	2000	32.00	0.0718	0.0011
6 & 6'	1500	24.00	0.0539	0.0009
7 & 7'	1000	16.00	0.0359	0.0006
8	500	8.00	0.0180	0.0003

Table 4.3 and Fig. 4.30 show the flow rates and pressure responses (Case 14b), by repeating the same experiments in Case 14a using 0.5 wt% concentration of Cedepal FA-406 surfactant. In contrast to Case 14a, the experiments increase the flow rate from the lowest to the highest (i.e., “1” to “10”), followed by a stepwise reduction back to the lowest flow rate (i.e., “9’” to “1’”). Again the steady-state pressure drops are consistent irrespective of the direction of flow rate change.

Table 4.3 Flow rates used for Case 14b (cf. Fig. 4.30) at fixed foam quality of 98.4%

Test No.	Gas Rate Scc/min	Liquid Rate ml/min	Gas Velocity [m/sec]	Liquid Velocity [m/sec]
1 & 1'	500	8.00	0.0180	0.0003
2 & 2'	1000	16.00	0.0359	0.0006
3 & 3'	1500	24.00	0.0539	0.0009
4 & 4'	2000	32.00	0.0718	0.0011
5 & 5'	2500	40.01	0.0898	0.0014
6 & 6'	3000	48.01	0.1077	0.0017
7 & 7'	3500	56.01	0.1257	0.0020
8 & 8'	4000	64.01	0.1437	0.0023
9 & 9'	4500	72.00	0.1616	0.0026
10	5000	80.00	0.1796	0.0029

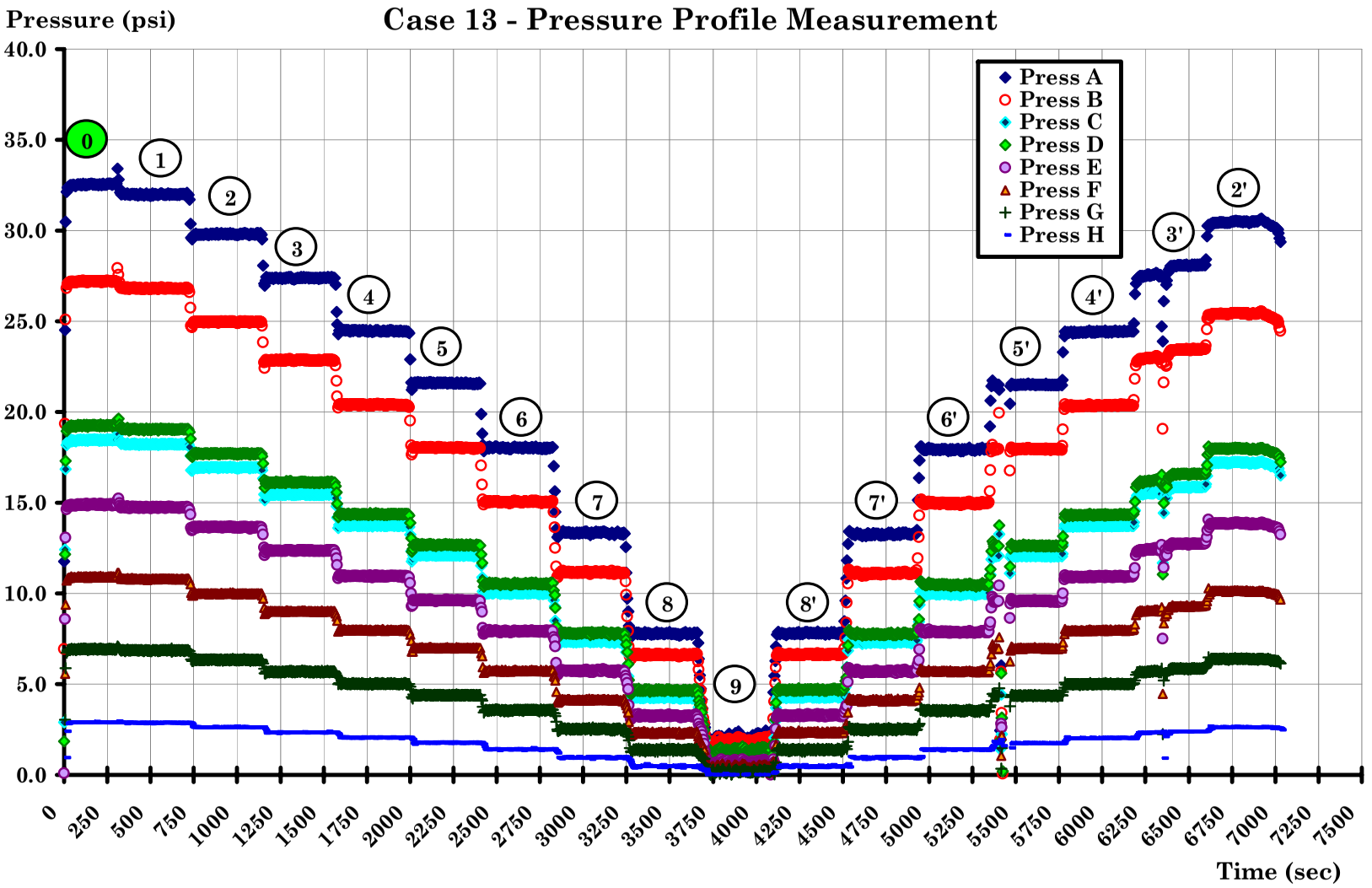

Fig. 4.28. Pressure response as a function of time with a stepwise change in gas and liquid injection rates (Case 13): (0.5 inch NPS stainless steel pipe, 1 wt% surfactant concentration using Cedepal FA-406, 50 µm filter opening size)

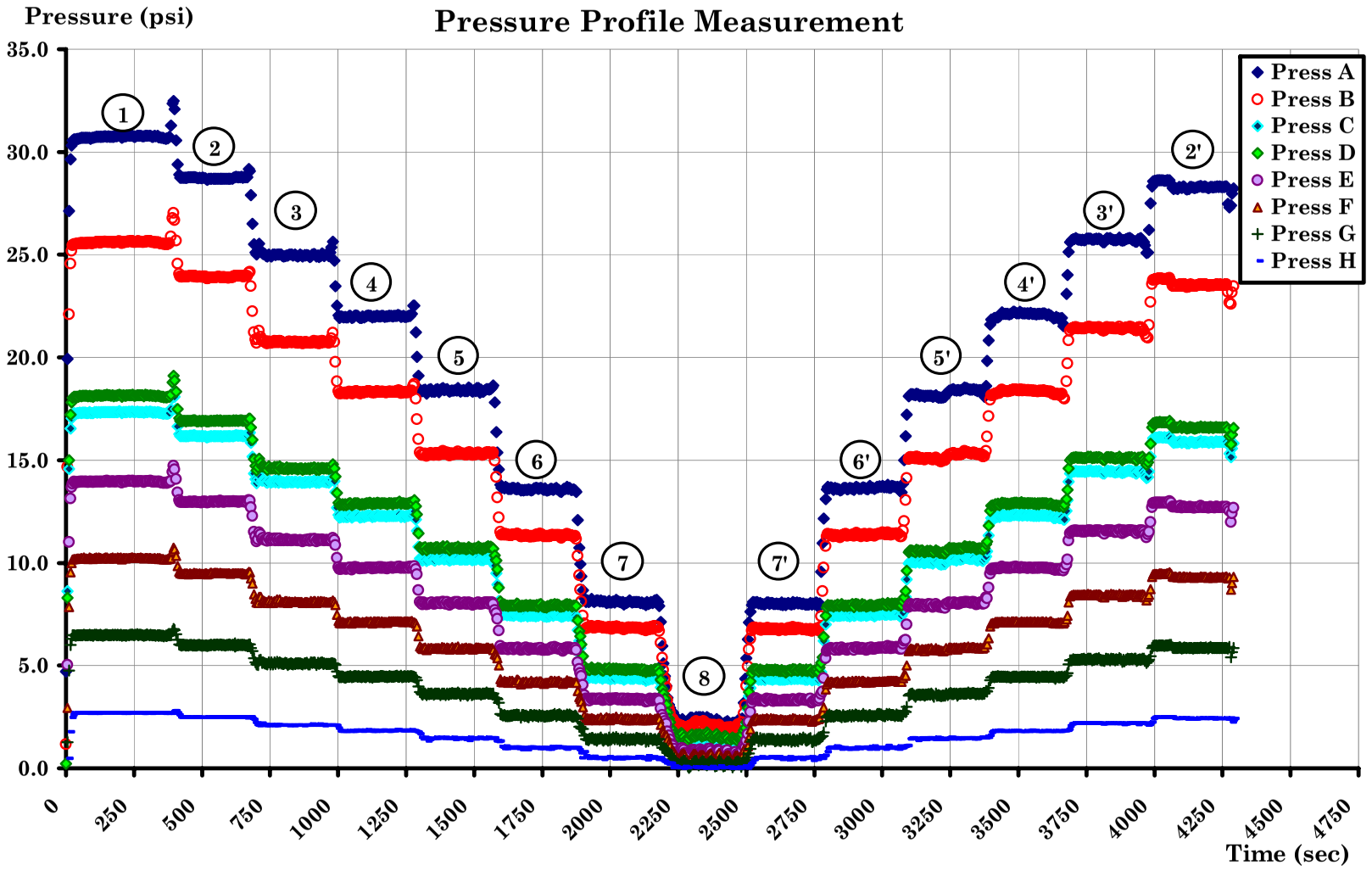

Fig. 4.29. Pressure response as a function of time with a stepwise change in gas and liquid injection rates (Case 14a): (0.5 inch NPS stainless steel pipe, 1 wt% surfactant concentration using Cedepal FA-406, 50 µm filter opening size)

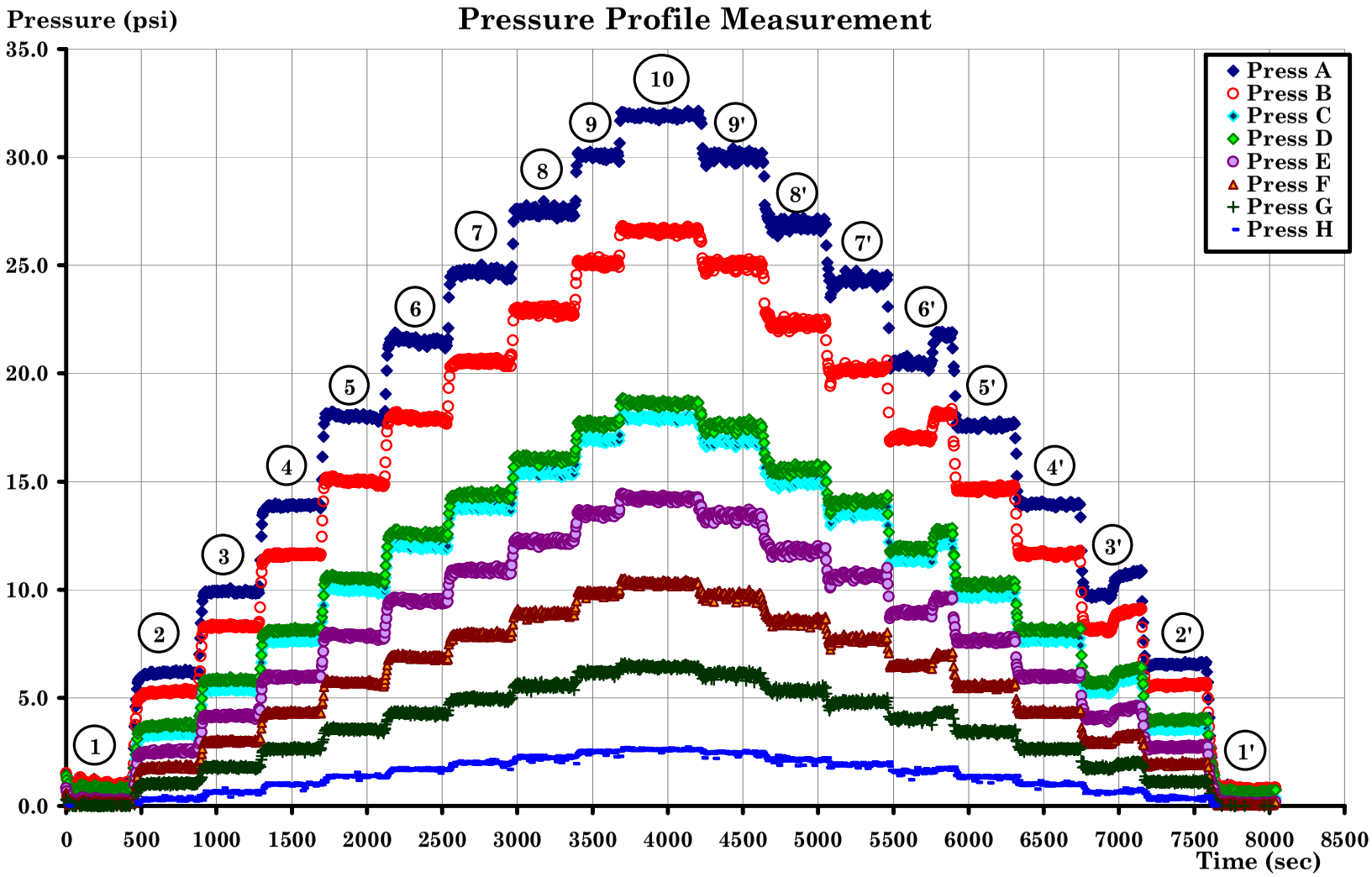

Fig. 4.30. Pressure response as a function of time with a stepwise change in gas and liquid injection rates (Case 14b): (0.5 inch NPS stainless steel pipe, 0.5 wt% surfactant concentration using Cedepal FA-406, 50 µm filter opening size)

4.8. Discussions

The experiments conducted in this study consistently show the presence of two flow regimes as shown in Fig. 4.31 schematically: a high-quality regime in which the pressure response is oscillating and a low-quality regime in which the pressure response is stabilized. This is because the two regimes are governed by different mechanisms.

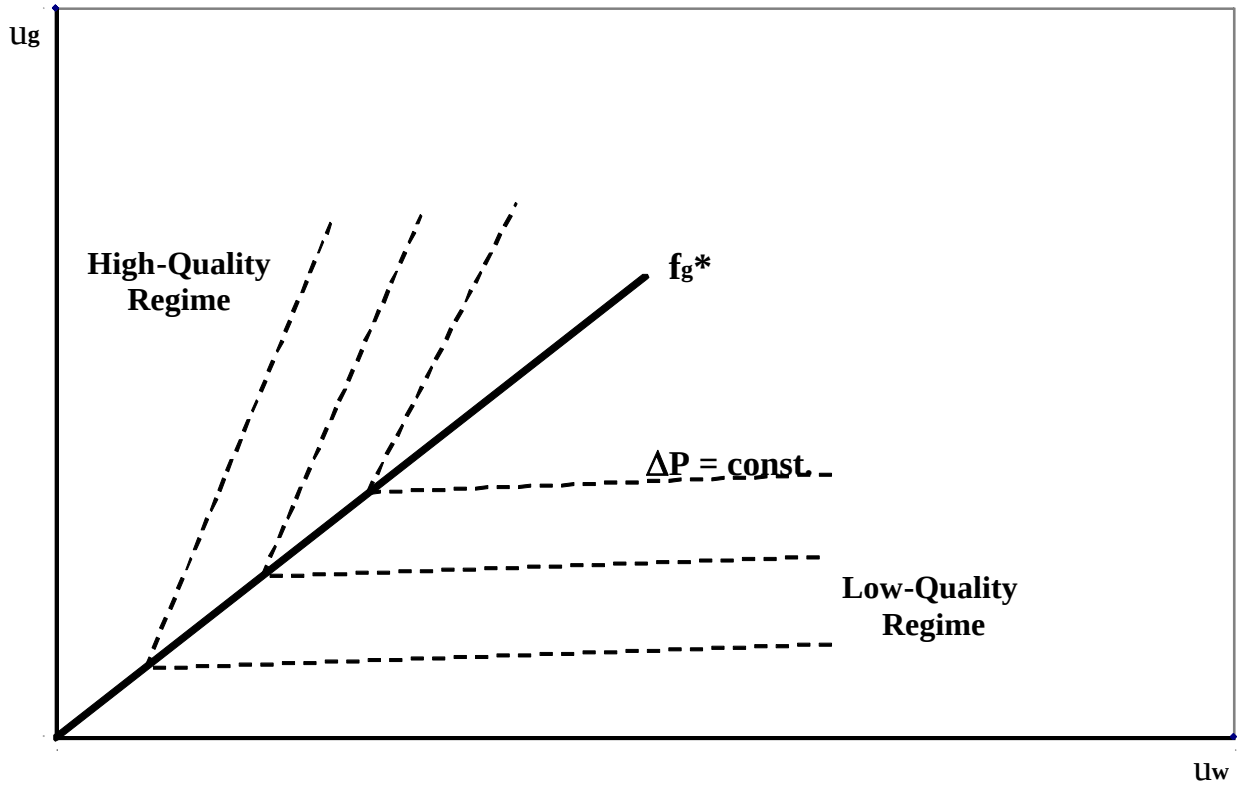

Fig. 4.31. Schematic representation of two flow regimes and pressure contours

The flow in the high-quality regime, as observed at the outlet of the pipe, is alternating slugs of gas and foam, as shown by the photos in Fig. 4.32. This recurring behavior is due to the fact that creating a continuous flow of fine-textured foam is not easy at high f_g (i.e., dry condition), implying that the unstable flow pattern in this regime is characterized by active bubble generation and coalescence mechanisms. The term, “steady-state” pressure drop, used in

this study may not be appropriate for foam in the high-quality regime because it does not seem to reach a steady state as shown in most of experiments.

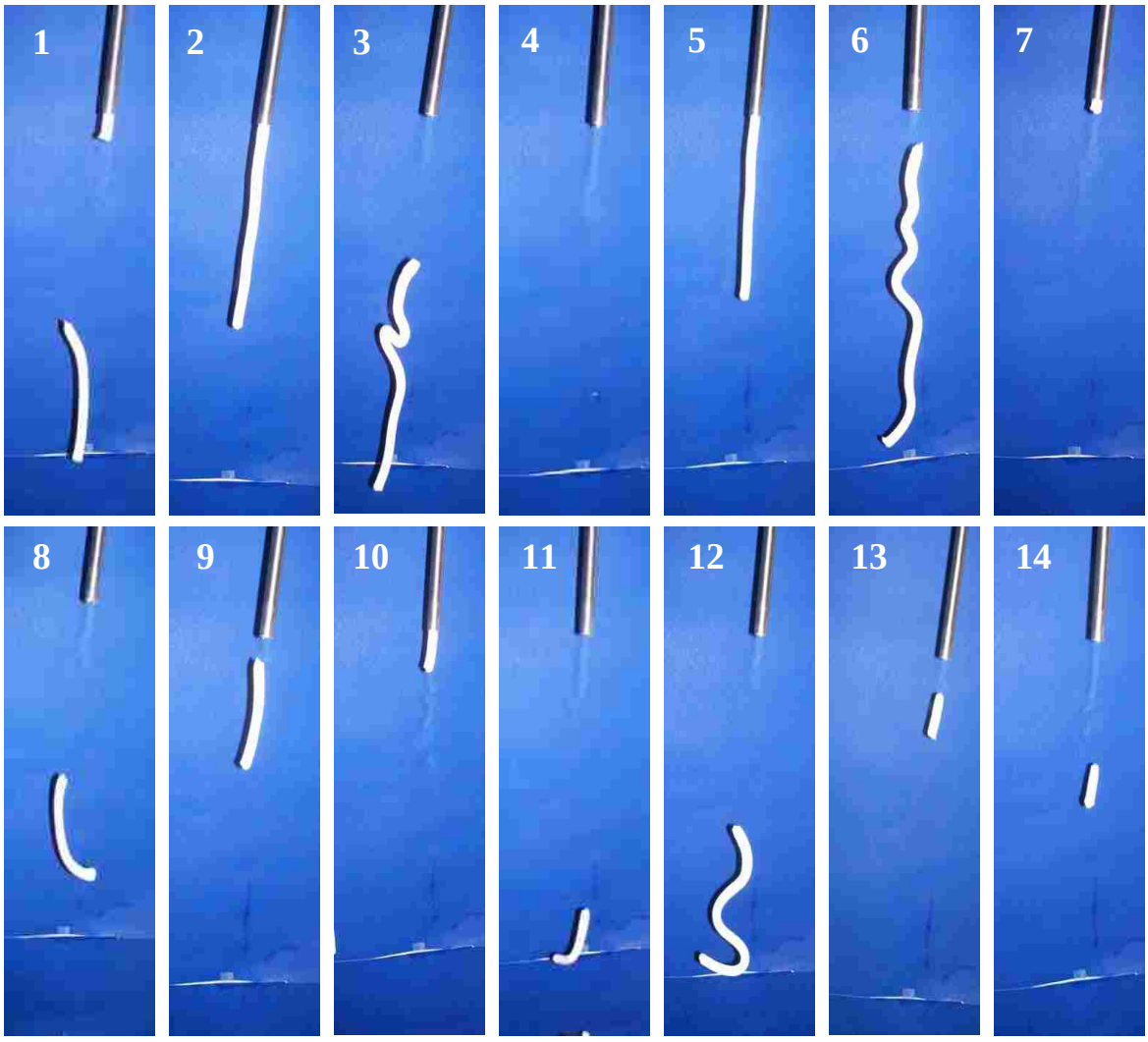

Fig. 4.32. Sequence of photos taken from the 0.5 inch pipe outlet showing repetition of free gas and foam slug within high-quality regime at foam quality above 99%.

The stable flow pattern that characterizes low-quality regime indicates that the flow rheology is governed by the movement of uniform and homogeneous fine-textured foam already present in the system, which is supported by the observation at the pipe outlet, shown in Fig. 4.33. The continuous flow of fine-textured foam in the low-quality regime implies that (1) the mechanisms of bubble creation and coalescence is less important for foams in the low-quality

regime because the steady-state fine foam texture is already obtained and maintained in the system, and (2) the interactions between bubbles and/or the interactions between bubbles and pipe surface under shear stress play a crucial role in overall flow behavior of foam in pipes. Fig. 4.34 shows the photos taken at the upstream visual cell.

Fig. 4.33. Sequence of homogeneous foam flow within low-quality regime at 0.5 inch pipe outlet at foam quality below 99%.

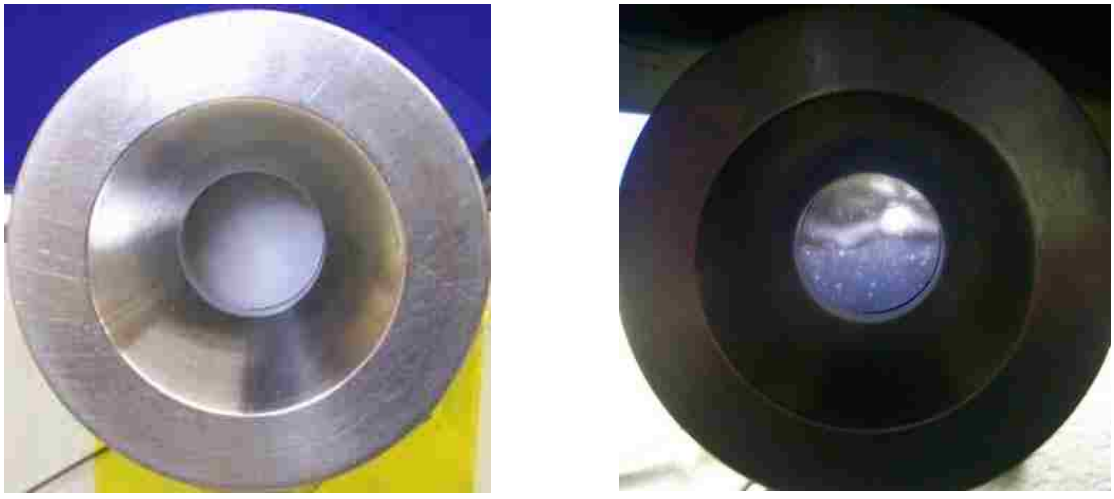

Fig. 4.34. Photos taken in the upstream visual cell: left with stable foam in the lower quality and right with unstable foam in the higher foam qualities.

The presence of two flow regimes during foam flow in pipes observed in this study is reminiscent of two steady-state strong-foam regimes during foam flow in porous media [Osterloh and Jante, 1992; Alvarez et al., 2001; Kam et al., 2007a]. Although a direct comparison cannot be made, the flow in pipes and the flow in porous media share a common ground in that the stability of foam films in dynamic motion is the key to the two flow regimes.

Another important aspect that should be noticed is the pattern of the pressure contours. As shown by the dotted lines in Fig. 4.31, the pressure contours are relatively steep in the high-quality regime and relatively gentle in the low-quality regime. This implies that in the high-quality regime, the additional amount of liquid supplied during the flow is used to create more stable bubbles contributing to more active interactions between bubbles and thus higher pressure gradients. In the low-quality regime, however the additional liquid is used to create thicker water films between bubbles or between bubbles and pipe surface, leading to the lower pressure gradients. This behavior in the low-quality regime seems similar to the lubricating effect reported by Briceño and Joseph, [2003]. Foams in the high-quality regime exhibit shear thickening behavior to the liquid injection velocity in all experiments throughout this study, whereas foams in the low-quality regime were shear thickening to the gas injection velocity in most of experiments in 0.5 inch NPS pipe and nearly Newtonian (or very slightly shear thinning) in 1 inch NPS pipe.

The boundary between the two regimes can be represented by a threshold value f_g called f_g* as shown in Fig. 4.35. The experiments in this study demonstrate that the f_g* shifts depending on experimental conditions. The value of f_g* increases as surfactant concentration increases and/or as the foamability of the surfactant increases. This observation also indicates that the high-quality regime is primarily governed by an unstable behavior, so any change that causes foams less stable is likely to expand the high-quality regime and contract the low-quality regime.

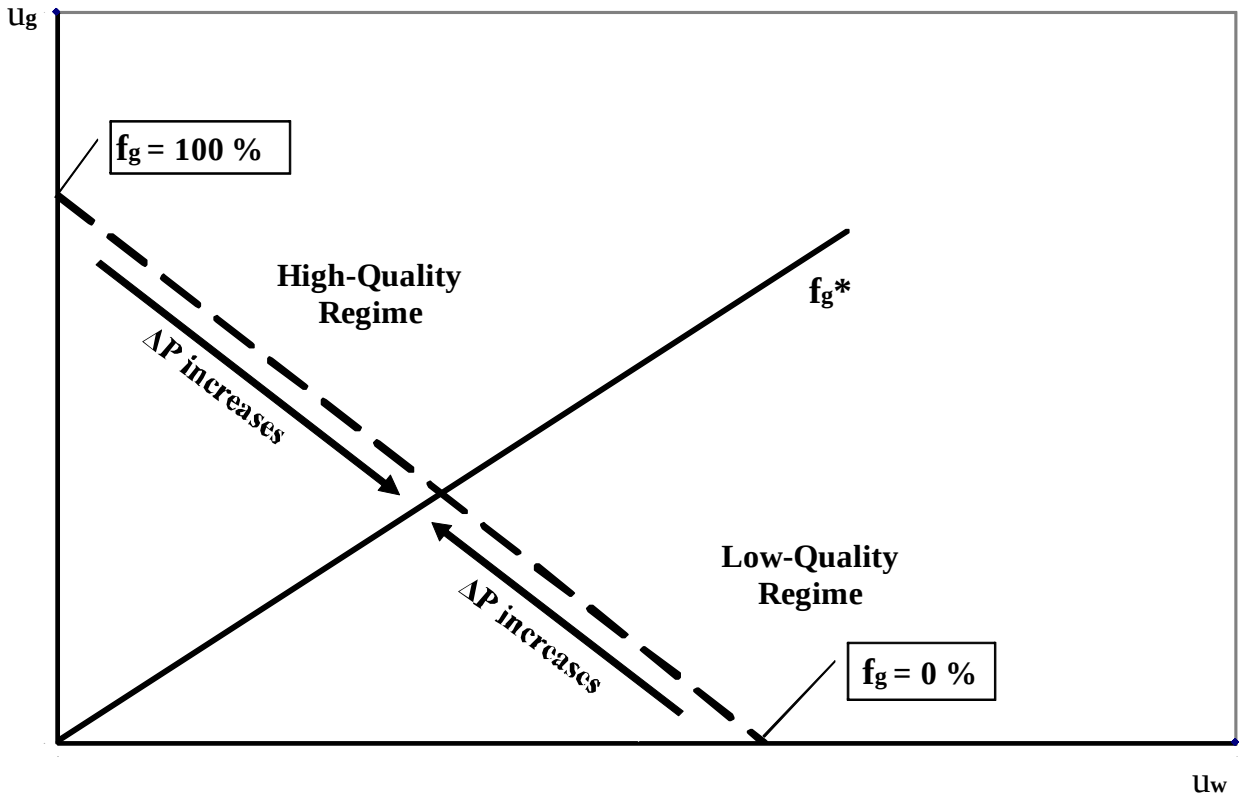

Fig. 4.35. Schematic representation of constant-total-injection-velocity experiment at varying foam quality (f_g)

The effect of the critical micelle concentration (CMC), above which interfacial tension does not change significantly with surfactant concentration, may play a role here such that the f_g* does not increase beyond a certain surfactant concentration.

Fig. 4.35 can be used to consider the effect of varying foam quality while keeping the total injection velocity (u_t) constant. Note that the constant-u_t experiment with increasing foam quality corresponds to moving along the broken straight line from f_g = 0% to f_g = 100% in Fig. 4.35. If the pressure contours in Fig. 4.31 are superimposed on Fig. 4.35, the pressure drop is expected to increase monotonically with increasing f_g until the pressure drop reaches its maximum value, and then the pressure drop decreases monotonically with increasing f_g. The maximum value in the pressure drop occurs at the boundary between the two flow regimes, or f_g*. Similar behavior can be found if one follows a vertical straight line (i.e., varying gas

injection velocity at fixed liquid injection velocity) or a horizontal straight line (i.e., varying liquid injection velocity at fixed gas injection velocity) in Fig. 4.35 in which the maximum pressure drop occurs near f_g*.

4.9. Implication of Two Flow Regimes in Field Applications

The two flow regimes demonstrated by the experiments in this study are believed to be crucial to the design and optimization of many foam applications because the flow rheology is very different depending on which regime the conditions fall. Changes in volume fraction of each phase, surfactant concentration, and/or surfactant performance may force the situation to cut across the boundary between the two regimes.

Fig. 4.36 can be used to investigate the significance of the two flow regimes, which show a few important features: (1) an application that undergoes a change in pressure and/or temperature may experience expansion or shrinkage of gas volume, which moves across the boundary between the two flow regimes (i.e., vertical dashed line in Fig. 4.36); (2) the loss or gain of liquid phase in the system may also go across the boundary (i.e., horizontal dashed line in Fig. 4.36); and (3) even though the injection velocities remain the same, any process that degrades surfactant molecules (i.e., deteriorating foamability of surfactant caused by, for example, high temperature or intrusion of foam-destabilizing oils) may shift the f_g* value substantially and cause the boundary to move across the existing operating conditions (i.e., diagonal dashed lines in Fig. 4.36). One example that has all these complexities is foam-assisted underbalanced drilling which can experience significant changes in pressure and temperature, influx of gas and/or liquid, dilution of surfactant solutions, degradation of foamability, change in flow conduit geometry, introduction of solid particles and so on. The knowledge gained about the two different foam flow regimes observed in this study is expected to greatly improve our understanding of these field applications.

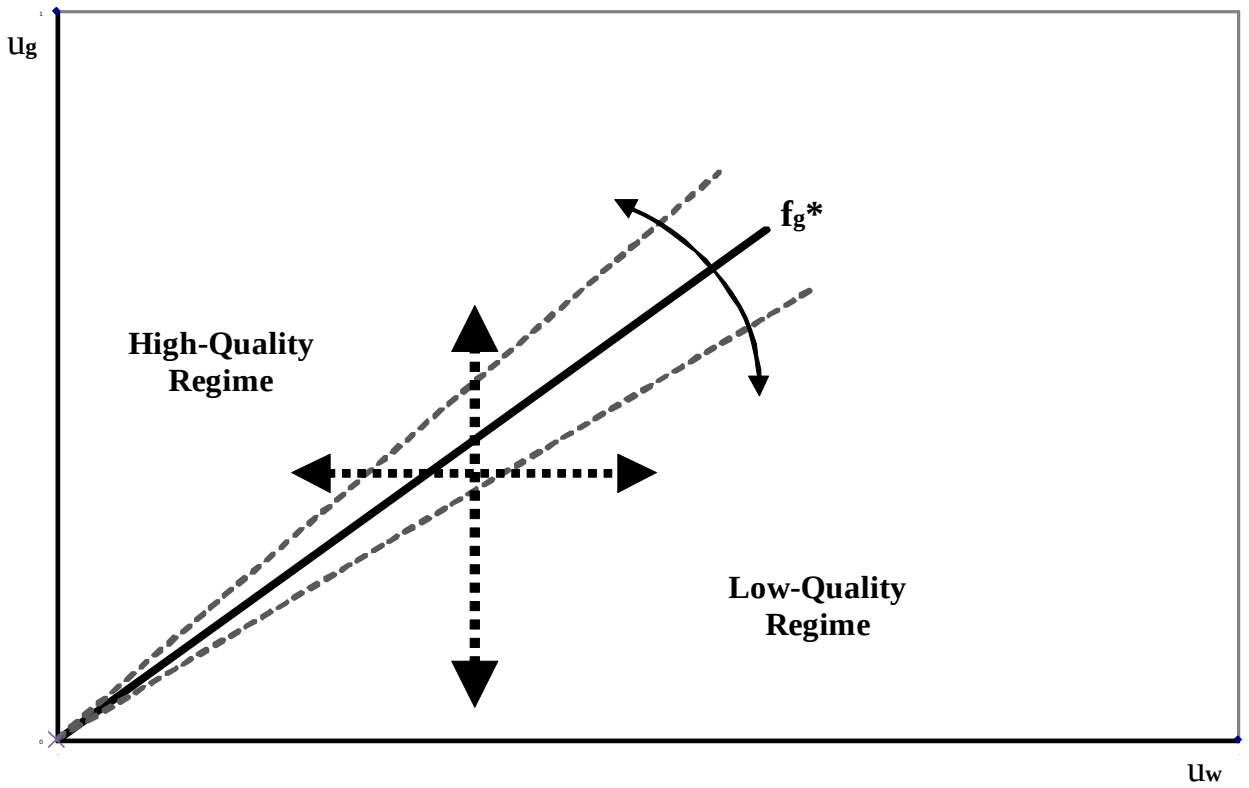

Fig. 4.36. Implication of the change in gas fraction (vertical dotted line), in liquid fraction (horizontal dotted line), or in f_g*.

5. CONCLUSIONS AND RECOMMENDATIONS

This experimental study investigates the rheological behavior of foams in horizontal pipes over a broad range of experimental conditions. These include two different pipe sizes (0.5 and 1 inch NPS stainless steel pipes), five different surfactant formulations (Cedepal FA-406, Petrostep CG-50, Stepanform 1050, Aquet TD-600, and Ultra Palmolive), three different surfactant concentrations (0.1 wt%, 1 wt%, and 5 wt%), and two different opening sizes of foam generating filters (50 μm and 90 μm). In all experiments, nitrogen gas and surfactant solutions were co-injected at pre-specified injection rates. Foam rheology in pipes was analyzed by looking into the pressure data measured from 8 different pressure ports (ports A through H) which were installed along the longitudinal pipe length. The following sections summarize more than 500 hundred experiments conducted in this study with conclusions and recommendations.

5.1. Conclusions

This experimental study can be summarized with the following conclusions:

1. The experimental results consistently showed two different flow regimes during foam flow in horizontal pipes: a high-quality regime and a low-quality regime. The high-quality foam flow regime was characterized by alternating flow of free gas and foam slugs causing an oscillating pressure response, while the low-quality regime was characterized by a flow of uniform and homogeneous foams showing stable pressure response. These two regimes were separated by a threshold value of foam quality (f_g) called f_g*.
2. The pressure contours plotted as a function of superficial gas and liquid injection velocities (u_g and u_w) in this study provided a convenient means of interpreting the regimes. The pressure contours, connecting the data points showing the same steady-state pressure drops, had a steep slope in the high-quality regime but a gentle (or negligible in some cases) slope in the low-quality regime. This suggests that these two flow regimes are controlled by different

governing mechanisms: the high-quality regime presumably by active competition between dynamic bubble creation and coalescence mechanisms struggling to obtain uniform and stable foam; and the low-quality regime by interactions between individual bubbles and/or bubbles and pipe surface under shear flow with foams already in a homogeneous and fine-textured state. This concept explains different sensitivity of the pressure drop to liquid injection velocity quite well: any increment of liquid injection velocity in the high-quality regime tends to increase the pressure drop by making bubble generation more active and foams more stable. Any positive increment of liquid injection velocity in the low-quality regime tends to reduce the pressure drop presumably by thickening water films and thus lowering the friction between bubbles and/or bubbles and pipe surface.

3. In all experiments, foams in the high-quality regime exhibited shear-thickening behavior to liquid injection velocity with the power-law exponents ranging from 1.4 to 3.2 (many around 1.4-1.7). Foams in the low-quality regime, however, exhibited shear-thickening behavior to the gas injection velocity with the power-law exponents around 1.4-1.7 in 0.5 inch NPS pipe but near-Newtonian (or slightly shear thinning) behavior in 1 inch NPS pipes. The experimental results also showed that the pressure drop decreased as gas injection velocity increased at fixed liquid injection velocity in the high-quality regime. The pressure drop in the low-quality regime, however, decreased slightly or was unchanged as liquid injection velocity increased at fixed gas injection velocity.
4. The value of f_g* that divides two flow regimes seems crucial to the optimum design of foam field applications. The experimental results showed that the f_g* could be affected by many factors including surfactant formulations and concentrations such that the high-quality regime stretched as the surfactant concentration decreased and/or as the foamability decreased. The results in this study further imply that any changes which influence the performance of

surfactant as a foamer are likely to change the value of f_g*, which, for example, could be caused by surfactant degradation, dilution of surfactant solutions, and intrusion of oil-destabilizing phases such as oils.

5. The use of two different filter opening sizes, 50μm and 90μm, did not result in meaningful changes in foam rheology in pipes. This implies that the fine-textured foam created by these foam generators was re-adjusted quickly so that the foam could reach its steady-state foam texture in the pipe. The steady-state foam texture and pressure response in pipes, however, might be impacted by the layout in the upstream of the pipe such as tubing length, tubing size, and the number of connections.

5.2. Recommendations

Based on the outcome of this study, the following can be recommended as future research topics:

1. A research challenge lies in the up-scaling of the experimental results observed in this study. The results from 0.5 inch and 1 inch pipes may not be appropriate to represent foam rheology in pipes with larger pipe diameters. The experiments in larger diameters will require much longer pipes in order for foam flow to reach a steady-state.
2. A small-scale experimental study should be developed in order to further investigate (1) the dynamic mechanisms of bubble creation and coalescence and (2) the bubble-to-bubble or bubble-to-pipe-wall interactions. This will help characterize foam rheology in the high-quality and low-quality regimes, respectively.
3. It is not certain how the experimental observations made in this study can be translated into the situations where foam flows with upward or downward inclination angles. Together with different flow geometry, the presence of solids and/or a third phase such as oils should be accounted for to extend this study to foam applications in drilling, fracturing, cementing, and

well completion treatments in petroleum industry.

4. For the applications such as deepwater underbalanced drilling in which the surfactant solution can be diluted by the influx of foreign fluids and/or the temperature may change significantly, the effect of degrading surfactant should be investigated separately to optimize the process.

REFERENCES

1. Alvarez, J. M., Rivas, H. and Rossen, W.R.: "A Unified Model for Steady-State Foam Behavior at High and Low Foam Qualities", SPE Journal 6, p.325-333, September, 2001.

2. Aronson, A.S., Bergeron, V., Fagan, M.E. and Radke, C.J.: "The Influence of Disjoining Pressure on Foam Stability and Foam in Porous Media", Colloids and Surfaces A: Physicochemical and Engineering Aspects, 83, p. 109-120, 1994.

3. Becher, P.: "Emulsions: Theory and Practice", Reinhold Pub. & Co., N.Y., 1965.

4. Bejuijen, A., Schminee, P.E.L. and Kleinjan, J.A.: "Additive Testing for Earth Pressure Balance Shields", Proceedings of the 12th European Conference on Soil Mechanics and Geotechnical Engineering, Amsterdam, June 7 – 10, 1999.

5. Beyer, A.H., Millhone, R.S. and Foote, R.W.: "Flow behavior of Foam as a Well Circulating Fluid", SPE 3986 presented at 47th Annual Fall Meeting held in San Antonio, Texas, October 8-11, 1972.

6. Bikerman, J.: "Foams", Applied Physics and Engineering Vol. 10, Springer-Verlag, Berlin, 1973.

7. Bird, R.B. and Stewart, W.E. and Lightfoot, E.N.: "Transport Phenomena", John Wiley and Sons, Inc, NYC, 1960.

8. Blauer, R.E., Mitchell, B.J. and Kohlhaas, C.A.: "Determination of Laminar, Turbulent, and Transitional Foam Flow Losses in Pipes", SPE 4885 presented at the 44th Annual California Regional Meeting of the Society of Petroleum Engineers of AIME, San Francisco, California, April 4-5, 1974.

9. Blauer, R.E. and Kohlhaas, C.A.: "Formation Fracturing with Foam", SPE 5003 presented at 44th Annual Fall Meeting of the Society of Petroleum Engineers of AIME held in Houston, Texas, October 6-9, 1974.

10. Bonilla, L.F. and Shah, S.N.: "Experimental Investigation on the Rheology of Foams", SPE 59752 presented at the SPE/CERI Gas Technology Symposium held in Calgary, Alberta Canada, April 3-5, 2000.

11. Bourgoyne, A.T.Jr., Chenevert, M.E., Millheim, K.K. and Young, F.S.Jr.: "Applied Drilling Engineering", SPE Textbook Series, Vol.2, Richardson, TX, 2005.

12. Briceño, M.I. and Joseph, D.D.: "Self-Lubricated Transportation of Aqueous Foams in Horizontal Conduits", International Journal of Multiphase Flow, 29, p. 1817-1831, May 2003.

13. Brookbank, M.R. and Fagiano, P.M.J.: “A Review of the Theory and Practice of Two-Phase Flow in Gas-Liquid Transmission Systems”, SPE 5264 presented at the SPE-European Spring Meeting held in London, Great Britain, April 14-15, 1975.

14. Calvert, J.R. and Nezhati, K.: “A Rheological Model for a Liquid–Gas Foam”, International Journal of Heat and Fluid Flow, 7, p. 164-168, 1986.

15. David, A. and Marsden, S.S.: “The Rheology of Foam”, SPE 2544 presented at the 44th Annual Meeting of the SPE, Denver, CO, September 28, 1969.

16. Dholkawala, Z.F., Sarma, H.K. and Kam, S.I.: “Application of Fractional Flow Theory to Foams in Porous Media”, Journal of Petroleum Science and Engineering, Vol. 57, p. 138-160, May, 2007.

17. Einstein, A.: “Eine Neue Bestimmung Der Molekul-dimensionen”, Annalen Der Physik, Vol. 19, Ser. 4, p.289, 1906.

18. Gardiner, B.S., Dlugogorski, B.Z. and Jameson, G.J.: “Prediction of Pressure Losses in Pipe Flow of Aqueous Foams”, Industrial and Engineering Chemistry Research, 38, p. 1099-1106, May 1999.

19. Gaulitz, P.A., Friedmann, F., Kam, S.I. and Rossen, W.R.: “Foam Generation in Homogenous Porous Media”, SPE 75177 presented at SPE/DOE 13th Symposium on Improved Oil Recovery, Tulsa, Oklahoma, April 13-17, 2002; also published as "Foam Generation in Homogeneous Porous Media," Chemical Engineering and Science, Vol. 57, p. 4037-4052, October, 2002.

20. Guzman, N., Shoham, O. and Mohan R.: “Rheology of Aqueous Two-Phase Foam Flow in Horizontal Pipes”, Journal of Energy Resources Technology, 2005.

21. Guzman, N.: “Foam Flow in Gas-Liquid Cylindrical Cyclone (GLCC) Compact Separator”, PhD Dissertation, The University of Tulsa, Oklahoma, 2005.

22. Harris, P.C. and Reidenbach, V.G.: “High-Temperature Rheological Study of Foam Fracturing Fluids”, SPE 13177 presented at SPE Annual Technical Conference held in Houston, September 16-19, 1984.

23. Harris, P.C.: “Effects of Texture on Rheology of Foam Fracturing Fluids”, SPE 14257 presented at SPE Annual Technical Conference held in Las Vegas, September 22-25, 1985.

24. Harris, P.C., Klebenow, D.E. and Kundert, P.D.: “Constant-internal-phase Design Improves Simulation Results”, SPE Production Engineering, 6 (1), 1991.

25. Harris, P.C. and Heath, S.J.: “Rheology of Crosslinked Foams”, SPE 28512 presented at SPE Annual Technical Conference held in New Orleans, September 25-28, 1994.

26. Harris, P.C. and Heath, S.J.: “High-Quality Foam Fracturing Fluids”, SPE 35600 presented at the SPE Gas Technology Symposium held in Calgary, Alberta, Canada, April 28 – May 1, 1996.

27. Hatschek, E.: “Die Viscositat Der Dispersoide II. Die Emulsionen Uns Emulsoide”, Kolloid Z, Vol. 8. p. 34, 1910.

28. Hutchins, R.D. and Miller, M.J.: “A Circulating Foam Loop for Evaluating Foam at Conditions of Use”, SPE 80242 presented at the SPE International Symposium on Oilfield Chemistry held in Houston, Texas, U.S.A., February 5-7, 2003.

29. Irani, C.A. and Solomon Jr. C.: “Slim-Tube Investigation of CO_2 Foams”, SPE 14962 presented at the SPE/DOE Fifth Symposium on Enhanced Oil Recovery of the Society of Petroleum Engineers and the Department of Energy held in Tulsa, Oklahoma, April 20-23, 1988.

30. Kam, S. I. and Rossen, W.R.: “The Compressibility of Foamy Sands”, Colloids and Surfaces A: Physicochemical and Engineering Aspects, 202, p. 63-70 , 2002.

31. Kam, S. I., Gauglitz, P.A. and Rossen, W.R.: “The Yield Stress of Foamy Sands”, Colloids and Surfaces A: Physicochemical and Engineering Aspects, 202 (1), p. 53-62, 2002.

32. Kam, S.I. and Rossen, W.R.: “A Model for Foam Generation in Homogeneous Porous Media”, SPE Journal, 8, p. 417-425, December, 2003.

33. Kam, S.I., Frenier, W.W., Davies, S.N. and Rossen, W.R.: “Experimental Study of High-Temperature Foam for Acid Diversion”, Journal of Petroleum Science and Engineering, Vol. 58, p. 138–160, August 2007a.

34. Kam, S.I., Nguyen, Q.P., Li, Q. and Rossen, W.R.: “Dynamic Simulation with an Improved Model for Foam Generation”, SPE Journal, p. 35–48, March, 2007b.

35. Khatib, Z.I., Hirasaki, G.J. and Falls, A.H.: “Effect of Capillary Pressure on Coalescence and Phase Mobilities in Foams Flowing Through Porous Media”, SPE Reservoir Engineering, p. 919-926, August, 1988.

36. Kibodeaux, K.R.: “Experimental and Theoretical Studies of Foam Mechanisms in Enhanced Oil Recovery and Matrix Acidization Applications”, Ph.D. Dissertation, The University of Texas at Austin, 1997.

37. Kim, J. S., Dong, Y. and Rossen, W. R.: “Steady-State Flow Behavior of CO2 Foam”, SPE Journal, 10, p. 405-415, December, 2005.

38. Kovscek, A. R. and Radke, C. J.: “Fundamentals of Foam Transport in Porous Media”, in: L. L. Schramm (ed.), Foams: Fundamentals and Applications in the Petroleum Industry, ACS Advances in Chemistry Series No. 242, Am. Chem. Soc., Washington DC, 1994.

39. Kraynik, A.M.: “Foam Flows”, Annual Revision of Fluid Mechanics, 20, p. 325 – 357, 1988.

40. Lourenço, A.M.F., Miska, S.Z., Reed, T.D., Pickell, M.B. and Takach, N.E.: “Study of the Effects of Pressure and Temperature on the Rheology of Drilling Foams and Frictional Pressure Losses”, SPE 84175 presented at the SPE Annual Technical Conference held in Denver, Colorado, October 5-8, 2003.

41. Mamun, C.K., Rong, J.G., Kam, S.I., Liljestrand, H.M. and Rossen, W.R.: “Simulating Use of Foam in Aquifer Remediation”, Proceedings of the 14th International Conference on Computational Methods in Water Resources (CMWR XIV), June 23-28, 2002, Delft, The Netherlands, S.M. Hassanizadeh, R.J. Schotting, W.G. Gray, G.F. Pinder, eds., Volume 1, p. 867-874.

42. Mitchell, B.J.: “Viscosity of Foam”, PhD Thesis, University of Tulsa, Oklahoma, 1969.

43. Mitchell, B.J.: “Test data Fill Theory gap on Using Foam as a Drilling Fluid”, Oil and Gas Journal, p. 96-100, September, 1971.

44. Mooney, M.: “Explicit Formulas for Slip and Fluidity”, Journal of Rheology, 1931.

45. Okpobiri, G.A. and Ikoku, C.U.: “Volumetric Requirements for Foam and Mist Drilling Operations”, SPE 11723 presented at the SPE California Regional Meeting in Ventura, March 23-25, 1983.

46. Osterloh, W.T. and Jante, M.J.: “Effects of Gas and Liquid Velocity on Steady-State Foam Flow at High Temperature”, SPE 24179 presented at SPE/DOE eight Symposium on Enhanced Oil Recovery held in Tulsa, Oklahoma, April 22-24, 1992.

47. Ozbayoglu, E.M. and Akin, S.: “Foam Characterization Using Image Processing Techniques”, SPE 93860 presented at SPE Western Regional Meeting held in Irvine, California, March 30 – April 1, 2005.

48. Princen, H.M.: “Rheology of Foams and Highly Concentrated Emulsions. I. Elastic Properties and Yield Stress of a Cylindrical Model System”, Journal of Colloid and Interface Science, 105. p. 150-171, 1983.

49. Prud'homme, R.H. and Bird, R.B.: "The Dilatational Properties of Suspensions of Gas Bubbles in incompressible Newtonian and Non-Newtonian Fluids", Journal of Non-Newtonian Fluid Mechanics, 3: 261-279, 1978.

50. Prud'homme, R. H.: "Foam Flow", Presented at Ann. Meeting Soc. Rheol., Louisiana, KY., October 12-15, 1981.

51. Prud'homme, R. H. and Khan, S.(eds.), "Foams: Theory, Measurements and Applications", Marcel Dekker, New York, p. 413 – 464, 1996.

52. Raza, S.H. and Marsden, S.S.: "The Streaming Potential and the Rheology of Foam", SPE Journal, Vol. 7, p. 4, 1967.

53. Rong, J.G.: "Experimental Evaluation of Foam in Environmental Remediation", Department of Civil Engineering, PhD dissertation, The University of Texas at Austin, 2002.

54. Rossen, W. R.: "Foams in Enhanced Oil Recovery", in: R. K. Prud'homme and Khan, S. (eds.), "Foams: Theory, Measurements and Applications", Marcel Dekker, New York, 1996.

55. Rossen, W.R. and Wang, M.W.: "Modeling Foams for Acid Diversion", SPE Journal, 4, p. 92-100, June, 1999.

56. Rossen, W.R.: "Application of Percolation Concepts to Foam Flow Through Porous Media", Campus Theory presented at the Science at the Edge Seminar, May, 2003.

57. Saintpere, S., Herzhaft, B., Toure, A. and Jollet, S.: "Rheological Properties of Aqueous Foams for Underbalanced Drilling", SPE 56633 presented at SPE Annual Technical Conference and Exibition held in Houston, Texas, October 3-6, 1999.

58. Schramm, L.: "FOAMS: Fundamentals and Applications in the Petroleum Industry", Advances in Chemistry series 242, American Chemical Society, Washington, D.C., 1994.

59. Taitel, Y. and Dukler, A.E.: "A Model for Predicting Flow Regime Transition in Horizontal and Near-Horizontal Gas-Liquid Flow", American Institute of Chemical Engineers 22, p. 47-55, 1976.

60. Tan, H.C.S. and McGowen, J.M.: "Friction Pressure Correlation for CO_2 Foam Fluids", SPE 21856 presented at the Rocky Mountain Regional Meeting and Low-Permeability Reservoir Symposium held in Denver, Colorado, April 15-17, 1991.

61. Valko, P., Economides, M.J., Baumgarthner, S.A. and McElfresh, P.M.: “The Rheological Properties of Carbon Dioxide and Nitrogen Foams”, SPE 23778 presented at the SPE International Symposium on Formation Damage Control held in Lafayette, Louisiana, February 25-27, 1992.

62. Wilson, A. J. D.: “Foams: Physics, Chemistry and Structure”, Springer-Verlag, New York, 1989.

APPENDIX A

EXPERIMENTAL DATA FOR CASES 1 THROUGH 12

Case 1 (Base Case)

Pipe: 0.5" Nominal Pipe Size, 0.36 inch ID, 12.3 ft long, Stainless Steel **Surfactant: CEDEPAL FA-406**

Foam Generator Opening Size: 50 μm **Surfactant Concentration: 1 wt % in Liquid Solution**

Test No	Liquid Rate ml/min	Gas Rate Scc/min	Total Rate cc/min	fg %	Pavg at A Psi	Pavg at H Psi	Pavg Psi	ΔPA-H Psi	Qgas cc/min	Uliquid m/sec	Ugas m/sec	Ut m/sec	dP/dL psi/ft
1	60	3000	3060	98.04	23.25	1.98	12.62	21.27	1614.5	0.0152	0.410	0.425	1.74
2	60	4000	4060	98.52	29.53	2.52	16.03	27.01	1913.8	0.0152	0.486	0.501	2.21
3	60	5000	5060	98.81	35.07	3.04	19.06	32.03	2177.5	0.0152	0.553	0.568	2.62
4	40	5000	5040	99.21	24.31	1.85	13.09	22.45	2645.3	0.0102	0.671	0.682	1.83
5	40	4000	4040	99.01	30	2.51	16.26	27.49	1899.5	0.0102	0.482	0.492	2.25
6	80	4000	4080	98.04	27.77	2.4	15.09	25.37	1974.1	0.0203	0.501	0.521	2.07
7	80	5000	5080	98.43	33.45	2.92	18.19	30.53	2235.1	0.0203	0.567	0.588	2.49
8	80	3000	3080	97.40	21.53	1.74	11.64	19.79	1674.6	0.0203	0.425	0.445	1.62
9	40	3000	3040	98.68	25.93	2.18	14.06	23.75	1533.6	0.0102	0.389	0.399	1.94
10	20	3000	3020	99.34	8.51	0.49	4.50	8.02	2296.9	0.0051	0.583	0.588	0.66
11	20	4000	4020	99.50	4.16	0.14	2.15	4.02	3489.6	0.0051	0.886	0.891	0.33
12	20	5000	5020	99.60	2.68	0.04	1.36	2.64	4576.6	0.0051	1.162	1.167	0.22
13	20	2000	2020	99.01	19.18	1.4	10.29	17.78	1176.5	0.0051	0.299	0.304	1.45
14	20	1000	1020	98.04	10.04	0.65	5.35	9.39	733.3	0.0051	0.186	0.191	0.77
15	40	2000	2040	98.04	17.92	1.44	9.68	16.48	1205.9	0.0102	0.306	0.316	1.35
16	60	2000	2060	97.09	16.05	1.28	8.67	14.77	1258.3	0.0152	0.319	0.335	1.21
17	80	2000	2080	96.15	14.7	1.18	7.94	13.52	1298.6	0.0203	0.330	0.350	1.10
18	80	1000	1080	92.59	7.3	0.52	3.91	6.78	789.9	0.0203	0.200	0.221	0.55
19	60	1000	1060	94.34	7.52	0.53	4.03	6.99	785.0	0.0152	0.199	0.214	0.57
20	40	1000	1040	96.15	8.36	0.59	4.48	7.77	766.6	0.0102	0.195	0.205	0.63
21	20	500	520	96.15	4.85	0.23	2.54	4.62	426.3	0.0051	0.108	0.113	0.38
22	40	500	540	92.59	4	0.19	2.10	3.81	437.6	0.0102	0.111	0.121	0.31
23	60	500	560	89.29	3.42	0.15	1.79	3.27	445.9	0.0152	0.113	0.128	0.27
24	80	500	580	86.21	2.94	0.11	1.53	2.83	453.0	0.0203	0.115	0.135	0.23

Case 2

Pipe: 0.5" Nominal Pipe Size, 0.36 inch ID, 12.3 ft long, Stainless Steel **Surfactant: CEDEPAL FA-406**

Foam Generator Opening Size: 50 μm **Surfactant Concentration: 5 wt % in Liquid Solution**

Test No.	Liquid Rate ml/min	Gas Rate Scc/min	Total Rate cc/min	fg %	Pavg at A Psi	Pavg at H Psi	Pavg Psi	ΔPA-E Psi	Qgas cc/min	Uliquid m/sec	Ugas m/sec	Ut m/sec	dP/dL psi/ft
1	60	3000	3060	98.04	23.87	1.74	12.81	22.13	1503.3	0.0152	0.407	0.422	1.81
2	60	4000	4060	98.52	30.36	2.26	16.31	28.1	1896.2	0.0152	0.481	0.496	2.30
3	60	5000	5060	98.81	36.16	2.72	19.44	33.44	2152.9	0.0152	0.546	0.562	2.73
4	40	5000	5040	99.21	39.4	2.88	21.14	36.52	2050.8	0.0102	0.520	0.531	2.98
5	40	4000	4040	99.01	33.07	2.9	17.99	30.17	1799.0	0.0102	0.457	0.467	2.47
6	80	4000	4080	98.04	28.11	2.1	15.11	26.01	1972.8	0.0203	0.501	0.521	2.13
7	80	5000	5080	98.43	33.57	2.5	18.04	31.07	2245.3	0.0203	0.570	0.590	2.54
8	80	3000	3080	97.40	22.05	1.58	11.82	20.47	1563.2	0.0203	0.422	0.442	1.67
9	40	3000	3040	98.68	26.5	2.4	14.45	24.1	1512.9	0.0102	0.384	0.394	1.97
10	20	3000	3020	99.34	30.38	2.1	16.24	28.28	1425.3	0.0051	0.362	0.367	2.31
11	20	4000	4020	99.50	37.55	2.68	20.12	34.87	1688.9	0.0051	0.429	0.434	2.85
12	20	5000	5020	99.60	44.05	3.22	23.64	40.83	1917.3	0.0051	0.487	0.492	3.34
13	20	2000	2020	99.01	22.09	1.5	11.80	20.59	1109.6	0.0051	0.282	0.287	1.68
14	20	1000	1020	98.04	11.42	0.71	6.07	10.71	707.9	0.0051	0.180	0.185	0.88
15	40	2000	2040	98.04	18.8	1.52	10.16	17.28	1182.6	0.0102	0.300	0.310	1.41
16	60	2000	2060	97.09	16.75	1.22	8.99	15.53	1241.3	0.0152	0.315	0.330	1.27
17	80	2000	2080	96.15	16.03	1.24	8.64	14.79	1259.9	0.0203	0.320	0.340	1.21
18	80	1000	1080	92.59	8.3	0.59	4.45	7.71	767.8	0.0203	0.195	0.215	0.63
19	60	1000	1060	94.34	8.42	0.57	4.50	7.85	765.8	0.0152	0.194	0.210	0.64
20	40	1000	1040	96.15	8.95	0.59	4.77	8.36	755.0	0.0102	0.192	0.202	0.68
21	20	500	520	96.15	4.65	0.23	2.44	4.42	428.8	0.0051	0.109	0.114	0.36
22	40	500	540	92.59	4.2	0.21	2.21	3.99	434.8	0.0102	0.110	0.120	0.33
23	60	500	560	89.29	3.8	0.17	1.99	3.63	440.5	0.0152	0.112	0.127	0.30
24	80	500	580	86.21	3.4	0.15	1.78	3.25	446.1	0.0203	0.113	0.134	0.27

Case 3

Pipe: 0.5" Nominal Pipe Size, 0.36 inch ID, 12.3 ft long, Stainless Steel **Surfactant: CEDEPAL FA-406**

Foam Generator Opening Size: 50 μm **Surfactant Concentration: 0.1 wt % in Liquid Solution**

Test	Liquid Rate	Gas Rate	Total Rate	fg	Pavg at A	Pavg at H	Pavg	ΔP_{A-H}	Qgas	Uliquid	Ugas	Ut	dP/dL
No.	ml/min	Scc/min	cc/min	%	Psi	Psi	Psi	Psi	cc/min	m/sec	m/sec	m/sec	psi/ft
1	60	3000	3060	98.04	0.12	0	0.06	0.12	2987.8	0.0152	0.758	0.774	0.01
2	80	3000	3080	97.40	0.31	0	0.16	0.31	2968.7	0.0203	0.753	0.774	0.03
3	80	2000	2080	96.15	0.88	0	0.44	0.88	1941.9	0.0203	0.493	0.513	0.07
4	60	2000	2060	97.09	0.41	0	0.21	0.41	1972.5	0.0152	0.501	0.516	0.03
5	40	2000	2040	98.04	0.18	0	0.09	0.18	1987.8	0.0102	0.505	0.515	0.01
6	80	1000	1080	92.59	3.06	0.09	1.58	2.97	903.2	0.0203	0.229	0.250	0.24
7	60	1000	1060	94.34	2.02	0.01	1.02	2.01	935.4	0.0152	0.237	0.253	0.16
8	40	1000	1040	96.15	1.4	0	0.70	1.4	954.5	0.0102	0.242	0.252	0.11
9	20	1000	1020	98.04	0.74	0	0.37	0.74	975.4	0.0051	0.248	0.253	0.06
10	20	500	520	96.15	1.83	0.01	0.92	1.82	470.6	0.0051	0.119	0.125	0.15
11	40	500	540	92.59	1.96	0.03	1.00	1.93	468.3	0.0102	0.119	0.129	0.16
12	60	500	560	89.29	2.14	0.05	1.10	2.09	465.3	0.0152	0.118	0.133	0.17
13	80	500	580	86.21	2.13	0.05	1.09	2.08	465.5	0.0203	0.118	0.138	0.17

Case 4

Pipe: 0.5" Nominal Pipe Size, 0.36 inch ID, 12.3 ft long, Stainless Steel

Surfactant: CEDEPAL FA-406

Foam Generator Opening Size: 90 μm

Surfactant Concentration: 1 wt % in Liquid Solution

Test No.	Liquid Rate ml/min	Gas Rate Scc/min	Total Rate cc/min	fg %	Pavg at A Psi	Pavg at H Psi	Pavg Psi	ΔP_{A-H} Psi	Qgas cc/min	Uliquid m/sec	Ugas m/sec	Ut m/sec	dP/dL psi/ft
1	80	3000	3080	97.40	21.63	1.84	11.74	19.79	1668.2	0.0203	0.423	0.444	1.62
2	80	4000	4080	98.04	27.95	2.44	15.20	25.51	1966.9	0.0203	0.499	0.519	2.08
3	80	5000	5080	98.43	33.8	3.07	18.44	30.73	2218.2	0.0203	0.563	0.583	2.51
4	60	5000	5060	98.81	35.3	3.05	19.18	32.25	2169.7	0.0152	0.551	0.566	2.64
5	40	5000	5040	99.21	24.23	1.86	13.05	22.37	2649.1	0.0102	0.672	0.682	1.83
6	20	5000	5020	99.60	2.77	0.07	1.42	2.7	4559.6	0.0051	1.157	1.162	0.22
7	20	4000	4020	99.50	4.23	0.1	2.17	4.13	3486.5	0.0051	0.885	0.890	0.34
8	20	3000	3020	99.34	8.67	0.63	4.65	8.04	2279.1	0.0051	0.578	0.583	0.66
9	20	2000	2020	99.01	18.1	1.31	9.71	16.79	1204.7	0.0051	0.306	0.311	1.37
10	20	1000	1020	98.04	3.04	0.5	4.27	7.54	774.9	0.0051	0.197	0.202	0.62
11	40	3000	3040	98.68	24.85	2.04	13.45	22.81	1566.9	0.0102	0.398	0.408	1.86
12	40	4000	4040	99.01	29.47	2.39	15.93	27.08	1919.7	0.0102	0.487	0.497	2.21
13	60	2000	2060	97.09	15.61	1.28	8.45	14.33	1270.3	0.0152	0.322	0.338	1.17
14	60	3000	3060	98.04	23.31	2	12.66	21.31	1612.1	0.0152	0.409	0.424	1.74
15	60	4000	4060	98.52	30	2.62	16.31	27.38	1896.2	0.0152	0.481	0.496	2.24
16	80	2000	2080	96.15	14.5	1.19	7.85	13.31	1304.1	0.0203	0.331	0.351	1.09
17	40	2000	2040	98.04	17.23	1.38	9.31	15.85	1224.7	0.0102	0.311	0.321	1.30
18	80	1000	1080	92.59	6.57	0.45	3.51	6.12	807.2	0.0203	0.205	0.225	0.50
19	60	1000	1060	94.34	6.75	0.45	3.60	6.3	803.3	0.0152	0.204	0.219	0.51
20	40	1000	1040	96.15	7.44	0.49	3.97	6.95	787.6	0.0102	0.200	0.210	0.57
21	20	500	520	96.15	3.61	0.09	1.85	3.52	444.1	0.0051	0.113	0.118	0.29
22	40	500	540	92.59	2.42	0.05	1.24	2.37	461.2	0.0102	0.117	0.127	0.19
23	60	500	560	89.29	2.28	0.04	1.16	2.24	463.4	0.0152	0.118	0.133	0.18
24	80	500	580	86.21	2.38	0.07	1.23	2.31	461.5	0.0203	0.117	0.137	0.19

Case 5

Pipe: 0.5" Nominal Pipe Size, 0.36 inch ID, 12.3 ft long, Stainless Steel **Surfactant: CEDEPAL FA-406**

Foam Generator Opening Size: 90 μm **Surfactant Concentration: 5 wt % in Liquid Solution**

Test	Liquid Rate	Gas Rate	Total Rate	fg	Pavg at A	Pavg at H	Pavg	ΔP_{A-H}	Qgas	Uliquid	Ugas	Ut	dP/dL
No.	ml/min	Scc/min	cc/min	%	Psi	Psi	Psi	Psi	cc/min	m/sec	m/sec	m/sec	psi/ft
1	80	3000	3080	97.40	21.77	1.64	11.71	20.13	1670.1	0.0203	0.424	0.444	1.64
2	80	4000	4080	98.04	27.81	2.1	14.96	25.71	1982.8	0.0203	0.503	0.524	2.10
3	80	5000	5080	98.43	33.63	2.57	18.10	31.06	2240.9	0.0203	0.569	0.589	2.54
4	60	5000	5060	98.81	36.15	2.73	19.44	33.42	2152.9	0.0152	0.546	0.562	2.73
5	40	5000	5040	99.21	39.33	2.92	21.13	36.41	2051.6	0.0102	0.521	0.531	2.98
6	20	5000	5020	99.60	44.04	3.28	23.66	40.76	1916.1	0.0051	0.486	0.491	3.33
7	20	4000	4020	99.50	37.37	2.69	20.03	34.68	1693.1	0.0051	0.430	0.435	2.83
8	20	3000	3020	99.34	30.04	2.11	16.08	27.93	1433.0	0.0051	0.364	0.369	2.28
9	20	2000	2020	99.01	20.89	1.46	11.18	19.43	1136.2	0.0051	0.288	0.293	1.59
10	20	1000	1020	98.04	9.71	0.62	5.17	9.09	740.0	0.0051	0.188	0.193	0.74
11	40	3000	3040	98.68	26.42	1.99	14.21	24.43	1525.7	0.0102	0.387	0.397	2.00
12	40	4000	4040	99.01	33.11	2.42	17.77	30.69	1811.2	0.0102	0.460	0.470	2.51
13	60	2000	2060	97.09	16.62	1.26	8.94	15.36	1243.7	0.0152	0.316	0.331	1.26
14	60	3000	3060	98.04	24.02	1.83	12.93	22.19	1596.4	0.0152	0.405	0.420	1.81
15	60	4000	4060	98.52	30.48	2.31	16.40	28.17	1891.0	0.0152	0.480	0.495	2.30
16	80	2000	2080	96.15	15.42	1.16	8.29	14.26	1278.8	0.0203	0.325	0.345	1.17
17	40	2000	2040	98.04	18.46	1.37	9.92	17.09	1194.4	0.0102	0.303	0.313	1.40
18	80	1000	1080	92.59	7.66	0.55	4.11	7.11	781.7	0.0203	0.198	0.219	0.58
19	60	1000	1060	94.34	7.77	0.55	4.16	7.22	779.4	0.0152	0.198	0.213	0.59
20	40	1000	1040	96.15	8.38	0.57	4.48	7.81	766.6	0.0102	0.195	0.205	0.64
21	20	500	520	96.15	3.44	0.13	1.79	3.31	445.9	0.0051	0.113	0.118	0.27
22	40	500	540	92.59	2.96	0.11	1.54	2.85	452.7	0.0102	0.115	0.125	0.23
23	60	500	560	89.29	2.99	0.13	1.56	2.86	452.0	0.0152	0.115	0.130	0.23
24	80	500	580	86.21	2.96	0.13	1.55	2.83	452.4	0.0203	0.115	0.135	0.23

Case 6

Pipe: 0.5" Nominal Pipe Size, 0.36 inch ID, 12.3 ft long, Stainless Steel **Surfactant: CEDEPAL FA-406**

Foam Generator Opening Size: 90 μm **Surfactant Concentration: 0.1 wt % in Liquid Solution**

Test	Liquid Rate	Gas Rate	Total Rate	fg	Pavg at A	Pavg at H	Pavg	ΔP_{A-H}	Qgas	Uliquid	Ugas	Ut	dP/dL
No.	ml/min	Scc/min	cc/min	%	Psi	Psi	Psi	Psi	cc/min	m/sec	m/sec	m/sec	psi/ft
1	60	3000	3060	98.04	0.05	0	0.03	0.05	2994.9	0.0152	0.760	0.775	0.00
2	80	3000	3080	97.40	0.25	0	0.13	0.25	2974.7	0.0203	0.755	0.775	0.02
3	80	2000	2080	96.15	0.63	0	0.32	0.63	1958.0	0.0203	0.497	0.517	0.05
4	60	2000	2060	97.09	0.22	0	0.11	0.22	1985.1	0.0152	0.504	0.519	0.02
5	80	1000	1080	92.59	2.02	0	1.01	2.02	935.7	0.0203	0.237	0.258	0.17
6	60	1000	1060	94.34	1.15	0	0.58	1.15	962.4	0.0152	0.244	0.259	0.09
7	40	1000	1040	96.15	0.93	0	0.47	0.93	969.3	0.0102	0.246	0.256	0.08
8	20	1000	1020	98.04	0.55	0	0.28	0.55	981.6	0.0051	0.249	0.254	0.04
9	20	500	520	96.15	0.86	0	0.43	0.86	485.8	0.0051	0.123	0.128	0.07
10	40	500	540	92.59	1.13	0	0.57	1.13	481.5	0.0102	0.122	0.132	0.09
11	60	500	560	89.29	1.31	0	0.66	1.31	478.7	0.0152	0.121	0.137	0.11
12	80	500	580	86.21	1.5	0	0.75	1.5	475.7	0.0203	0.121	0.141	0.12

Case 7

Pipe: 0.5" Nominal Pipe Size, 0.36 inch ID, 12.3 ft long, Stainless Steel

Surfactant: PETROSTEP CG-50

Foam Generator Opening Size: 50 µm

Surfactant Concentration: 1 wt % in Liquid Solution

Test No.	Liquid Rate ml/min	Gas Rate Scc/min	Total Rate cc/min	fg %	Pavg at A Psi	Pavg at H Psi	Pavg Psi	ΔPA-H Psi	Qgas cc/min	Ulquid m/sec	Ugas m/sec	Ut m/sec	dP/dL psi/ft
1	80	3000	3080	97.40	10.87	0.8	5.84	10.07	2147.6	0.0203	0.545	0.565	0.82
2	80	4000	4080	98.04	8.32	0.53	4.43	7.79	3074.5	0.0203	0.780	0.801	0.64
3	80	5000	5080	98.43	5.05	0.33	2.69	4.72	4226.6	0.0203	1.073	1.093	0.39
4	60	5000	5060	98.81	2.74	0.04	1.39	2.7	4568.1	0.0152	1.159	1.175	0.22
5	40	5000	5040	99.21	1.21	0	0.61	1.21	4802.4	0.0102	1.219	1.229	0.10
6	20	5000	5020	99.60	0.14	0	0.07	0.14	4976.3	0.0051	1.263	1.268	0.01
7	20	4000	4020	99.50	0.19	0	0.10	0.19	3974.3	0.0051	1.009	1.014	0.02
8	20	3000	3020	99.34	0.34	0	0.17	0.34	2965.7	0.0051	0.753	0.758	0.03
9	20	2000	2020	99.01	0.61	0	0.31	0.61	1959.3	0.0051	0.497	0.502	0.05
10	20	1000	1020	98.04	0.96	0	0.48	0.96	968.4	0.0051	0.246	0.251	0.08
11	40	3000	3040	98.68	2.39	0.04	1.22	2.35	2771.0	0.0102	0.703	0.713	0.19
12	40	4000	4040	99.01	1.81	0	0.91	1.81	3768.0	0.0102	0.956	0.966	0.15
13	60	2000	2060	97.09	6.34	0.4	3.37	5.94	1627.0	0.0152	0.413	0.428	0.49
14	60	3000	3060	98.04	6.28	0.4	3.34	5.88	2444.6	0.0152	0.620	0.636	0.48
15	60	4000	4060	98.52	3.99	0.23	2.11	3.76	3497.9	0.0152	0.888	0.903	0.31
16	80	2000	2080	96.15	9.67	0.72	5.20	8.95	1477.8	0.0203	0.375	0.395	0.73
17	40	2000	2040	98.04	3.09	0.06	1.58	3.03	1806.5	0.0102	0.458	0.469	0.25
18	80	1000	1080	92.59	6.27	0.47	3.37	5.8	813.5	0.0203	0.206	0.227	0.47
19	60	1000	1060	94.34	4.67	0.29	2.48	4.38	855.6	0.0152	0.217	0.232	0.36
20	40	1000	1040	96.15	2.3	0.03	1.17	2.27	926.6	0.0102	0.235	0.245	0.19
21	20	500	520	96.15	4.26	0.19	2.23	4.07	434.3	0.0051	0.110	0.115	0.33
22	40	500	540	92.59	2.84	0.11	1.48	2.73	454.4	0.0102	0.115	0.125	0.22
23	60	500	560	89.29	2.38	0.07	1.23	2.31	461.5	0.0152	0.117	0.132	0.19
24	80	500	580	86.21	2.12	0.03	1.08	2.09	465.9	0.0203	0.118	0.139	0.17

Case 8

Pipe: 0.5" Nominal Pipe Size, 0.36 inch ID, 12.3 ft long, Stainless Steel **Surfactant: STEPANFORM 1050**

Foam Generator Opening Size: 50 μm **Surfactant Concentration: 1 wt % in Liquid Solution**

Test No.	Liquid Rate ml/min	Gas Rate Scc/min	Total Rate cc/min	fg %	Pavg at A Psi	Pavg at H Psi	Pavg Psi	ΔP_{A-H} Psi	Qgas cc/min	Uliquid m/sec	Ugas m/sec	Ut m/sec	dP/dL psi/ft
1	80	3000	3080	97.40	22.4	2.02	12.21	20.38	1638.8	0.0203	0.416	0.435	1.67
2	80	4000	4080	98.04	28.55	2.66	15.61	25.89	1940.3	0.0203	0.492	0.513	2.12
3	80	5000	5080	98.43	34.03	3.18	18.61	30.85	2206.9	0.0203	0.560	0.580	2.52
4	60	5000	5060	98.81	32.03	2.84	17.44	29.19	2287.2	0.0152	0.580	0.595	2.39
5	40	5000	5040	99.21	9.51	0.6	5.06	8.91	3720.6	0.0102	0.944	0.954	0.73
6	20	5000	5020	99.60	1.53	0	0.77	1.53	4752.7	0.0051	1.206	1.211	0.13
7	20	4000	4020	99.50	2.39	0	1.20	2.39	3699.3	0.0051	0.939	0.944	0.20
8	20	3000	3020	99.34	3.94	0	1.97	3.94	2645.5	0.0051	0.671	0.676	0.32
9	20	2000	2020	99.01	9.09	0.56	4.83	8.53	1505.8	0.0051	0.382	0.387	0.70
10	20	1000	1020	98.04	12.33	0.86	6.60	11.47	690.3	0.0051	0.175	0.180	0.94
11	40	3000	3040	98.68	21.1	1.78	11.44	19.32	1687.1	0.0102	0.428	0.438	1.58
12	40	4000	4040	99.01	18.19	1.45	9.82	16.74	2398.0	0.0102	0.609	0.619	1.37
13	60	2000	2060	97.09	16.74	1.39	9.07	15.35	1237.1	0.0152	0.314	0.329	1.25
14	60	3000	3060	98.04	22.81	2.13	12.47	20.68	1623.1	0.0152	0.412	0.427	1.69
15	60	4000	4060	98.52	28.25	2.61	15.43	25.64	1951.5	0.0152	0.495	0.511	2.10
16	80	2000	2080	96.15	15.65	1.3	8.48	14.35	1268.6	0.0203	0.322	0.342	1.17
17	40	2000	2040	98.04	16.64	1.45	9.05	15.19	1238.2	0.0102	0.314	0.324	1.24
18	80	1000	1080	92.59	7.8	0.57	4.19	7.23	778.4	0.0203	0.198	0.218	0.59
19	60	1000	1060	94.34	8.54	0.61	4.58	7.93	762.6	0.0152	0.194	0.209	0.65
20	40	1000	1040	96.15	9.76	0.68	5.22	9.08	738.0	0.0102	0.187	0.197	0.74
21	20	500	520	96.15	5.41	0.27	2.84	5.14	419.0	0.0051	0.106	0.111	0.42
22	40	500	540	92.59	3.94	0.17	2.06	3.77	438.7	0.0102	0.111	0.121	0.31
23	60	500	560	89.29	3.34	0.15	1.75	3.19	446.9	0.0152	0.113	0.129	0.26
24	80	500	580	86.21	2.95	0.11	1.53	2.84	452.9	0.0203	0.115	0.135	0.23

Case 9

Pipe: 0.5" Nominal Pipe Size, 0.36 inch ID, 12.3 ft long, Stainless Steel **Surfactant: AQUET TD-600**

Foam Generator Opening Size: 50 μm **Surfactant Concentration: 1 wt % in Liquid Solution**

Test No.	Liquid Rate ml/min	Gas Rate Scc/min	Total Rate cc/min	fg %	Pavg at A Psi	Pavg at H Psi	Pavg Psi	ΔPA-H Psi	Qgas cc/min	Uliquid m/sec	Ugas m/sec	Ut m/sec	dP/dL psi/ft
1	80	3000	3080	97.40	4.35	0.3	2.33	4.05	2590.3	0.0203	0.657	0.678	0.33
2	80	4000	4080	98.04	2.46	0.07	1.27	2.39	3683.1	0.0203	0.935	0.955	0.20
3	80	5000	5080	98.43	1.55	0.01	0.78	1.54	4748.1	0.0203	1.205	1.225	0.13
4	60	5000	5060	98.81	1.08	0	0.54	1.08	4822.8	0.0152	1.224	1.239	0.09
5	40	5000	5040	99.21	0.62	0	0.31	0.62	4896.7	0.0102	1.243	1.253	0.05
6	20	5000	5020	99.60	0.12	0	0.06	0.12	4979.7	0.0051	1.264	1.269	0.01
7	20	4000	4020	99.50	0.2	0	0.10	0.2	3973.0	0.0051	1.008	1.013	0.02
8	20	3000	3020	99.34	0.27	0	0.14	0.27	2972.7	0.0051	0.754	0.760	0.02
9	20	2000	2020	99.01	0.56	0	0.28	0.56	1962.6	0.0051	0.498	0.503	0.05
10	20	1000	1020	98.04	1.53	0	0.77	1.53	950.5	0.0051	0.241	0.246	0.13
11	40	3000	3040	98.68	1.33	0	0.67	1.33	2870.2	0.0102	0.728	0.739	0.11
12	40	4000	4040	99.01	0.82	0	0.41	0.82	3891.5	0.0102	0.988	0.998	0.07
13	60	2000	2060	97.09	2.85	0.09	1.47	2.76	1818.2	0.0152	0.461	0.477	0.23
14	60	3000	3060	98.04	2.36	0.08	1.22	2.28	2770.1	0.0152	0.703	0.718	0.19
15	60	4000	4060	98.52	1.5	0.01	0.76	1.49	3804.6	0.0152	0.966	0.981	0.12
16	80	2000	2080	96.15	4.63	0.28	2.46	4.35	1713.8	0.0203	0.435	0.455	0.36
17	40	2000	2040	98.04	1.92	0.01	0.97	1.91	1876.8	0.0102	0.476	0.486	0.16
18	80	1000	1080	92.59	6.27	0.51	3.39	5.76	812.6	0.0203	0.206	0.227	0.47
19	60	1000	1060	94.34	4.67	0.33	2.50	4.34	854.7	0.0152	0.217	0.232	0.35
20	40	1000	1040	96.15	4.05	0.26	2.16	3.79	872.1	0.0102	0.221	0.231	0.31
21	20	500	520	96.15	4.71	0.29	2.50	4.42	427.3	0.0051	0.108	0.114	0.36
22	40	500	540	92.59	3.12	0.17	1.65	2.95	449.7	0.0102	0.114	0.124	0.24
23	60	500	560	89.29	2.58	0.13	1.36	2.45	457.8	0.0152	0.116	0.131	0.20
24	80	500	580	86.21	2.32	0.09	1.21	2.23	462.1	0.0203	0.117	0.138	0.18

Case 10

Pipe: 0.5" Nominal Pipe Size, 0.36 inch ID, 12.3 ft long, Stainless Steel **Surfactant: ULTRA-PALMOLIVE**

Foam Generator Opening Size: 50 µm **Surfactant Concentration: 1 wt % in Liquid Solution**

Test	Liquid Rate	Gas Rate	Total Rate	fg	Pavg at A	Pavg at H	Pavg	ΔPa-h	Qgas	Uliq.	Ugas	Ut	dP/dL
No.	ml/min	Scc/min	cc/min	%	Psi	Psi	Psi	Psi	cc/min	m/sec	m/sec	m/sec	psi/ft
1	80	3000	3080	97.40	14.28	1.3	7.79	12.98	1960.9	0.0203	0.498	0.518	1.06
2	80	4000	4080	98.04	11.43	1.01	6.22	10.42	2810.7	0.0203	0.713	0.734	0.85
3	80	5000	5080	98.43	8.42	0.7	4.56	7.72	3816.2	0.0203	0.969	0.989	0.63
4	60	5000	5060	98.81	3.93	0.16	2.05	3.77	4389.4	0.0152	1.114	1.129	0.31
5	40	5000	5040	99.21	1.77	0.05	0.91	1.72	4708.5	0.0102	1.195	1.205	0.14
6	20	5000	5020	99.60	0.34	0	0.17	0.34	4942.8	0.0051	1.254	1.260	0.03
7	20	4000	4020	99.50	0.48	0	0.24	0.48	3935.7	0.0051	0.999	1.004	0.04
8	20	3000	3020	99.34	0.6	0	0.30	0.6	2940.0	0.0051	0.746	0.751	0.05
9	20	2000	2020	99.01	1.21	0	0.61	1.21	1920.9	0.0051	0.488	0.493	0.10
10	20	1000	1020	98.04	2.2	0.01	1.11	2.19	930.1	0.0051	0.236	0.241	0.18
11	40	3000	3040	98.68	3.53	0.13	1.83	3.4	2667.9	0.0102	0.677	0.687	0.28
12	40	4000	4040	99.01	2.43	0	1.22	2.43	3694.6	0.0102	0.938	0.948	0.20
13	60	2000	2060	97.09	10.08	0.76	5.42	9.32	1461.2	0.0152	0.371	0.386	0.76
14	60	3000	3060	98.04	10.6	0.81	5.71	9.79	2161.2	0.0152	0.549	0.564	0.80
15	60	4000	4060	98.52	5.29	0.26	2.78	5.03	3364.8	0.0152	0.854	0.869	0.41
16	80	2000	2080	96.15	12.8	1.1	6.95	11.7	1358.0	0.0203	0.345	0.365	0.96
17	40	2000	2040	98.04	6.84	0.4	3.62	6.44	1604.8	0.0102	0.407	0.417	0.53
18	80	1000	1080	92.59	6.63	0.51	3.57	6.12	804.6	0.0203	0.204	0.225	0.50
19	60	1000	1060	94.34	5.93	0.43	3.18	5.5	822.1	0.0152	0.209	0.224	0.45
20	40	1000	1040	96.15	5.75	0.39	3.07	5.36	827.2	0.0102	0.210	0.220	0.44
21	20	500	520	96.15	5.23	0.27	2.75	4.96	421.2	0.0051	0.107	0.112	0.41
22	40	500	540	92.59	5.5	0.37	2.94	5.13	416.8	0.0102	0.106	0.116	0.42
23	60	500	560	89.29	3.46	0.28	1.87	3.18	443.6	0.0152	0.113	0.128	0.26
24	80	500	580	86.21	1.92	0.04	0.98	1.88	468.8	0.0203	0.119	0.139	0.15

Case 11

Pipe: 1" Nominal Pipe Size, 0.957 inch ID, 8.5 ft long, Stainless Steel **Surfactant: CEDEPAL FA-406**

Foam Generator Opening Size: 50 μm **Surfactant Concentration: 1 wt % in Liquid Solution**

Test No.	Liquid Rate ml/min	Gas Rate Scc/min	Total Rate cc/min	fg %	Pavg at B Psi	Pavg at G Psi	Pavg Psi	ΔPb-g Psi	Qgas cc/min	Uliquid m/sec	Ugas m/sec	Ut m/sec	dP/dL psi/ft
1	40	1000	1040	96.15	1.77	1.01	1.39	0.76	913.6	0.0014	0.033	0.034	0.09
2	40	2000	2040	98.04	3.61	2.23	2.92	1.37948	1668.6	0.0014	0.060	0.061	0.16
3	40	3000	3040	98.68	4.38	2.73	3.56	1.65	2415.8	0.0014	0.087	0.088	0.19
4	60	3000	3060	98.04	5.27	3.26	4.27	2.01	2325.3	0.0022	0.084	0.086	0.24
5	80	3000	3080	97.40	5.56	3.34	4.45	2.22	2302.9	0.0029	0.083	0.086	0.26
6	80	2000	2080	96.15	4.03	2.45	3.24	1.58	1638.8	0.0029	0.059	0.062	0.19
7	80	1000	1080	92.59	2.11	1.36	1.74	0.75	894.4	0.0029	0.032	0.035	0.09
8	20	1000	1020	98.04	1.36	1.33	1.35	0.03	916.2	0.0007	0.033	0.034	0.00
9	20	2000	2020	99.01	2.08	1.29	1.69	0.79	1794.3	0.0007	0.064	0.065	0.09
10	20	3000	3020	99.34	1.55	0.97	1.26	0.58	2763.2	0.0007	0.099	0.100	0.07
11	60	2000	2060	97.09	3.89	2.24	3.07	1.65	1654.9	0.0022	0.059	0.062	0.19
12	60	4000	4060	98.52	6.02	3.78	4.90	2.24	3000.0	0.0022	0.108	0.110	0.26
13	60	5000	5060	98.81	5.68	3.83	4.76	1.85	3777.9	0.0022	0.136	0.138	0.22
14	80	5000	5080	98.43	7.62	5.02	6.32	2.6	3496.7	0.0029	0.126	0.128	0.30
15	80	4000	4080	98.04	6.89	4.66	5.78	2.23	2871.8	0.0029	0.103	0.106	0.26
16	40	4000	4040	99.01	4.05	2.88	3.47	1.17	3237.0	0.0014	0.116	0.118	0.14
17	60	1000	1060	94.34	1.74	0.99	1.37	0.75	915.0	0.0022	0.033	0.035	0.09
18	40	5000	5040	99.21	3.04	2.21	2.63	0.83	4242.4	0.0014	0.152	0.154	0.10
19	20	4000	4020	99.50	1.08	0.72	0.90	0.36	3769.2	0.0007	0.135	0.136	0.04
20	20	5000	5020	99.60	0.9	0.63	0.77	0.27	4752.7	0.0007	0.171	0.171	0.03

Case 12

Pipe: 1" Nominal Pipe Size, 0.957 inch ID, 8.5 ft long, Stainless Steel **Surfactant: CEDEPAL FA-406**

Foam Generator Opening Size: 50 μm **Surfactant Concentration: 5 wt % in Liquid Solution**

Test	Liquid Rate	Gas Rate	Total Rate	fg	Pavg at B	Pavg at G	Pavg	ΔPb-g	Qgas	Uliq.	Ugas	Ut	dP/dL
No.	ml/min	Scc/min	cc/min	%	Psi	Psi	Psi	Psi	cc/min	m/sec	m/sec	m/sec	psi/ft
1	60	3000	3060	98.04	6.27	3.71	4.99	2.56	2239.7	0.0022	0.080	0.083	0.30
2	60	4000	4060	98.52	8.10	4.80	6.45	3.3	2780.1	0.0022	0.100	0.102	0.39
3	60	5000	5060	98.81	9.73	5.77	7.75	3.96	3273.9	0.0022	0.118	0.120	0.46
4	40	5000	5040	99.21	8.75	5.41	7.08	3.34	3374.7	0.0014	0.121	0.123	0.39
5	40	4000	4040	99.01	8.15	4.76	6.46	3.39	2779.5	0.0014	0.100	0.101	0.40
6	80	4000	4080	98.04	7.81	4.66	6.24	3.15	2808.7	0.0029	0.101	0.104	0.37
7	80	5000	5080	98.43	9.18	5.35	7.27	3.83	3346.2	0.0029	0.120	0.123	0.45
8	80	3000	3080	97.40	6.02	3.59	4.81	2.43	2261.0	0.0029	0.081	0.084	0.28
9	40	3000	3040	98.68	6.12	3.56	4.84	2.56	2256.9	0.0014	0.081	0.082	0.30
10	20	3000	3020	99.34	4.33	2.72	3.53	1.61	2419.8	0.0007	0.087	0.088	0.19
11	20	4000	4020	99.50	4.8	2.87	3.84	1.93	3172.4	0.0007	0.114	0.115	0.23
12	20	5000	5020	99.60	2.43	1.71	2.07	0.72	4382.8	0.0007	0.157	0.158	0.08
13	20	2000	2020	99.01	3.67	2.03	2.85	1.64	1675.2	0.0007	0.060	0.061	0.19
14	20	1000	1020	98.04	1.77	0.99	1.38	0.78	914.2	0.0007	0.033	0.034	0.09
15	40	2000	2040	98.04	3.73	2.03	2.88	1.7	1672.4	0.0014	0.060	0.061	0.20
16	60	2000	2060	97.09	3.71	2.02	2.87	1.69	1673.8	0.0022	0.060	0.062	0.20
17	80	2000	2080	96.15	3.73	2.07	2.90	1.66	1670.5	0.0029	0.060	0.063	0.19
18	80	1000	1080	92.59	1.97	1.21	1.59	0.76	902.4	0.0029	0.032	0.035	0.09
19	60	1000	1060	94.34	1.89	1.13	1.51	0.76	906.8	0.0022	0.033	0.035	0.09
20	40	1000	1040	96.15	1.84	1.09	1.47	0.75	909.4	0.0014	0.033	0.034	0.09

APPENDIX B

DERIVATION OF REYNOLDS NUMBER AND POWER-LAW EXPONENT

Foam can be described by a power-law fluid, which is explained in Chapter 2.

$\tau = K\dot{\gamma}^n$, for power-law fluid .....……..... (B-1)

Eq. (B-1) is valid only for laminar flow [Bourgoyne et al., 2005], and the Reynolds number during foam flow can be calculated as follows:

$$R_e = \frac{\rho_f \, u_t \, d}{\mu_f} \quad \text{,.....……... (B-2)}$$

where u_t is the total velocity (i.e., u_{gas} + u_{liq}) whose maximum is about 1.2 m/s in this study corresponding to the maximum gas and liquid flow rates (5000 scc/min and 80 ml/min, respectively) (see Appendix A). The inner diameter (d) of 0.5 inch pipe is about 0.36 inch and ρ_f and μ_f are the density and viscosity of foam mixture.

Nitrogen density can be determined by

$$\rho_g = \frac{2.7\,(P_{inlet} + 14.7)\,\gamma_g}{Z\,(T+459.6)} \quad \text{,.....……... (B-3)}$$

where P_{inlet} is the maximum inlet pressure recorded during experiments which is around 35 psi, γ_g is the specific gravity of nitrogen which is around 0.9737 at standard condition, and Z is the compressibility factor. Density of compressed nitrogen is around 0.25 lb/ft^3 (or 4.03 kg/m^3) at this experimental condition.

Further, foam density can be calculated by

$$\rho_f = \rho_l \, f_l + \rho_g \, f_g \quad \text{,.....……... (B-4)}$$

where ρ and f are the density and volume fraction of liquid and gas phases, respectively. ρ_l is assumed to be 62.4 lb/ft^3 (or 1000 kg/m^3), which is roughly the density of pure water, due to low surfactant concentration in liquid solution (from 0.1 to 5 wt%). The maximum foam density

calculated from the experimental conditions is about 2.42 lb/ft^3 (or, 38.8 kg/m^3) by using the maximum liquid flow rate (i.e., 80 ml/min) and the lowest value of actual gas flow rate adjusted at the elevated system pressure (i.e., 2200 cc/min from the range of 2200 to 4800 cc/min; see Appendix A). More specifically, ρ_f = 62.4 lb/ft^3 · (80/(80+2200)) + 0.25 lb/ft^3 · (2200/(80+2200)) = 2.42 lb/ft^3. For the pressure and temperature not changing significantly, the actual gas flow rate (q_{gas}) can be estimated by

$$q_{gas} = \frac{14.7\, q_{gas,sc}}{14.7 + P_{avg}} \quad \text{,.....} \quad \text{(B-5)}$$

Finally, substituting the maximum foam velocity of 1.2 m/s, inner pipe diameter of 0.36 inch, and the maximum foam density of 2.42 lb/ft^3, and assuming foam viscosity to be 1 cp into Eq. (B-2) yields Reynolds number of 426.

This calculation shows that all experimental conditions in this study lie within the pattern of laminar flow keeping the Reynolds number far lower than the transition between laminar and turbulent flow pattern (i.e., 2100).. In reality, foam viscosity can vary from 60 to 500 cps in most of the experiments, which would further reduce the Reynolds number.

Previous studies show that foam can be approximated by shear-thickening, shear-thinning, or Newtonian fluid. A general way to analyze the power-law fluid behavior is the evaluation of power-law exponent through the shear-stress and shear-rate relationship for laminar flow in the pipe. Given that all experimental data in this study are within the pattern of laminar flow, the following relationship [Bourgoyne et al., 2005] should be applicable.

The shear-stress at the pipe wall is given by

$$\tau_w = \frac{r}{2}\frac{dP}{dL} \quad \text{,.....} \quad \text{(B-6)}$$

where τ_w is the shear-stress at the pipe wall, and r is radius of circular pipe. The frictional

pressure gradient (dP/dL) for a circular pipe can be expressed by

$$\frac{dP}{dL} = \frac{8\,\mu\,u}{r^2} \quad \text{,.....} \quad \text{(B-7)}$$

Substituting Eq. (B-7) into Eq. (B-6) yields

$$\tau_w = \frac{r\,8\,\mu\,u}{2\,r^2} = \frac{4\,\mu\,u}{r} = \frac{8\,\mu\,u}{d} \quad \text{,.....} \quad \text{(B-8)}$$

Because the shear-rate at the pipe wall is defined as

$$\dot{\gamma} = \frac{\tau_w}{\mu} \quad \text{,.....} \quad \text{(B-9)}$$

the shear stress vs. shear-rate relationship for power-law model is given by

$$\tau_w = K_f \left(\frac{8\,u}{d}\right)^{\alpha} \quad \text{,.....} \quad \text{(B-10)}$$

For two different flow rates and corresponding pressure drops, Eq. (B-10) can be written as follows

$$\frac{\tau_{w2}}{\tau_{w1}} = \frac{K_f\left(8\frac{\frac{q_2}{A}}{d}\right)^{\alpha}}{K_f\left(8\frac{\frac{q_1}{A}}{d}\right)^{\alpha}} \quad \text{,.....} \quad \text{(B-11)}$$

Substituting Eq. (B-7) into Eq. (B-11) yields

$$\frac{\frac{r_w}{2}\frac{\Delta P_2}{\Delta L}}{\frac{r_w}{2}\frac{\Delta P_1}{\Delta L}} = \frac{K_f\left(8\frac{\frac{q_2}{A}}{d}\right)^{\alpha}}{K_f\left(8\frac{\frac{q_1}{A}}{d}\right)^{\alpha}} \quad \text{,.....} \quad \text{(B-12)}$$

which becomes

$$\frac{\Delta P_2}{\Delta P_1} = \left(\frac{q_2}{q_1}\right)^{\alpha} \quad \text{,.....} \quad \text{(B-13)}$$

and finally, power-law exponent can be expressed as:

$$\alpha = \frac{\ln\left(\frac{\Delta P_2}{\Delta P_1}\right)}{\ln\left(\frac{q_2}{q_1}\right)} \quad \text{,.....} \quad \text{(B-14)}$$

Eqs. (B-13) and (B-14) are identical to Eqs. (3.9) and (3.10), respectively, used in this study to determine the power-law exponent, α, from the steady-state pressure drops as a function of superficial gas and liquid velocities.

VITA

Miodrag Bogdanovic was born to Vladimir and Javorka Bogdanovic in Belgrade, Serbia, in May, 1976. Miodrag received his primary and secondary education in public schools in Belgrade. He graduated from the University of Belgrade in September, 2000 with Bachelor of Science degree in mechanical engineering with specialization in thermal-engineering and HVAC Systems. After graduation, Miodrag worked for three years with Energoproject, Energy-construction company as piping stress analysis engineer in several thermal power plants in Serbia, and as pipeline engineer in Qatar and Oman. He later became a facility engineer working for PM Lucas Enterprises in Serbia, Kazakhstan, and Iran, for three years. He was accepted by Craft and Hawkins Petroleum Engineering Department at Louisiana State University and began his graduate studies in petroleum engineering in August 2006.

His interests include oilfield facilities and rotating equipment, production engineering, underbalanced drilling, well control and natural gas.